A Field and Numerical Investigation of the Pressure Pulsing Reagent Delivery Approach

by

Tyler Gale

A thesis
presented to the University of Waterloo
in fulfillment of the
thesis requirement for the degree of
Master of Applied Science
in
Civil Engineering

Waterloo, Ontario, Canada, 2011

Author's Declaration

I hereby declare that I am the sole author of this thesis. This is a true copy of the thesis, including my required final revisions, as accepted by my examiners.

I understand that my thesis may be made electronically available to the public.

Abstract

The efficacy of injection-driven remediation techniques for non-aqueous phase liquid (NAPL) source zones is limited by the principle that fluid flow is focused along paths of least hydraulic resistance. The pressure pulse technology stands among a number of innovative methods that have been developed with the aim of overcoming or mitigating this limitation. The objective of this research was to observe and document differences in saturated groundwater flow and solute transport between an injection using a conventional or continuous pressure delivery approach and an injection using a pressure pulsing instrument. The underlying motivation was to identify engineering opportunities presented by pressure pulsing with the potential to improve remediation efficiency at contaminated sites.

A series of tracer injections were conducted in the unconfined aquifer at the University of Waterloo Groundwater Research Facility at Canadian Forces Base (CFB) Borden near Alliston, ON (homogeneous fine sand), and in the shallow aquifer at a groundwater research site located on the North Campus at the University of Waterloo (moderately heterogeneous with discrete layers varying from fine sand to silt). A single injection well was used at each site for both the conventional and pressure pulsing injections. Different tracers were used for consecutive injections. Bromide, Lithium, Chloride, and fluorescent dyes (Rhodamine WT and Sulforhodamine B) were used. Formation pressurization data was captured by pressure transducers. The spatial distribution of the injected tracers was monitored at a series of multilevel wells. A groundwater flow and solute transport modeling exercise (MODFLOW and MT3DMS numerical engines) simulating the rapid boundary pressure modulation that occurs in association with pressure pulsing was conducted to complement the field injections. A two-dimensional domain was used to conduct a parametric investigation of pressure modulation and its effect on flow and transport. A three-dimensional domain served to scale-up the two-dimensional results and for benchmarking against field observations.

Pressure pulsing simulation results reveal that repeated sudden onset of injection cessation produces brief periods of gradient reversal near the injection well and the development of a mixing zone around the injection well. The spatial extents of this mixing zone are highly dependent upon the hydraulic diffusivity of the medium. Greater heterogeneity in combination with presence of high hydraulic diffusivity pathways maximized the extent of the mixing zone and the magnitude of transverse and reversal hydraulic gradients. Lower pulsing frequency and higher pulsing amplitude favoured a more significant mixing zone, though these effects were secondary to geologic properties.

Use of the pressure pulsing tool did not manifest into distinct changes in tracer breakthrough at either field research site. Comparison between tracer tests was complicated by sorption of fluorescent dyes and ongoing well development. Solute transport simulation results demonstrated augmentation of dispersion arising from the mixing zone phenomenon, but no distinct changes in advection.

Acknowledgements

Department of Earth and Environmental Science field technicians Bob Ingleton and Paul Johnson provided field support. Their wisdom reflected many years of field experience and was an invaluable resource for the development of field procedures and installations.

Department of Civil and Environmental Engineering Lab Technician Mark Sobon provided support and advise for water sample analysis.

Pat Hicks, Wavefront Technology Solutions V.P. Environmental, provided access to a Sindewinder tool and provided instruction and advise on its use.

Neil Thomson and Jim Barker, advisors from departments of Civil and Environmental Engineering and Earth and Environmental Science respectively, provided insight for experiment development, high-level planning, interpretation of results, and tracking down relevant information in the seemingly never ending body of groundwater research litterature.

Financial support was provided by the Ontario Graduate Scholarship, Natural Science and Engineering Research Council of Canada Graduate Scholarship, and the NSERC Discovery Grant awarded to Dr. Neil Thomson.

Table of Contents

List of Figures

List of Tables

Chapter 1 – Introduction

1.1 Background

The efficacy of injection-driven in situ groundwater remediation techniques is limited by the principle that fluid flow concentrates in paths of least resistance. According to the Darcian flow model (Hubbert, 1940), flow in lower permeability zones is slower than higher permeability zones. When a chemical amendment is injected through a screened well, the distribution of the injected fluid will be greater in higher permeability zones than adjacent lower permeability zones. According to Payne et al (2008) even the least heterogeneous sites exhibit at least 1,000-fold variations in hydraulic conductivity at scales of 1 to 10 cm. Therefore it is very difficult, particularly given financial constraints, to achieve a level of control over the distribution of an injected amendment such that the final outcome is contact with all the target contamination within a non-aqueous phase (NAPL) source zone (Zhong et al 2011; Saeton et al 2002).

Attempts to remediate groundwater contamination in situ have been shown to be characterised by partial mass removal, temporary decreases in measured contamination levels, and an eventual rebound, sometimes approaching pre-existing conditions (Thomson et al 2008). Contamination becomes a persistent source where it remains in diffusion-controlled zones, or where contact with an emplaced amendment is otherwise impeded by heterogeneity (e.g., Parker et al 1994). The slow process of diffusion becomes the only means of contact with contamination in such zones.

Pressure pulse technology stands among a number of innovations that have been developed and marketed with the aim of overcoming amendment delivery challenges. It is an injection system that introduces controlled, rapid (4 – 125 complete pulse cycles per second) releases of pressurized water at the well head. The sudden increases in water pressure are theorized to generate high-amplitude dynamic excitation in the porous medium (Davidson 1999). To date marketing in the environmental sector has focussed on suppression of preferred flow paths. It has also been suggested that pressure pulsing can increase flow rate under a given pressure constraint and therefore expedite injections and improve the attainable radius of influence for any given injection. However experimental evidence demonstrating these effects, particularly field-scale evidence, is scarce.

1.2 Thesis Objectives

The over-arching objective of this research was to observe and document differences in saturated groundwater flow and solute transport between injection under a standard screened well method and that using a pressure pulsing instrument. Specific questions upon-which experimental and analytical method development was based include the following:

(1) Does the Darcian groundwater flow model apply for injection using a pressure pulsing tool?
(2) Do solute transport characteristics change when pressure pulsing is applied?
(3) To what extent does pressure pulsing induce flow in the lower permeability zones of a heterogeneous porous medium?
(4) Are there injection design parameters that optimize the effectiveness of pressure pulsing as an aid in the delivery of aqueous amendments?

The underlying motivation for this research is a lack of experimental and analytical evidence that clarifies the benefits of pressure pulsing for the purpose of aqueous amendment delivery. Identifying such engineering opportunities has the potential to play a role in remediation efficiency at contaminated sites.

1.3 Scope and Limitations

Pilot field-scale aqueous conservative tracer injections were conducted at two geographically separated sites with contrasting hydrostraigraphic properties. A single injection well was used at each site for a series of conventional (not pulsing) and pressure pulsing injections.

A groundwater modelling exercise was undertaken to complement tracer injections. According to a small body of literature there are strain excitations which occur in association with pressure pulsing that lead to flow behaviour that cannot be represented under Darcy's law (Refer to section 2.1). Groundwater modelling served as a tool to examine whether flow and transport observations in the field could be validated using Darcy's law. Parametric analysis of pressure pulsing presented an additional opportunity to reveal injection performance considerations that might otherwise be unaccounted for in existing performance criteria. The accuracy of modeling was constrained by the approach used to simulate pressure pulsing as a prescribed pressure boundary condition (Refer to section 4.2.3).

The well-head technology used to induce pressure pulsing has evolved considerably since it was first deployed in the mid 1990s, and will probably continue to evolve after this research effort is complete. For the experiments described and discussed herein, pressure pulsing was generated using the most recent build of the Sidewinder© tool (Refer to section 4.1.2), patented by Wavefront Reservoir Technologies Ltd. The extent to-which results will vary where different technology is used to generate pressure pulsing is unknown.

Research and industry use of pressure pulsing has targeted applications in petroleum recovery and contaminated site remediation. Petroleum production occurs in porous media much deeper and under much more lithostatic pressure than groundwater remediation. The application of pressure pulsing in petroleum recovery is water flooding, and involves a focus on mobilizing NAPLs. The application of pressure pulsing in this research project is limited to delivery of amendments to target soil and groundwater contamination in situ. Water is assumed to be the only mobile phase, and mobilization of NAPL is not investigated nor a desired outcome.

The nature of pressure pulse technology is such that it is only effective under liquid-saturated conditions (refer to section 2.1). Therefore the focus of experiments and discussion is on contamination in water-saturated media. Some liquid amendments are non-aqueous (e.g. Emulsified Zero-Valent Iron solutions), and are more or less viscous than water. The impact of viscosity on flow under pressure pulsing conditions has been examined in past research focussed on petroleum recovery applications (refer to section 2.2). This investigation focussed exclusively on aqueous phase injections.

Chapter 2 – Pressure Pulsing and Other Delivery Enhancement Technologies

Pressure pulse technology has been marketed in the contaminated sites sector as a tool that facilitates the amendment delivery process. This chapter outlines existing documentation describing how pressure pulsing works, with an emphasis on evidence suggesting potential to facilitate amendment delivery. The theoretical model often referred to in association with pressure pulsing is presented. Existing experimental evidence is summarized. Other technologies that attempt to facilitate amendment delivery are briefly discussed.

2.1 Pressure Pulsing Theory

The observation that earthquakes impact water levels in wells and lakes has been documented for a number of decades (e.g. Waller et al 1965, Nikolaevskiy et al 1992). This was the motivation behind early interest in exploring the application of pressure perturbations to manipulate fluid flow through porous media.

The de la Cruz – Spanos model is documented as the early theoretical foundation upon-which pressure pulse technology has been developed (Davidson et al 1999). It describes wave propagation in porous media saturated with a single, viscous, compressible fluid using a set of coupled, first order macroscopic equations. A volume averaging approach is used, whereby equations describing the porous medium at the microscopic scale are averaged over a minimum representative elemental volume (REV). The complete set of equations and their derivations are presented in de la Cruz & Spanos (1989). Fundamental pore-scale equations used to derive the macroscopic equations include the following:

- Equations of motion for a fluid and an elastic solid,
- Continuity equations for a fluid and a solid, and
- Solid and fluid heat equations.

A considerable contrast with the theories of Gassman (1951) and Biot (1956) is the treatment of porosity as a dynamic variable. First-order changes in static porosity (static porosity refers to the

undisturbed porosity of the medium) are suggested to occur when the porous medium is subjected to a transient compression (de la Cruz & Spanos 1985).

Geilkman et al (1993) used the fundamentals of the de la Cruz – Spanos theory to predict a pressure-porosity diffusion process when compression is initiated in a porous medium filled with an incompressible fluid. Spanos (2002) developed a model which predicts pressure-porosity waves when inertial terms are included in the analysis of Geikeman et al (1993). Theses waves are predicted to propagate much slower than acoustic waves and faster than steady-state fluid flow. The analogy of pulsing fluid associated with a heart beat has been used. Udey (2009) expanded upon the model of Spanos (2002) to predict enhancement of dispersion under fluid flow driven by the pressure-porosity wave process.

In the case of a pressure pulsing instrument, compression would be initiated by a sudden, temporary increase in fluid pressure, causing acceleration of the fluid phase. Inertial coupling between the fluid phase (for the case of a fluid with very low compressibility and measurable viscosity) and the solid phase forces a momentary widening or choking of pore channels. This porosity wave follows as the pulse of pressure (or pressure wave) propagates radially from the source.

Darcy theory contains no inertial term (Hubbert 1940). Therefore the argument has been made that, due to the associated accelerations, Darcy theory cannot adequately model flow under a pressure pulsing regime (Davidson et al 1999). Proponents of the de la Cruz – Spanos model have also argued that the wave propagation models of Biot (1956) and Gassman (1951) are limited by their assumptions that porosity is a constant and a porous medium can be represented as two spatially superimposed interacting media (de la Cruz et al 1993).

The predicted pressure-porosity wave attenuates very rapidly in circumstances involving large ratios of gas in pore spaces, because this fluid phase is characterised by considerable compressibility. Fluid flow following cessation of pulsing occurs due to re-expansion of the gas phase. Therefore application of pressure pulsing at contaminated sites has been limited to delivery into the saturated zone, and where only liquid amendments are in use.

2.2 Laboratory and field experiments focussed on pressure pulsing for enhanced oil recovery

A body of literature was generated in the late 1990s and early 2000s exploring the suitability of pressure pulsing as an enhancement in a water flood oil recovery setting. Early experiments involved singe-phase flow at the laboratory scale. Experiments of increasing complexity (e.g., two flowing immiscible liquid phases) and field scale followed.

Wang (1999) and Davidson et al (1999) describe applying pressure pulsing to sand-packed columns and flat sheet cells in laboratory settings. Perturbations were generated by repeatedly impacting tygon© tubing with a rubber mallet upstream of the cell inlets (Figure 2.1).

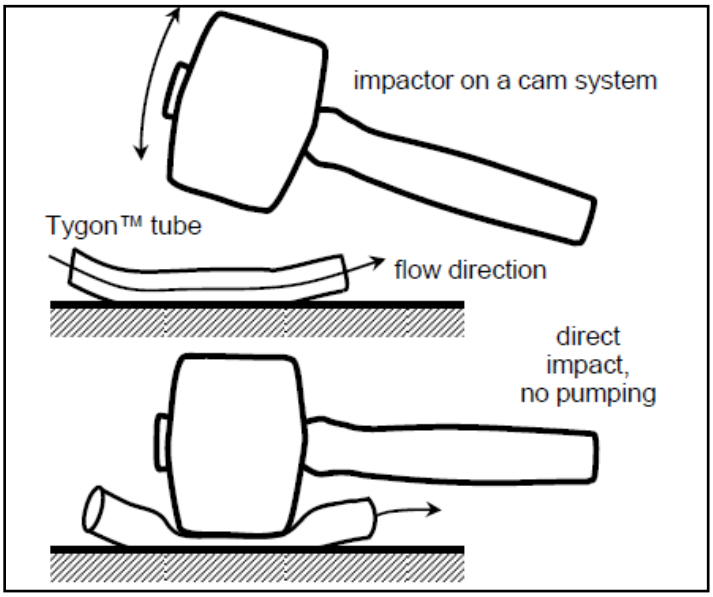

Figure 2.1 - Manual impact pulse generation method (Davidson et al 1999)

Both Wang (1999) and Davidson (1999) demonstrate increased flow rates aligned with the hydraulic gradient. The observation that flow rate increased without a change to the inlet water pressure indicated that the flow rate increase must have been associated with the applied perturbation. Wang (1999) demonstrated that the pressure response to such a perturbation is characterised by a rapid pressure rise followed by a slower decay back to the original pressure. The net result of repeated pulsing is a synergetic pressure build-up (Figure 2.2) where the return to the pre-existing pressure after each pulse does not occur completely before arrival of the next pulse.

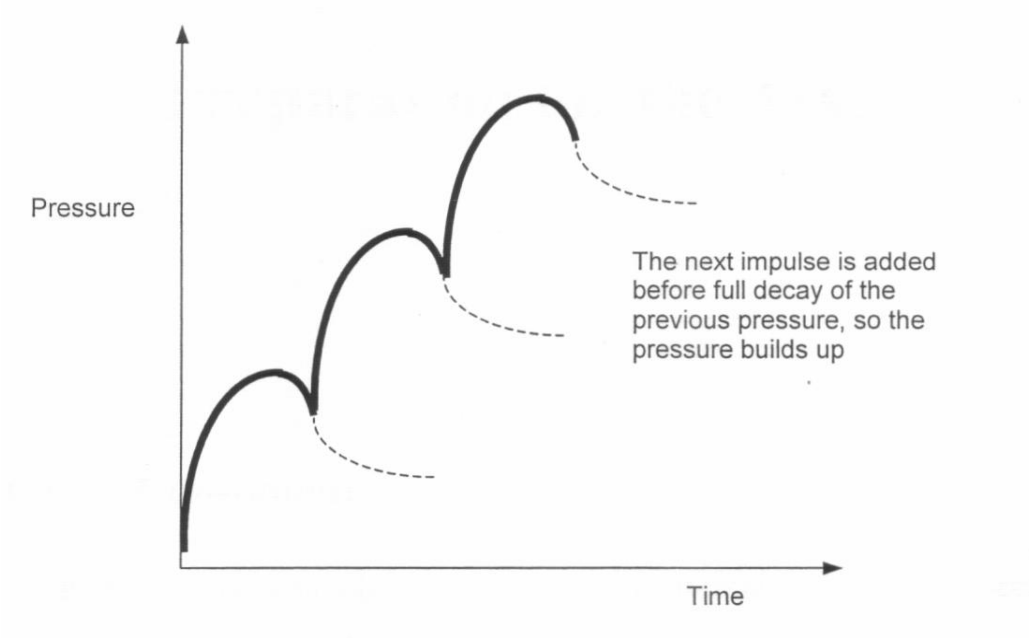

Figure 2.2 – Conceptual plot illustrating synergetic pressure build-up

Davidson et al (1999) and Zschuppe (2001) document experiments involving two mobile immiscible liquid phases in flat plate flow cells. Davidson (1999) demonstrated suppression of viscous fingering in a water-flooding experiment when pressure pulsing was applied (Figure 2.3). Fingers were shown to be shorter and to reach a steady-state length during pressure pulsing, whereas they grew continuously under a conventional flow regime. This resulted in increased oil sweep efficiency and later water breakthrough at the cell outlet. Zschuppe (2001) repeatedly quantified oil recovery improvements of 10% or greater over a given time period, achieved by pressure pulsing in a flat plate flow cell. Zschuppe (2001) made use of temporary pneumatic pressurization of the inlet reservoir to generate pressure pulses.

Cable et al (2001) reported on sand pack and consolidated sandstone column experiments involving single- and two-phase flow. Pressure pulses were generated using the manual impact method described by Davidson (1999), as well as pulsed pumping. Results contrasted previous findings. Flow rate enhancements were observed during pulsed pumping, and were attributed to increases in the average pressure drop across the column. Measurements indicated that a component of pumping was being introduced by the pulsing action, which had the effect of increasing average pressure at the column inlet. No increase in flow rate was observed when the manual impact method was used to generate pulsing. Only the pulsed pumping method was used to generate pressure pulses for two-phase experiments. Earlier water breakthrough was observed during pulsing water flood experiments, suggesting no

suppression of viscous fingering. These findings, which contradict those of Wang (1999), Davidson et al (1999), and Zschuppe (2001), may have their root in the method by which pulsing is generated. Contact materials at the pulsing source for the manual impact method (e.g. rubber mallet and Tygon tubing) were not reported. The pulsed pumping method was not used by other authors. Davidson et al (1999) emphasized the importance of method and materials used to generate the pressure-porosity wave theorized to occur in association with pressure pulsing.

Figure 2.3 – Photographs of viscous fingering developing in two phase systems. Left: No pressure pulsing. Right: Pressure Pulsing (Davidson et al 1999)

Oil removal from porous media has also been explored at the lab scale in the context of shallow mobile NAPL at contaminated sites. At the site scale this can be accomplished by installing a pumping well such that it is screened at depths corresponding with the mobile NAPL pool. The mobile liquid can then be pumped out, leaving behind NAPL at a reduced saturation level, rendering it immobile. Woynillowicz (2000) compared the reduced saturation levels attained under pressure pulsing and conventional flow regimes in the lab. Experiments were conducted in a flat plate flow cell similar to those of Zschuppe (2001) and Davidson et al (1999) using paraffin oil and water. The residual oil saturation was shown to decrease by 3% when pressure pulsing was introduced after a seven pore-volume flush under conventional flow. While the additional mass removal obtained with pressure pulsing is considerable, in terms of arriving at environmentally acceptable standards it is not likely economical.

Samaroo (1999) documents an investigation of reservoir-scale oil production. During a period when pressure pulsing was applied at one water injection well, reservoir-wide oil production was determined to be 37% higher than it had been previously. Accelerometers were installed down-hole in an attempt to detect seismic activity associated with pressure pulsing, but findings were inconclusive.

2.3 Pressure Pulsing Field Trials at Contaminated Sites

Nichols et al (2009) conducted a field investigation to compare the radius of influence and vertical distribution of an injected amendment obtained using pressure pulsing with that of a conventional direct-push injection. Different locations were used for the two types of injection. Down-hole electrical-conductivity profiles were generated at a series of points around each injection site before and after injection using a Geo Probe Direct Image® system. Changes in electrical conductivity post-injection were interpreted to indicate the presence of sodium lactate (a component of the injected amendment). A subset of the generated electrical conductivity profiles were presented in this conference paper (Figure 2.4).

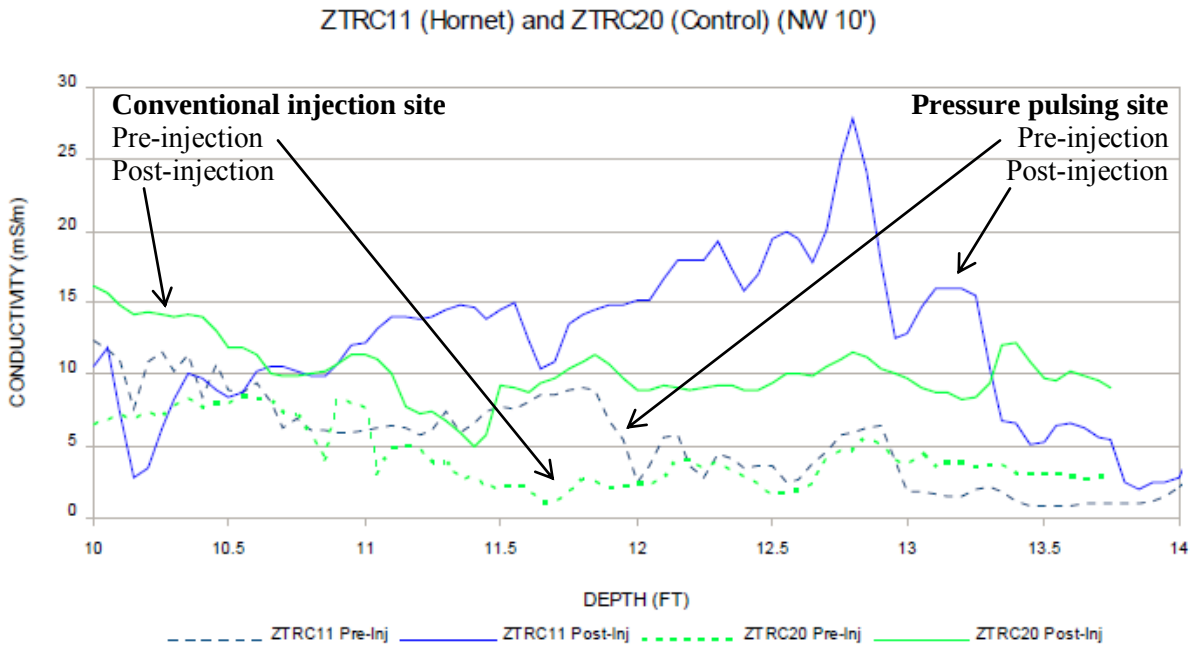

Figure 2.4 – Electrical conductivity profiles recorded 3 m northwest of the pulsing and non-pulsing injection points pre- and post-injection at the Nichols (2009) Site

Nichols et al (2009) reported an average post-injection increase in electrical conductivity of 8.79 mS/m around the pressure pulsing injection point, and an average increase of 5.6 mS/m around the conventional injection site. The trend of higher post-injection EC around the pressure pulsing site was more pronounced further away from the injection point. This suggested that a greater ROI was attainable with pressure pulsing. The pressure pulsing Hornet Tool was subsequently integrated into the full scale remediation program at this site, involving injection at 112 points.

Chang et al (2007) used pressure pulse technology to inject an amendment into fine-grained soils. A comparison between standard direct push injection and pressure pulsing was inconclusive, and a maximum radius of influence of 6 m was reported for both.

Quinn et al (2004) (also refer to Federal Remediation Technologies Roundtable 2004) reported on a series of four pilot injections of emulsified zero-valent iron (EZVI) using standard direct-push, pressure pulsing, and pneumatic and hydraulic fracturing. Distribution of the injected EZVI was evaluated post-injection using soil cores and FLUTe© liners. At the pressure pulsing injection site EZVI was observed to have migrated upwards upon entering the porous medium, suggesting presence of a considerable preferred flow pathway. EZVI was also described to have been well dispersed within the sediments along the path of migration. Results indicated that pressure pulsing might not be best suited for highly viscous amendments such as EZVI.

The experimental research conducted to date has clearly demonstrated opportunity for gains in the petroleum industry. Opportunities presented to the environmental industry remain undetermined. The linkage between experimental findings and the porosity diffusion wave predicted by the de la Cruz – Spanos model also remains undetermined.

2.4 Other Delivery Enhancement Technologies

A number of other innovations have been developed with the aim of overcoming amendment delivery challenges associated with preferred flow paths. A brief discussion of these tools and related research findings are discusses here.

Direct Push Injections

The drill rod systems of certain percussion hammer drill rigs have been designed such that they may act as a mobile injection well. A well screen is fixed to the bottom rod. Sequential, progressively deeper or shallower injections, each spanning a short interval, can be conducted. This presents an opportunity to attain greater hydraulic control in media with moderate to high permeability than would be attainable with a long–screen well (ITRC 2005).

Soil Mixing

Originally designed to serve geotechnical purposes, soil mixing involves homogenising soils using mixing augers as large as 4 m in diameter (Day & Ryan 1995). A cement slurry has often been injected during mixing as a means of encapsulating contamination, thus reducing its availability to the mobile groundwater system. Nutrients and reagents have been injected during mixing to serve the purpose of biological or chemical treatment in situ (e.g., Brough et al 1998). Soil vapour extraction has also been employed in combination with soil mixing, and mass removal on the scale of 90% have been documented (Day & Ryan 1995). The number of mixing sites required to complete a remediation program depends on remediation goals. For example, if preventing migration is a goal, mixing points might only be required along a line to create a low-permeability barrier. If mass removal is a goal, mixing points covering the entire surface area of the contamination would be required. The costs of moving and treating soil offsite are eliminated by soil mixing. Hydraulic processes preventing contact with contamination in low-permeability soils may also be suppressed. However operational costs are much greater than well-based delivery methods.

Hydraulic and Pneumatic Fracturing

Hydraulic fracturing has been successfully used in the petroleum industry since the 1940s, and was first adopted on contaminated sites in the late 1980s (Murdoch & Slack 2002). The utility of this technology arises from the ability to create a network of high-permeability pathways within a fine-grained, low-permeability soil where injection would otherwise be unfeasible. Development has been founded on the observation that fractures nucleate when water pressure in a sealed well exceeds a critical threshold (Frank & Barkley 1995) approximately equivalent to effective stress. Current methods involve

fracture nucleation with a hydraulic jet followed by well pressurization to propagate these fractures. While fractures grow a gel-based slurry is injected to distribute granular solids throughout the system. Once in place these sediments act to hold fractures open. One remediation approach is to inject a reactive granular solid to serve as a permeable reactive barrier (e.g. Siegrist et al 1999). It is also possible to employ a soil vapour extraction system, whereby contamination in and near fracture walls can be accessed for mass removal (e.g. Frank & Barkley 1995). Diffusion distances in low permeability media are considerably reduced in proximity of the induced fracture network.

Pneumatic fracturing is conceptually very similar to hydraulic fracturing. Pressurized gas is injected to nucleate and propagate fractures in low-permeability media. Together hydraulic and pneumatic fracturing have sometimes been referred to as environmental fracturing. The argument has been made that air injection has the added benefit of aeration, which can facilitate biodegradation or vapour extraction. Schuring et al (1995) documents case studies integrating pneumatic fracturing with vapour extraction and NAPL recovery. Predictive capabilities regarding how fractures distribute in different media remains limited (Christiansen et al 2008).

Polymer Injections

Polymer solutions, such as Xanthan gum, have been used widely in the petroleum industry because they have been shown to reduce viscous instabilities along contact surfaces between water and oil (Martel et al 1998). Polymer injection has been shown to increase cross-flow between layers of differing permeability during transient injection as a result of increased fluid viscosity (McCray et al 2010). It has also been suggested that polymer chains act to clog smaller pore channels, thus concentrating polymer flow into higher-permeability zones and having the net effect of decreasing differences in hydraulic conductivity (Darwish et al 2003). The application of polymers in surfactant and alcohol injections has been widely examined (e.g., Maret et al 1998; Lunn & Kueper 1999). Use of polymers during amendment injection for in situ bioremediation and chemical oxidation has also been documented (e.g. Oostrom et al 2007, McCray et al 2010). Laboratory and numerical modelling experiments have demonstrated that polymers can increase sweep efficiency in heterogeneous porous media (McCray et al 2010; Zhong et al 2011). Polymer injection presents an opportunity to suppress preferred flow path tendencies and obtain a more uniform distribution in target zones that are accessible by advection.

Chapter 3 – Field Sites

Field experiments were conducted at two sites with contrasting hydrogeologic properties. The well-characterised Canadian Forces Base Borden Site is considered to be of low heterogeneity, while the University of Waterloo North Campus Research Site is moderately heterogeneous. Site locations, hydrostratigraphy, and installations are described in this chapter.

3.1 Canadian Forces Base Borden

3.1.1 Site Location and Hydrogeology

A series of injections were conducted in the sandpit area of the Canadian Forces Base Borden Groundwater Research Site, near Alliston, Ontario (Figure 3.1). The sandpit area can be described in broad terms as an unconfined aquifer of thickness ranging 9 to 11 m underlain by an aquitard approximately 8 m thick (Morrison 1998). The aquifer consists of fine to medium-grained well sorted sand (median grain size of 0.15 mm according to Frind et al 1999) derived from a glaciofluvial depositional environment (Refer to core photograph in Appendix A). Laminations and evidence of cross-lamination are visible in cross-section, with occasional stringers of silty clay and coarse sand (Sudicky et al 1986). Depth to the water table varies seasonally from surface to 1.65 m below grade (mbg) (Mocanu 2007). Other documented flow and transport parameters include the following:

- Porosity of 0.33 (Mackay et al 1986)
- Hydraulic gradient ranging 0.0065 to 0.0034 (Sudicky 1986) and $K_V=0.33K_H$
- Average hydraulic conductivity of 7E-5 m/s (Mackay et al 1986)
- Longitudinal and transverse vertical dispersivities of 0.36 m and 0.03 m respectively (Sudicky et al 1983)
- Average seepage velocity of 9 cm/day (Mackay et al 1986)
- Specific storage of 0.001 m^{-1} (Frind et al 1999)

A plume of elevated inorganic ion concentrations emanating from a landfill several hundred meters up-gradient contaminates the unconfined aquifer in the sand pit area from approximately 6 mbg to bottom.

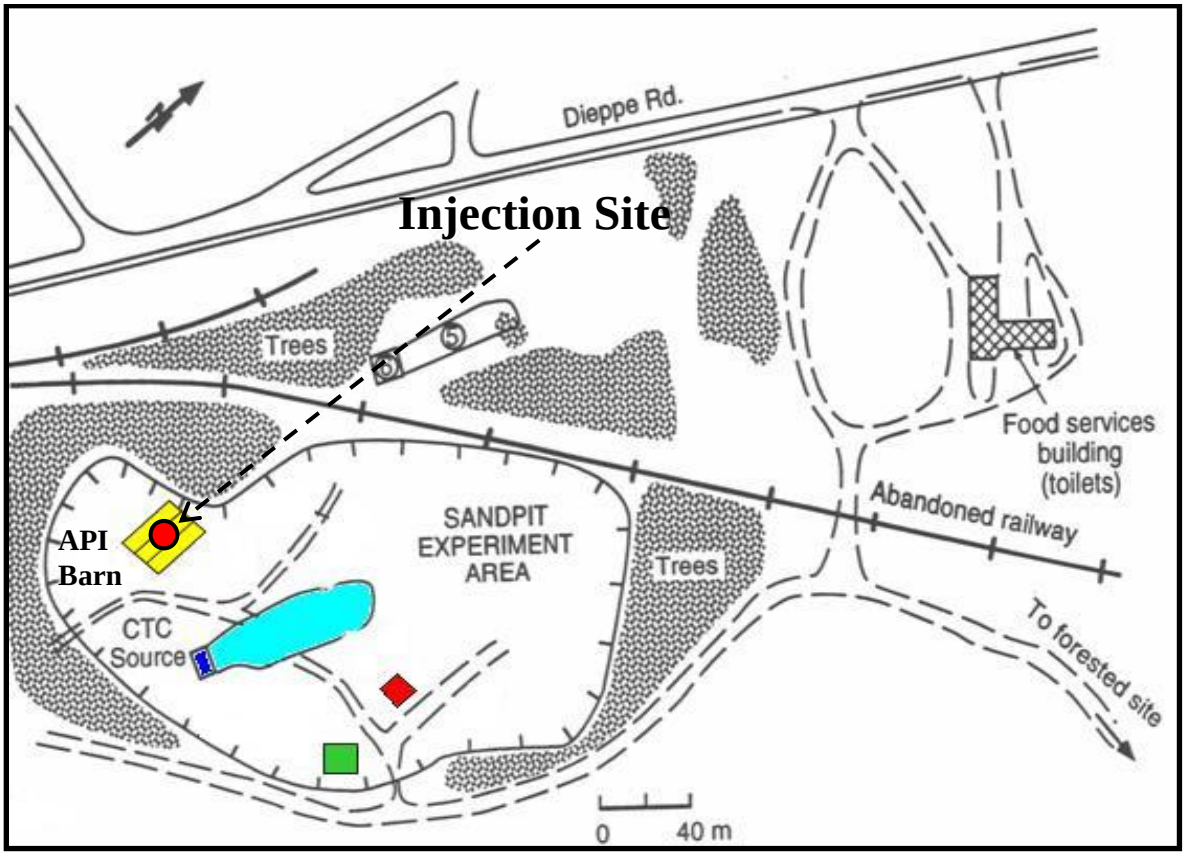

Figure 3.1 – Location of the CFB Borden injection site with respect to the base and sandpit area (Adapted from Mocanu 2007)

3.1.2 Installations

A series of wells were installed at the CFB Borden site, including an injection well and a monitoring network surrounding it in close proximity (Figure 3.2). The injection well was a 5 cm inner diameter (ID) PVC tube screened along a 1 m interval from 8.2 to 9.2 meters below datum (mbd). The elevation datum at the Borden injection site was the top of the injection well tube stickup. Two 2.5 cm ID PVC tubes with 30 cm screens were installed to serve as monitoring wells for hydraulics (HWB1 and HWB2). HWB1 was screened 8.4 to 8.7 mbd, 1 m away from the injection well. HWB2 was screened 7.85 to 8.15 mbd, 2 m away from the injection well. Three multilevel clusters served as water sampling

ports 1, 2, and 3 m away from the injection well. Each sampling port consisted of 1.5 mm ID polyethylene tubing with 100 µm Nytex® screen wrapped around the down-hole end. Each multilevel cluster included seven sampling ports installed to depths ranging approximately 10.5 to 7.5 mbd at 50 cm intervals. A total station survey was conducted after installation (Figure 3.2).

3.2 North Campus Research Site

3.2.1 Site Location and Hydrogeology

A series of injections were conducted at the University of Waterloo North Campus. The injection site was located in a grassy area bounded to the North by Frank Tompa Drive, to the West by Hagey Boulevard, and to the South and East by a parking lot (Figure 3.2).

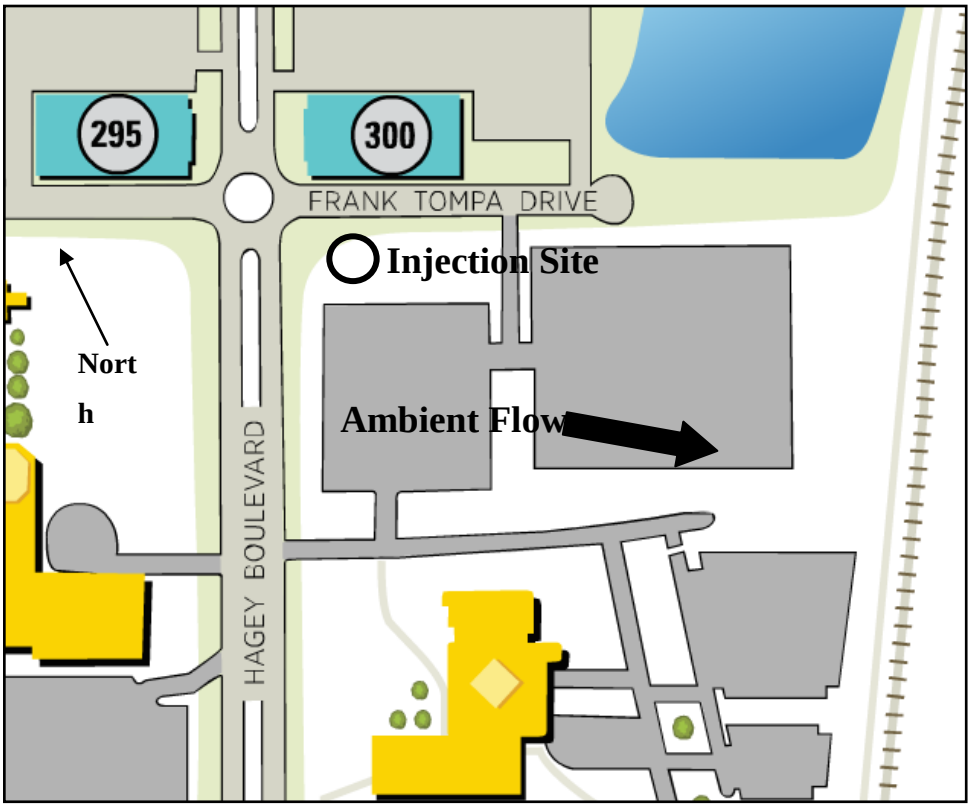

Figure 3.2 – Location of injection site on University of Waterloo North Campus (Adapted from University of Waterloo 2011)

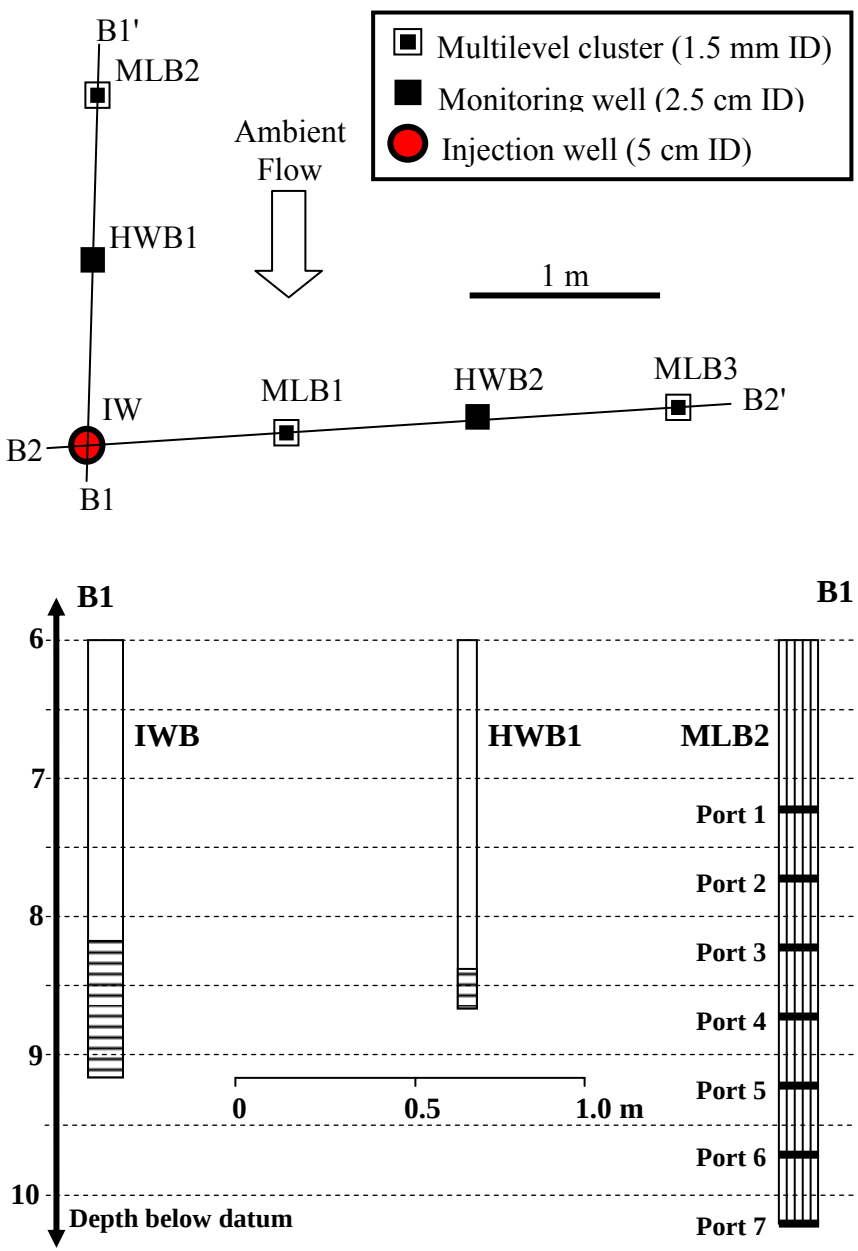

Figure 3.3 - Well network installed at CFB Borden. Clockwise from top left: plan view, cross-section B2-B2', cross-section B1-B1'. Scale indicated on individual drawings.

The dominant regional quaternary soil feature in the Waterloo Region is the Waterloo moraine, characterised by semi-alternating aquifer-aquitard units (Karrow 1979). Analysis of core collected from North Campus documented by Karrow (1979) identified a sequence of sandy to clayey silt to be the near-surface feature, identified as the Tavistock Till. Later work by Sebol (2000) demonstrated considerable heterogeneity and discontinuity of granular deposits. Cross-sections produced by Alexander (2009) 50 m from the injection site reflect this discontinuity, demonstrating granular formations being pinched out between more continuous layers of low permeability silts and clays.

Sebol (2000) indicates that groundwater in the vicinity of the North Campus injection site flows generally towards the Southeast. Water table depth fluctuates seasonally from 1.5 to 3 mbg. Hydraulic gradient has been observed to vary from 0.029 to 0.014, horizontally within aquifer units (Alexander 2009).

Soil cores were collected from the North Campus injection site (NCIS) prior to designing the injection and monitoring systems. These cores were logged and subsequently cut into samples representing intervals approximately 10 cm long. Falling head permeameter tests (ASTM D7100-06) were conducted on repacked samples to determine hydraulic conductivity. Hydraulic Conductivity results were used to design installation depths. A series of hydrostratigraphic units was identified based on logs, hydrometer test results and permeameter test results (Figure 3.4).

3.2.2 Installations

A series of wells were installed at the NCIS, including an injection well and a monitoring network surrounding it in close proximity (Figure 3.5). The injection well was a 5 cm ID PVC tube screened along a 2.5 m interval from 3.9 to 6.4 meters below datum (mbd). The elevation datum at the NCIS was ground surface immediately next to the injection well. Two 2.5 cm ID PVC tubes with 30 cm screens were installed to serve as monitoring wells for hydraulics (HWNC05 and HWB1). HWB05 was screened 6.1 to 5.8 mbd, 0.5 m away from the injection well. HWNC1 was screened 6.05 to 5.75 mbd, 1.0 m away from the injection well. Two multilevel tubing clusters served as water sampling ports 0.5 and 1.0 m away from the injection well. Each sampling port consisted of 9.5 mm ID polyethylene tubing with 100 µm Nytex® screen wrapped around the down-hole end. Each multilevel cluster included ten sampling

ports installed to depths ranging approximately 6.75 to 3.25 mbd at 35 cm intervals. A total station survey was conducted after installation (Figure 3.5).

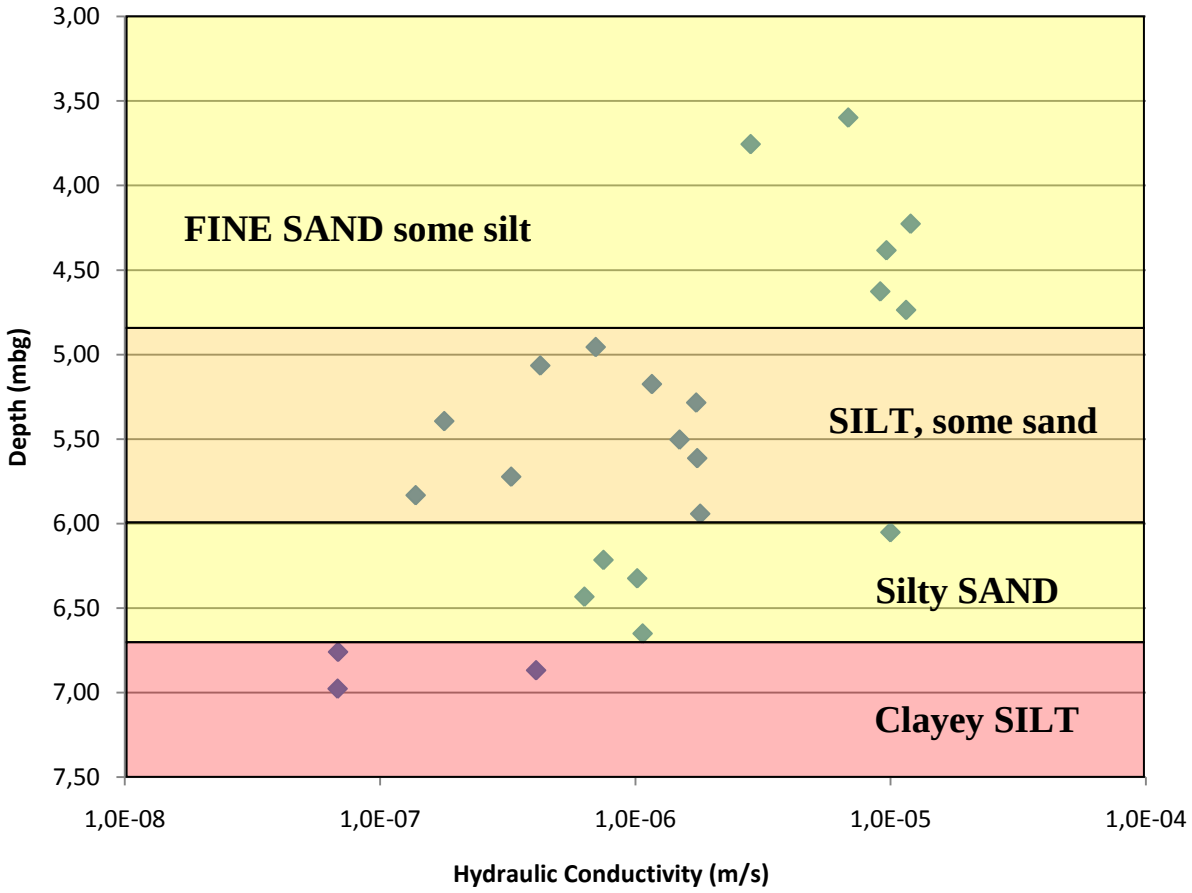

Figure 3.4 – Measured hydraulic conductivity and interpreted layers at the North Campus injection site. Hydraulic conductivity values determined by permeameter tests. Soil type based on combination of hydrometer and core logging. Cores recovered from injection well hole.

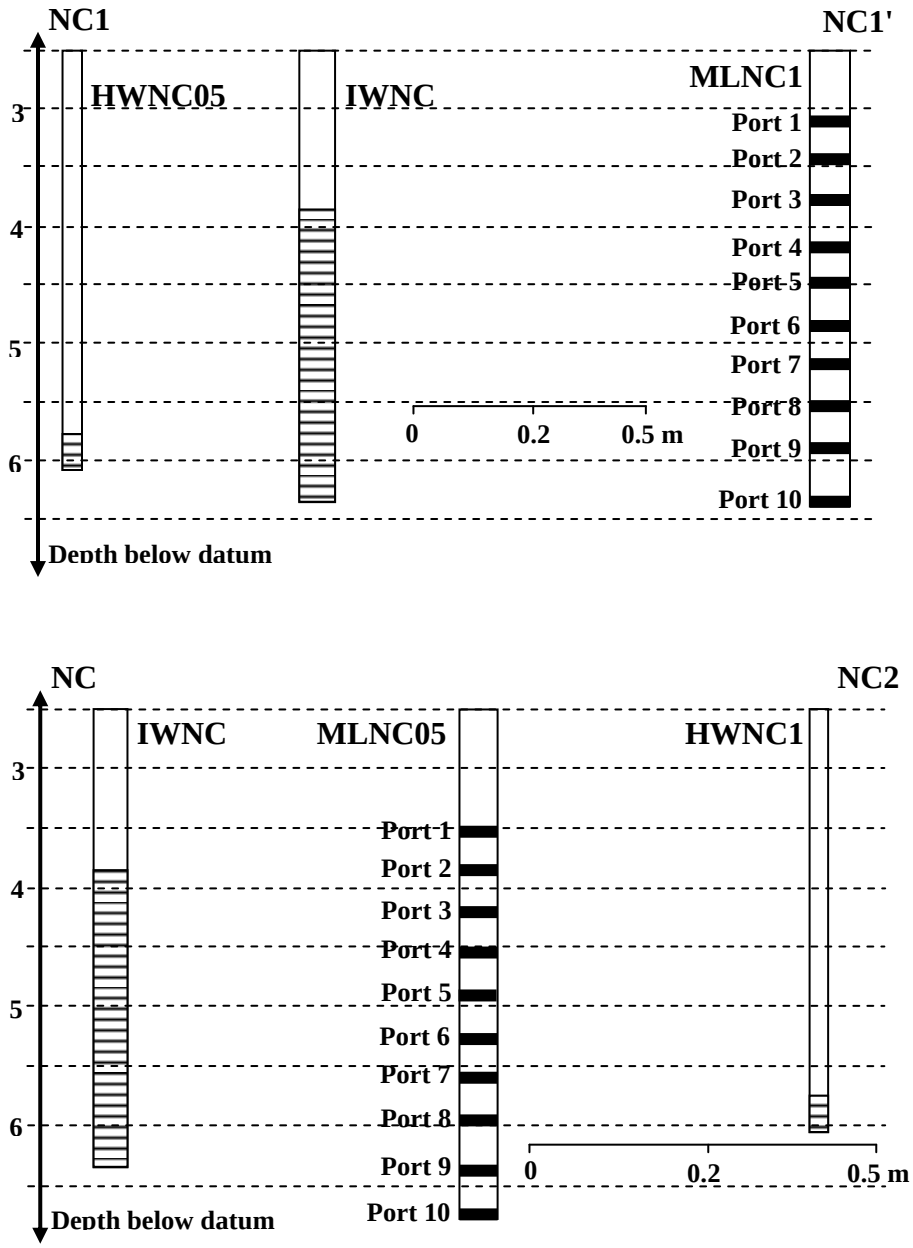

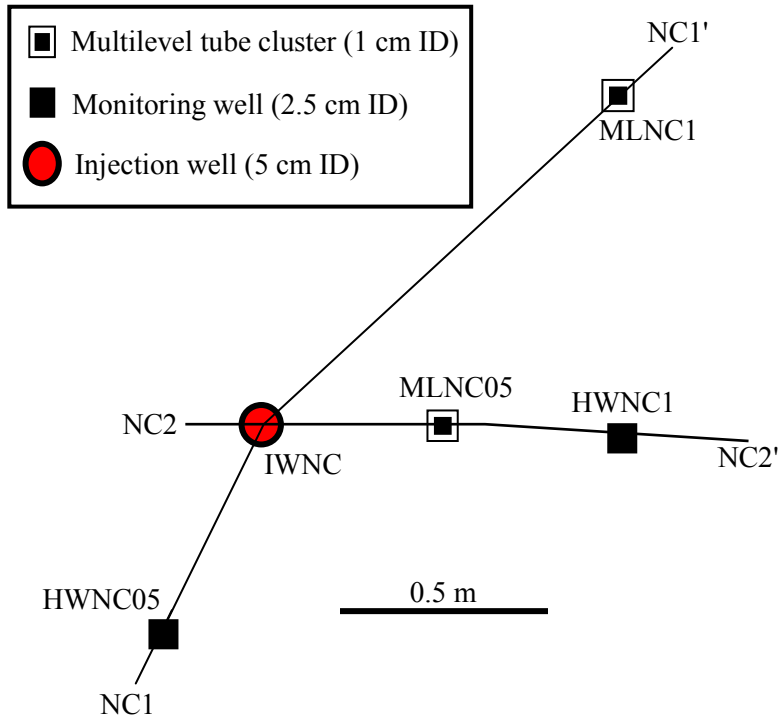

Figure 3.5 - Injection well and monitoring network installed at University of Waterloo North Campus. Clockwise from top left: plan view, cross-section B2-B2', cross-section B1-B1'. Scale indicated on individual drawings.

Chapter 4 – Materials and Methods

Materials and materials used for field and numerical experiments are described here. The functionality of the tool used to generate pressure pulses in the field is described, as well as the methods used to simulate pressure pulsing for modelling exercises. Field procedures, including those for injection and data collection, are described. Numerical engines, input data, and post-processing procedures for modelling exercises are described.

4.1 Field Injections

4.1.1 Injection Procedure and Equipment

All injections were conducted under pressure supplied by a pump (Goulds ½ HP, J5 Jet model). PVC holding tanks were used to contain water at ground surface. From the tank outlets water was routed through PVC piping to the pump, and subsequently to the well head. Flow rate and pressure were measured at regular intervals using an impeller flow meter (Kent C700) and analogue pressure gauge respectively (United States Gauge P-570, 0-15 or 0-100 psi range). Pulsing and conventional injections were paired such that target injection flow rates were consistent for a pair. Refer to Appendix A for photographs of the injection set-up at the Borden site and Appendix B for the North Campus Site.

Target tracer plume radius was dictated by the spatial distribution of the monitoring networks. Numerical models were used to estimate the injection volumes required to achieve the desired radius of influence at each site. The groundwater flow model Modflow 2005 (Harbough 2005) was used in combination with the MT3DMS contaminant transport code (Zheng & Wang 1999) to conduct three dimensional modeling. Injection wells and monitoring networks were placed at the centre of grids built to approximate the respective sites based on available data.

The criterion used to estimate the required injection volume at the CFB Borden site was arrival of tracer concentrations of C/C_0 of 0.5 2 m horizontally away from the injection point. A homogeneous porous medium was assumed (medium properties as detailed in section 3.1.1 were used). An injection of 7500 L satisfied this requirement.

The criterion used to estimate the required injection volume at the North Campus site was arrival of tracer concentrations of C/C_0 of 0.75 1 m from the injection point in the anticipated highest conductivity layer. A horizontally stratified porous medium was assumed. Hydraulic conductivities of each layer were taken to be the geometric mean of those determined by repacked permeameter (Refer to section 3.2.1). According to model results, a 3800 L injection was sufficient. The model also predicted C/C_0 of 0.75 0.5 m from the injection well in the deeper, lower conductivity silty sand layer.

4.1.2 Pressure Pulsing: The Sidewinder© Tool

The instrument used to generate pressure pulses for field injections, referred to as a Sidewinder Tool (Figure 4.1), was designed and patented (Wavefront Reservoir Technologies 2009) by Wavefront Technology Solutions Inc. A brief explanation of its functionality and performance considerations is provided here-in.

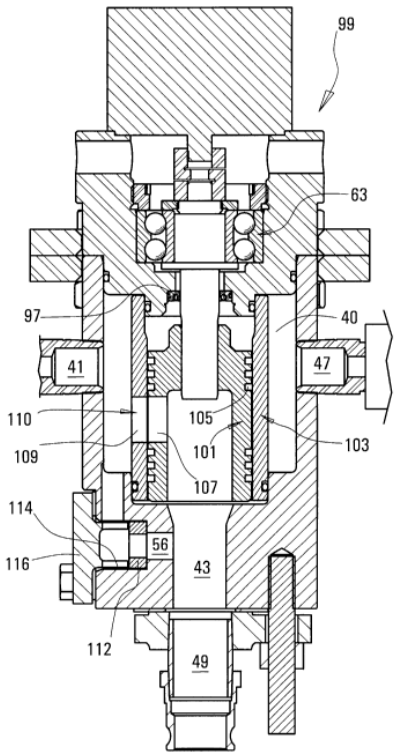

Figure 4.1 – Cross-sectional schematic diagram of the Sidewinder tool
(Wavefront Reservoir Technologies 2009)

Two steel cylinders (no. 101 and 103 in Figure 4.1), one within the other and each cut to contain an aperture, are oriented perpendicular to the incoming flow (no. 41). Chambers immediately up- (no. 40) and down-stream (no. 43) of the cylinders are filled with water during operation. An electric motor rotates the inner cylinder (no. 101). When the aperture of the inner cylinder is not aligned with that of the outer, a seal is formed between the upper and lower chambers. During this stage of the cycle a gas-pressurized accumulator connected to the upper chamber (connected at no. 47) fills with water and pressure builds. When the aperture of the inner cylinder aligns with that of the outer cylinder, built up pressure in the upstream chamber and accumulator is allowed to release, resulting in an increase in pressure and flow downstream (no. 49).

A controller connected to the motor is calibrated to adjust rotational speed. Control over the rate at which the inner cylinder rotates is used to set the frequency at which apertures of the inner and outer cylinders align, and is therefore the mechanism by which the pulsing frequency is controlled. The sidewinder tool was designed to operate at frequencies ranging from 1 to 125 Hz (Hz corresponds to pulses per second).

Performance optimization considerations for a Sidewinder tool, according to Wavefront Tecnology Solutions Inc. (2009), include the following:

(1) **Rate of pressure rise at commencement of a pulse**: A near-instantaneous rise in pressure is considered to be ideal. Adjustable parameters that enable control over rise-time include the shape of the rotating and stationary apertures, and the speed of the rotating cylinder. Leading aperture edges that are straight and align to open the aperture everywhere at once would maximize the rate of pressure rise. Faster rotation would increase the speed at-which the opening allowing flow to pass grows to its full size.

(2) Amplitude of pulsing: higher amplitude changes in pressure are considered more favourable. Maximum amplitude is achieved by maximizing the pumping rate and the time that pressure is allowed to build-up in the upper chamber of the tool between releases.

(3) Pressure build-up: in order to achieve the synergetic pressure build-up and related flow-rate enhancement described by Wang (1999) and Davidson (1999), individual pressure waveforms must not dissipate completely prior to arrival of the subsequent pulse. As such a higher frequency is favourable.

The requirements to achieve optimal pulsing rise-time, amplitude, and frequency are contradictory in nature (e.g., optimized amplitude calls for low frequency, but optimized synergetic pressure build-up calls for high frequency). Therefore optimal performance is a delicate balance between all of these considerations. The theoretical basis of de la Cruz & Spanos (1985, 1989) suggests that optimal performance maximizes the probability of generating an elastic perturbation and its potential size.

Pulsing frequency is the key variable available to optimize pulsing performance. Pump supply pressure is typically constrained by the pump's size and the system's capacity (particularly that of down-hole well seals and formation stability). Pulsing frequency is set to balance pulse amplitude, pressure build-up, and pulse rise-time.

Pulsing performance is affected considerably by hydrogeologic conditions. Very high-permeability media are particularly challenging to work with. Pulsing amplitude can be limited if a medium is able to transmit water very rapidly. A low pulsing frequency must be used and it is quite possible that medium pressurization will be minimal, thereby limiting the ability of a Sidewinder tool to generate a pressure-porosity wave.

Pressure build-up in the downstream chamber of the tool during the low-pressure period of the cycle is often taken to be a symptom of good pulsing performance (Wavefront Technology Solutions Inc. 2009). A temporary flow reversal has sometimes been observed under such conditions, as indicated by an increasing pressure in the downstream chamber during the low-pressure period. This flow reversal has been referred to as "suckback effect" or "matrix back-pressure." Its nature is poorly documented.

The Sidewinder tool was incorporated into the injection system for a subset of the injections at each site. It was installed immediately upstream of the wellhead, with the inlet water being fed from the pump. Pulsing frequencies were determined prior to each injection by consultation with Wavefront Technology Solutions. Refer to Appendix C for Sidewinder tool start-up procedure and photographs of Sidewinder tool configurations.

4.1.3 Hydraulic monitoring

Down-hole pressure transducers (Schlumberger Water Services Diver® model) served as the primary mode of hydraulic monitoring. The 2.5 cm ID monitoring wells were used to house the transducers. Extensions were installed on these wells to accommodate water levels rising above ground surface. Water level measurements were also taken by hand using a water level meter to tie pressure data to a reference datum. Barometric correction was achieved by subtracting pressure data down-hole from pressure data collected by a transducer kept stationary at surface. Recording intervals of 1.0 s or 0.5 s were used. This model of transducer was constrained to a minimum recording interval of 0.5 s and a maximum pressure of 15 m H_2O.

Pressure and flow rate were monitored at the well head using an impeller flowmeter and analogue pressure gauge(s) respectively. When pulsing was used pressure gauges were installed immediately up- and down-stream of the Sidewinder tool. An impeller flowmeter was installed upstream of the pump to monitor flow rates and volumes. A video camera was sometimes used to allow slow-motion observation of pressure gauge fluctuations during pressure pulsing.

4.1.4 Solute Transport Monitoring: Aqueous-Phase Tracers

Solute transport data were collected by injecting and sampling for an aqueous-phase tracer. Ideal tracer properties include maximum conservation in the aqueous phase and high accuracy of the analytical method. Prior to each injection one of four tracers (Sodium Bromide, Lithium Chloride, Sulforhodamine B, or Rhodamine WT) was mixed into the surface tanks to achieve a target concentration. Tank mixing was conducted by water re-circulation using the injection pump. Repeated sample collection from multilevel wells throughout injections allowed development of tracer breakthrough curves.

Sampling methods were developed based on recommendations by Yeskis & Zavala (2002). Negative pressure was applied at surface to draw water from multilevel tubing for sampling. 60 mL syringes were used to draw water at CFB Borden. Early background sampling at the Borden site indicated that a purge volume of at least 1.5 times the full volume of the tubing from screen to syringe was sufficient to collect samples representative of formation conditions. Peristaltic pumps and 0.6 cm (¼ inch) tubing were used to draw water from ports at the North Campus site. Ports were sealed between sampling events to prevent flow to surface. During sampling the seal was removed and the sample tubing was

inserted such that the inlet was located within the port screened interval. Early background sampling at North Campus indicated that a purge volume of at least one full volume of the port tubing from screen to ambient water level was sufficient to collect samples representative of formation conditions. Bottles were labeled with port ID and the time at which drawing water for the sample commenced.

Bromide is a widely-used groundwater tracer, in part because it has been shown to sorb very little and have very low natural concentrations in groundwater environments (Mackay et al 1986). Stock sodium bromide (VWR Inc.) was weighed and mixed into tanks prior to injection. Samples were stored in 30 mL PVC bottles or 40 mL glass bottles. Analysis was conducted using Ion Chromatography (IC) as described by Franson (1998). The Ion Chromatograph (Dionex AS9, 4 by 125mm column, Carbonate-bicarbonate eluent, 2.0 mL/min flow rate) was calibrated using a five-point calibration curve for concentrations ranging 1.0 to 100 mg/L Br^-. Standards and blanks were regularly run through the system to assess performance.

Rhodamine WT (RWT) and sulforhodamine B (SRB) are fluorescent dyes. Concentration analysis using fluorometry is a very rapid process with a particularly low method detection limit (0.5 ppb). Sorption is a consideration of significance for fluorescent dye tracers. While RWT has been used as a conservative tracer in groundwater (e.g., Pang et al. 1998), it has been shown to undergo measurable sorption and has also been used as a sorbing tracer for detection of organic contaminants (Sabatini et al. 1991). Shiau et al (1993) demonstrated that RWT undergoes a two-step sigmodal breakthrough curve arising from the presence of two structural isomers with distinct sorption characteristics. SRB has been shown to undergo less overall sorption than RWT in both silica and alumina environments, but with later initial arrival times (Kasanavia et al. 1999). Injection solutions of 50 ppb RWT were prepared from stock 2.5% w/w liquid (Bright Dyes FWT Red 25 Liquid). Injection solutions of 50 ppb SRB were prepared from stock 75% w/w solids acquired from Sigma-Aldrich Co. Samples were stored in 40 mL glass bottles out of direct sunlight. Analysis was conducted using a Turner Design digital fluorometer (model 10 AU) calibrated with a 40 ppb solution of the corresponding compound.

Successful use of lithium as a conservative aqueous tracer in acidic environments has been documented (Harvey & Bencala 1993; Wrenn et al 1997). Lithium has also been shown to sorb by cation exchange in near-neutral and basic waters (Bencala et al 1984). Chloride has been shown to be conservative in a variety of groundwater environments, however its use has frequently been pre-empted by considerable natural ambient concentrations. Lithium chloride was used as a groundwater tracer at the North Campus site. Chloride acted as a back-up tracer to assess lithium sorption. Stock lithium chloride

solids acquired from Alfa Aesar Inc. were weighed and mixed into holding tanks prior to injection. Samples were stored in 40 mL glass bottles. Lithium analysis was conducted by IC (Dionex DS 9, 4 by 125mm column, Methane Sulfonic acid eluent, 2.0 mL/min flow rate). Chloride analysis was conducted using the anion IC procedure, as described for bromide.

Background chloride concentrations were high and spatially variable at both sites, making chloride a poor option as a primary tracer. Concentrations ranging 11 mg/L to 192 mg/L were measured in background samples collected from the CFB Borden site. There was considerable vertical variability at Borden due to presence of the landfill leachate plume contaminating the bottom half of the aquifer. Concentrations ranging 36 to 147 mg/L were measure at the North Campus Site. Elevated levels at North Campus were likely the result of winter road salting.

4.1.5 NCIS Single-Well-Response Tests

A series of single-well-response tests (SWRT) were conducted at the NCIS prior to the first injection and subsequent to each injection. Water was poured into the Hydraulic monitoring wells (HWNC05 and HWNC1) and the injection well (IWNC) until water spilled over the top opening of the well. Hydraulic response was tracked using pressure transducers. Initial static water levels were recorded using a water level meter. Data analysis was conducted using the method of Bouwer & Rice (1976).

4.2 Numerical Modeling

Numerical groundwater flow and solute transport modeling experiments were conducted in two-dimensional (2D) and three-dimensional (3D) domains. Simulation development followed a process of gradually increasing complexity. Early modeling had the primary objective of simulating pressure pulsing in a homogeneous 2D domain using the boundary condition tools available in the Modflow 2005 (Harbough 2005) software. More complex hydraulic conductivity fields were then introduced, and a parametric investigation of pressure pulsing was conducted to assess effects on flow and transport. Implementing the third spatial dimension increased processing time considerably and served to scale up the 2D model and bridge the gap between detailed model results and field observations. A benchmarking approach was used to develop a 3D conductivity field that simulated the CFB Borden field site.

A brief description of the flow and transport modeling engines used is provided (sections 4.2.1 and 4.2.2), followed by a description of the approach used to represent pressure pulsing (section 4.2.3). The 2D and 3D domains and simulations are then described (sections 4.2.4 and 4.2.5).

4.2.1 Groundwater Flow Modeling – Modflow-2005

Numerical groundwater flow modeling was conducted using the Modflow 2005 code available through the United States Geological Survey (USGS), and documented by Harbaugh (2005). Modflow uses a block-centered finite-difference approach to solve the three-dimensional groundwater flow equation. Equation (1) is the backward-difference equation that forms the basis for generating a head solution from given initial conditions in a transient, saturated flow domain.

$$\begin{aligned} &CR_{i,j-\frac{1}{2},k}\left(h^m_{i,j-1,k}-h^m_{i,j,k}\right)+CR_{i,j+\frac{1}{2},k}\left(h^m_{i,j+1,k}-h^m_{i,j,k}\right)+\\ &CC_{i-\frac{1}{2},j,k}\left(h^m_{i-1,j,k}-h^m_{i,j,k}\right)+CC_{i+\frac{1}{2},j,k}\left(h^m_{i+1,j,k}-h^m_{i,j,k}\right)+\\ &CV_{i,j,k-\frac{1}{2}}\left(h^m_{i,j,k-1}-h^m_{i,j,k}\right)+CV_{i,j,k+\frac{1}{2}}\left(h^m_{i,j,k+1}-h^m_{i,j,k}\right)+\\ &P_{i,j,k}h^m_{i,j,k}+Q_{i,j,k}=SS_{i,j,k}(\Delta r_j\Delta c_i\Delta v_k)\frac{h^m_{i,j,k}-h^{m-1}_{i,j,k}}{t^m-t^{m-1}} \end{aligned} \quad \textbf{(1)}$$

Equation (1) represents the three-dimensional groundwater flow equation for cell i, j, k. C is hydraulic conductance, which combines hydraulic conductivity and cell dimensions in a single term. CR is conductance along rows; CC along columns; CV between layers. Darcy's law is applied between cell i, j, k and the six adjacent cells. The Ph term accounts for external sources and sinks to cell i, j, k that are head-dependent, where P is a constant representing resistance to flow. The term q accounts for external sources and sinks that are not head-dependent. SS is specific storage, Δr ΔcΔv is the volume of cell i, j, k, and t is simulation time. The superscript m is used to denote the current time step number, where m-1 is the previous time step number containing the initial conditions required to solve in the current time step. When Equation 1 is applied to all variable-head cells in a model domain there is one unknown for each cell and the system of equations is solved by iteration (Harbaugh 2005).

Discretization consists of cubic cells stacked in rows, columns and layers giving model domains the shape of a rectangular prism. Layers are always assumed to be stacked vertically. Cell faces at the edge of a model domain are treated as no-flow boundaries.

All modeling was conducted under transient, saturated conditions with water treated as incompressible and constant-density. Boundary conditions available in the Modflow package that were used in this modeling effort are discussed in sections 4.2.3, 4.2.4, and 4.2.5.

4.2.2 Solute Transport Modeling – MT3D

Numerical solute transport modeling was conducted using the MT3DMS code available through the United States Army Corps of Engineers, and documented by Zheng & Wang (1999). This code is compatible with Modflow-2005, making direct use of the discretization conventions and flow solution as input. The user has a number of solution method options. The Third-Order TVD Method and Method of Characteristics were used to solve advection terms and are outlined here. The implicit finite-difference method was used to solve for dispersion and is also outlined here.

The third-order total variation diminishing method (TVD) makes use of third-order polynomial interpolation of nodal concentrations at the previous transport time step with an upstream weighting to determine interface concentrations at the current transport time step. Numerical oscillation can be an issue where sharp concentration gradients are present. A universal flux limiter is implemented to ensure computational monotonicity after interface concentrations are interpolated. Local monotoncity is assessed by comparing normalized concentrations at interfaces and adjacent nodes, with the expectation that a trend of consistent increasing or decreasing concentration should occur. If local monotonicity does not hold the interface concentration is set equal to the nearest upstream nodal concentration (Zhang & Wang 1999). This procedure is repeated for each finite difference cell in the domain. The TVD method is mass-conservative and implements mitigative measures for numerical oscillation, making it a viable option for advection-dominated problems.

The Method of Characteristics (MOC) is a Lagrangian particle tracking method for simulating advection. At the beginning of a simulation a specified number of particles are distributed throughout the domain. These particles are assigned concentrations based on initial conditions in the grid cells within-which they are positioned. Particles are tracked as they migrate according to the flow simulation results. At the end of each transport step the concentration in each cell (due to advection alone) is taken to be the average of that of the particles located within the cell. This concentration is then used to compute changes in concentration due to dispersion and sources/sinks with a finite difference method. After computation of new concentrations for all cells, new concentrations are assigned to particles and the next transport time

step begins. The MOC is effective for advection-dominated systems because numerical dispersion is eliminated. However the particle tracking methods can lead to localized mass balance errors. Solutions tend to be "rough" in appearance and require interpretation.

The implicit finite difference method was used to simulate solute dispersion and sources/sinks. Hydrodynamic dispersion is represented by a 19-component tensor, accounting for longitudinal and transverse dispersive fluxes into and out of a cell at the six boundaries. A single equation accounts for fluxes associated with external sources and sinks at each cell. The result is a matrix of equations of form $AC^{n+1} = b$. Here A is a component matrix containing 19 diagonals for dispersion terms as well as the source/sink term, C^{n+1} is the concentration at the next transport step, and b is a vector containing known quantities including concentration at the previous time step, cell dimensions, and sources with assigned concentrations and flow rates. Refer to Zheng & Wang (1999) for a complete list of components and equations.

4.2.3 Numerical representation of an injection well and pressure pulsing

Both two- and three-dimensional models involved a vertical series of cells used to simulate an injection well where water containing a prescribed concentration of solute was being injected into the formation under pressure supplied by a pump. Well hydraulics were simulated using the "High K_v in the Well Block" approach documented by Neville & Tonkin (2004). Cells representing the well were assigned a vertical conductivity based on Hagen-Poiseuille Pipe-Flow theory (Reilly et al 1989).

$$K_{pipe} = \frac{pgr_w^2}{8\mu} \quad \textbf{(2)}$$

Where p is the density of the fluid, g is acceleration due to gravity, r_w is the well radius, and μ is viscosity of the fluid. For a well radius of 2.5cm (equal to that of the injection well at CFB Borden) Equation 2 gives a vertical hydraulic conductivity of 780 m/s. A quality control check was conducted frequently to ascertain that head was uniform at any given time throughout the simulated well bore.

Injection with pressure pulsing was represented in all models using a general-head boundary condition (GHB). Unlike constant-head boundary conditions, a GHB can be toggled off and the cell allowed to respond fully to its surroundings. The GHB has a design purpose of representing flow between

the model domain and a distant constant-head source/sink. Modflow assigns conductance to be the constant of proportionality that dictates the rate at which flow between the source and cell is allowed to occur towards equilibrium (Figure 4.2). It can be determined from the hydraulic conductivity and spatial dimensions of the pathway from domain to source.

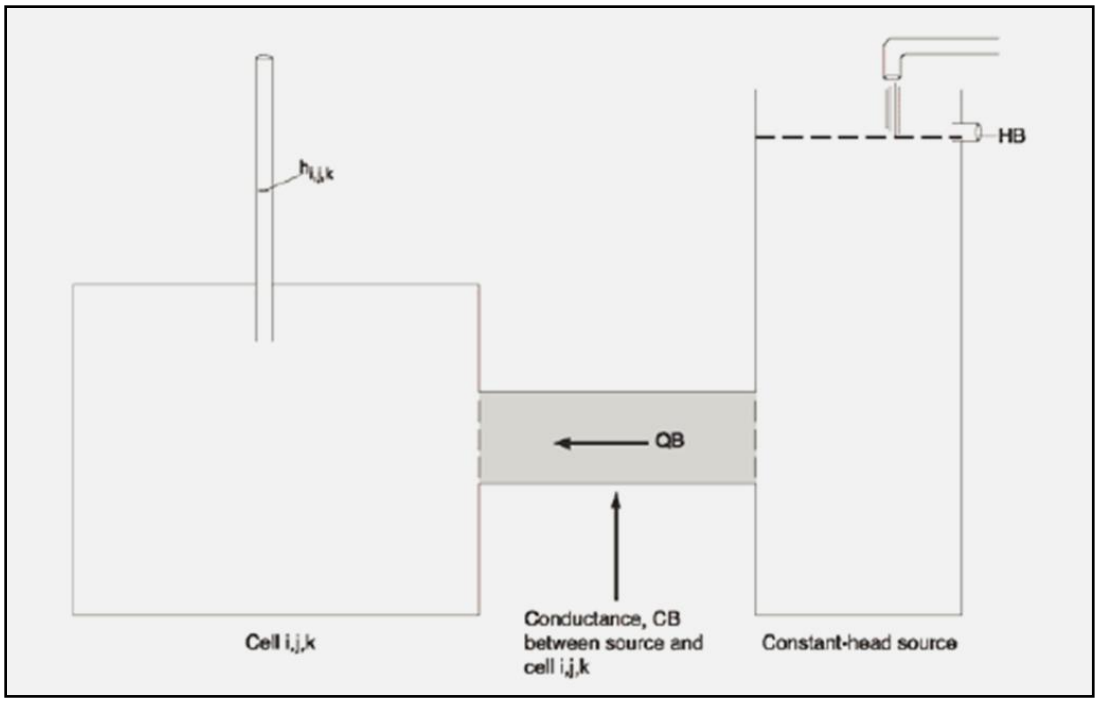

Figure 4.2 – Diagram illustrating the general-head boundary function used by Modflow (Harbaugh 2005)

For the case of a pump supplying pressurized water down a borehole the resistance to flow would be very low. A conductance of 780 m/s was used, representing the conductivity of the borehole upstream of the well screen. Results were monitored to ensure that a near-instantaneous response to assigned boundary pressure was simulated at the borehole cells.

Pressure pulsing was simulated by assigning a GHB pressure time series that was representative of the expected pressure signal downstream of the Sidewinder tool (Figure 4.3). This was determined by observation of an analogue pressure gauge downstream of the tool during operation, and consideration for the physical nature of the tool. A repeating sequence of five stress periods was used as follows:

Stress Period #1: Hydraulic head in GHB cells was assigned as H_{steady}. This corresponds to the period when the Sidewinder tool is in open position and the initial release of accumulated pressure has

dissipated. It represents the head supplied by the pump and is equivalent to the average pressure over a full pulsing cycle once the system has reached a quasi steady-state.

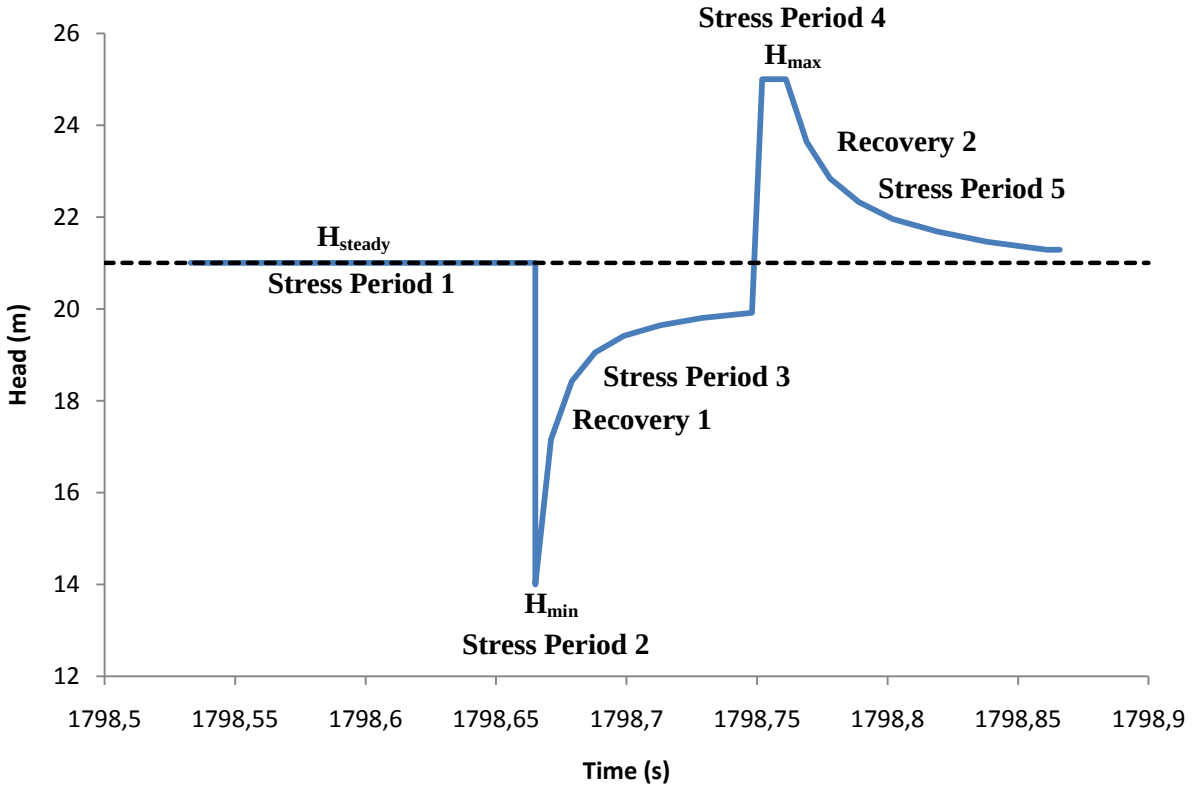

Figure 4.3 – Representation of the hydraulic head signal along the injection well screen downstream of a Sidewinder tool used for numerical modeling

Stress Period #2: Hydraulic head is briefly assigned as H_{min}. This corresponds to the brief moment when the Sidewinder tool enters the closed position and pressure in the well is equivalent to the column of water downstream of the tool. The duration of this stress period was set to 0.0001 s for all numerical experiments.

Stress Period #3: The GHB condition is toggled off for the duration of this stress period. This corresponds to the Sidewinder tool being in the closed position. The resulting pressure redistribution includes a rapid recovery at cells representing the injection well. The plateau pressure approached during this period is somewhat lower than H_{steady}.

Stress Period #4: Hydraulic head in GHB cells is assigned H_{max}. This corresponds to the release of accumulated pressurised water when the Sidewinder tool returns to open position. The duration of this

period is assigned based on the requirement to maintain an average cycle injection pressure of H_{steady} at late simulation time when the system has approached a quasi steady-state. The magnitude of H_{max} is a function of H_{steady} and H_{min} (Equation 3). Field experience has indicated that the magnitude of the rise to H_{max} from H_{steady} is approximately half the magnitude of the drop from H_{steady} to H_{min} (equation 3).

$$H_{max} = H_{steady} + {}^{1}/_{2}\,(H_{steady} - H_{\min}) \quad \textbf{(3)}$$

Stress Period #5: The GHB condition is toggled off for the duration of this stress period. This corresponds to the Sidewinder tool in the open position, where pressure is recovering to H_{steady} from H_{max}.

There are a few discrepancies between the approach used to model pressure pulsing and the true pressure fluctuations that would occur downstream of the Sidewinder tool. First, the model assumes that the drop to H_{min} and the rise to H_{max} are instantaneous. While the Sidewinder tool is designed to maximize the rate at which these changes take place, they would not be instantaneous. Physical parts must move to open and close the apertures that control flow through the tool. Second, the recovery from H_{max} to H_{steady} (Stress Period 5) in the model does not account for the presence of a pump supplying H_{steady} upstream. In reality this would entail a longer recovery period. The model allows for the possibility of artificial backflow at the transition from Stress Period 5 to Stress Period 1 if the recovery does not reach H_{steady} in the allotted time. Briefly sustaining H_{max} acts to compensate for potential gradient reversal, and for the recovery from H_{max} being too rapid. The onset of H_{min} requires that water be artificially removed from the model, resulting in artificial backflow to the well if formation pressure exceeds borehole pressure. In reality this backflow is prevented by the physical seal interrupting flow at the well head, and Recovery 1 is near-instantaneous.

The value of H_{min} was not confirmed by direct observation. Very sophisticated pressure-monitoring equipment would be required to capture this value because it is an instantaneous event followed by a rapid (less than 0.1s) recovery to a higher pressure.

A constant concentration boundary condition superimposed on injection well cells was used to simulate solute mixed into the water exiting the injection well at a prescribed concentration. At very early time it is possible that backflow to the well during Recovery 1 may contain water at a lower concentration than the boundary prescribes. This has the potential to artificially accelerate early-time advection. An assessment of artificial early-time concentration augmentation was performed.

4.2.4 Two-dimensional Model

Two-Dimensional (2D) modeling presented the opportunity to perform a preliminary, in-depth investigation of pressure pulsing as an injection mechanism. A series of simulations were conducted to assess the effect of varying different pulsing parameters on resulting flow and transport in the medium. A series of different porous medium structures were used as well.

The 2D model domain had a representative length of 100 m and height of 10 m, discretized into 141 columns and 40 layers (Figure 4.4). The simulated injection well was assigned to four cells at the centre of column 1 (layers 19, 20, 21, 22) at one edge of the domain. Layers were all 0.25 m high. Column widths were smallest near the injection well and grew progressively larger further away, as follows:

- 0.05 m Columns 1 & 2 (0 to 0.1 m)
- 0.1 m Columns 3,4,5,6 (0.1 to 0.5 m)
- 0.125 m Columns 7,8,9,10 (0.5 to 1 m)
- 0.25 m 1 to 20 m
- 1.0 m 20 to 50 m
- 2.0 m 50 to 100 m

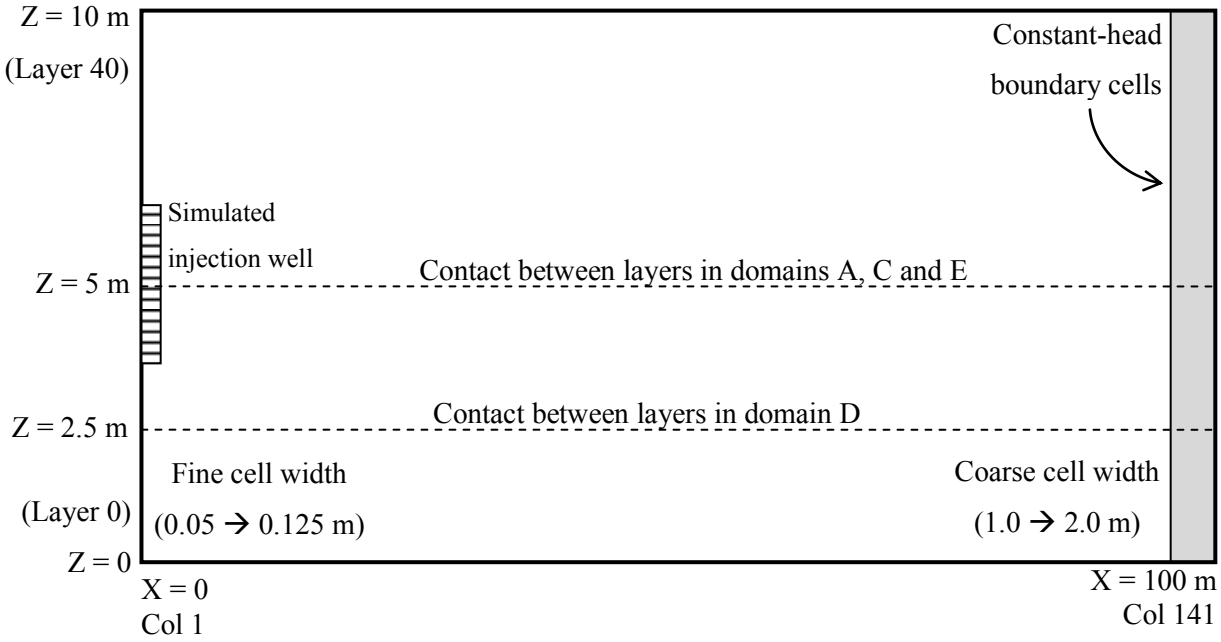

Figure 4.4 – 2D model domain sketch (not to scale)

Porosity was set at 0.33 and longitudinal dispersivity was set at 0.1 m throughout the domain for all simulations. Five different hydraulic conductivity fields were created to represent different hydrostratigraphic settings, as follows:

Domain A: Two distinct hydrostratigraphic layers splitting the model domain in symmetric halves. Injection well intersects both layers. Horizontal hydraulic conductivities are 4E-4 m/s and 9E-4 m/s for the top and bottom layers respectively, giving a domain geometric mean of 6E-4 m/s

Domain B: Homogeneous, K_x = 6E-4 m/s

Domain C: Identical to Domain A except the difference in hydraulic conductivity is greater. Horizontal hydraulic conductivities are 2E-4 and 1.8E-3 m/s for the top and bottom layers respectively, giving a domain geometric mean of 6E-4 m/s.

Domain D: High-hydraulic-conductivity aquifer (6E-4 m/s) overlying a low-hydraulic-conductivity aquitard (5E-6 m/s). Injection screen is within the aquifer only.

Domain E: Identical to domain A except both layers have lower hydraulic conductivities. Horizontal hydraulic conductivities are 2E-5 and 6E-5 m/s for the top and bottom layers respectively, giving a domain geometric mean of 3.5E-5 m/s. Hydraulic conductivity in this domain is similar to the CFB Borden site (refer to section 3.1).

A simulation time of 30 minutes was used for all runs. The number of stress periods varied depending on whether pulsing was being simulated, and the frequency of pulsing (Table 4.1)

Initial heads were set to 12.0 m (referenced to bottom of model domain) throughout the model domain. All cells along column 141, at the domain edge opposing the simulated injection well, were assigned as constant head boundaries with a sustained head of 12.0 m. This set-up simulated injection into an infinitely laterally extensive confined aquifer.

An injection concentration of 1.0 mg/L was assigned throughout all simulations. An initial concentration of zero was assigned throughout the domain for all simulations. Solute transport was simulated with the TVD method.

Eighteen unique simulations were conducted (Table 4.1). A Frequency of 3Hz pulsing in Domain A was taken to be a baseline case. Four different pulsing schemes were used in Domain A, including 2Hz, 3Hz, 4Hz, and higher amplitude pulsing. 3Hz pulsing was used in all four domains. 2Hz, 4Hz, and High Amplitude pulsing were subsequently used in domain C. Conventional injection simulations were paired with pulsing simulations, where H_{steady} from the pulsing simulation was taken to be the injection pressure for the conventional injection.

Pulsing parameters were selected to simulate a well-head located 2 m above the ambient potentiometric surface of 12.0 m. Therefore H_{min} was assigned as 14.0 m for all pulsing simulations. H_{steady} of 21 m is equivalent to pump-supplied hydraulic head of 7.0 m; H_{max} of 25 m is equivalent to release of accumulated pressure at 4.0 m in addition to the pump-supplied pressure. High amplitude pulsing was simulated under the assumption that higher pump-supplied pressure would be accompanied by a greater pressure release after accumulation (rise to H_{max} of 8.0 m relative to H_{Steady} for high-amplitude pulsing).

Post processing was conducted using a combination of proprietary and public domain software. A set of programs were written to extract head and concentration time series at cells of interest from Modflow and MT3D binary output files. Extracted data were used to generate head vs. time profiles and solute breakthrough curves. Cross-section data were extracted from output files using the PostMT3D|Modflow (PM) program supplied in the MT3D distribution (documented by Zheng & Wang 2005). Surfer 7 (Golden Software 1999) was used to generate cross section plots from data files produced by PM. The Zone Budget program supplied with the Modflow 2005 software package was used to calculate flow rates between zones of interest. A series of batch files and scripts were written to automate the post-processing sequence.

Table 4.1 – Summary of flow and pulsing parameters used for the 2D model parametric investigation. Shaded values emphasize differences with respect to the baseline pulsing case.

Model Run	K_1* (m/s)	K_2* (m/s)	H_{max}◊ (m)	H_{steady}◊ (m)	Pulsing frequency (cycles/sec)	# Stress Periods
1. Baseline: 3Hz pulsing in Domain A	4E-4	9E-4	25	21	3	27,000
2. 3Hz pulsing in Domain B	6E-4	6E-4	25	21	3	27,000
3. 3Hz pulsing in Domain C	2E-4	1.8E-3	25	21	3	27,000
4. 3Hz pulsing in Domain D	6E-4	5E-6	25	21	3	27,000
5. 4Hz pulsing in Domain A	4E-4	9E-4	25	21	4	36,000
6. 2Hz pulsing in Domain A	4E-4	9E-4	25	21	2	18,000
7. High-Amplitude 3Hz pulsing in Domain A	4E-4	9E-4	38	30	3	27,000
8. No Pulsing Domain A	4E-4	9E-4	n/a	21	n/a	1
9. No Pulsing Domain B	6E-4	6E-4	n/a	21	n/a	1
10. No Pulsing Domain C	2E-4	1.8E-3	n/a	21	n/a	1
11. No Pulsing Domain D	6E-4	5E-6	n/a	21	n/a	1
12. No pulsing high Injection pressure Domain A	4E-4	9E-4	n/a	30	n/a	1
13. High-Amplitude 3Hz pulsing in Domain C	2E-4	1.8E-3	38	30	3	27,000
14. No pulsing high injection pressure Domain C	2E-4	1.8E-3	n/a	30	n/a	1
15. 4Hz pulsing in Domain C	2E-4	1.8E-3	25	21	4	36,000
16. 2Hz pulsing in Domain C	2E-4	1.8E-3	25	21	2	18,000
17. 3Hz pulsing in Domain E	2E-5	6E-5	25	21	3	27,000
18. No Pulsing in Domain E	2E-5	6E-5	n/a	21	n/a	1

*K_1 overlies K_2, elevation varies

◊ Head values referenced to bottom of model domain

Hydraulic head data were extracted at cells along two horizontal and one vertical line segments (Figure 4.5). Concentration data were extracted along three vertical line segments (Figure 4.5). Node-to-node distances from the injection well to cells of interest were often used for analysis and discussion purposes, although these do not have a direct physical meaning for a two-dimensional model. Zone Budget zones were assigned such that cells representing the injection well, and the upper and lower hydrostratigraphic layers were grouped together. This allowed computation of flow into the formation from the injection well and across the contact between the two hydrostratigraphic layers.

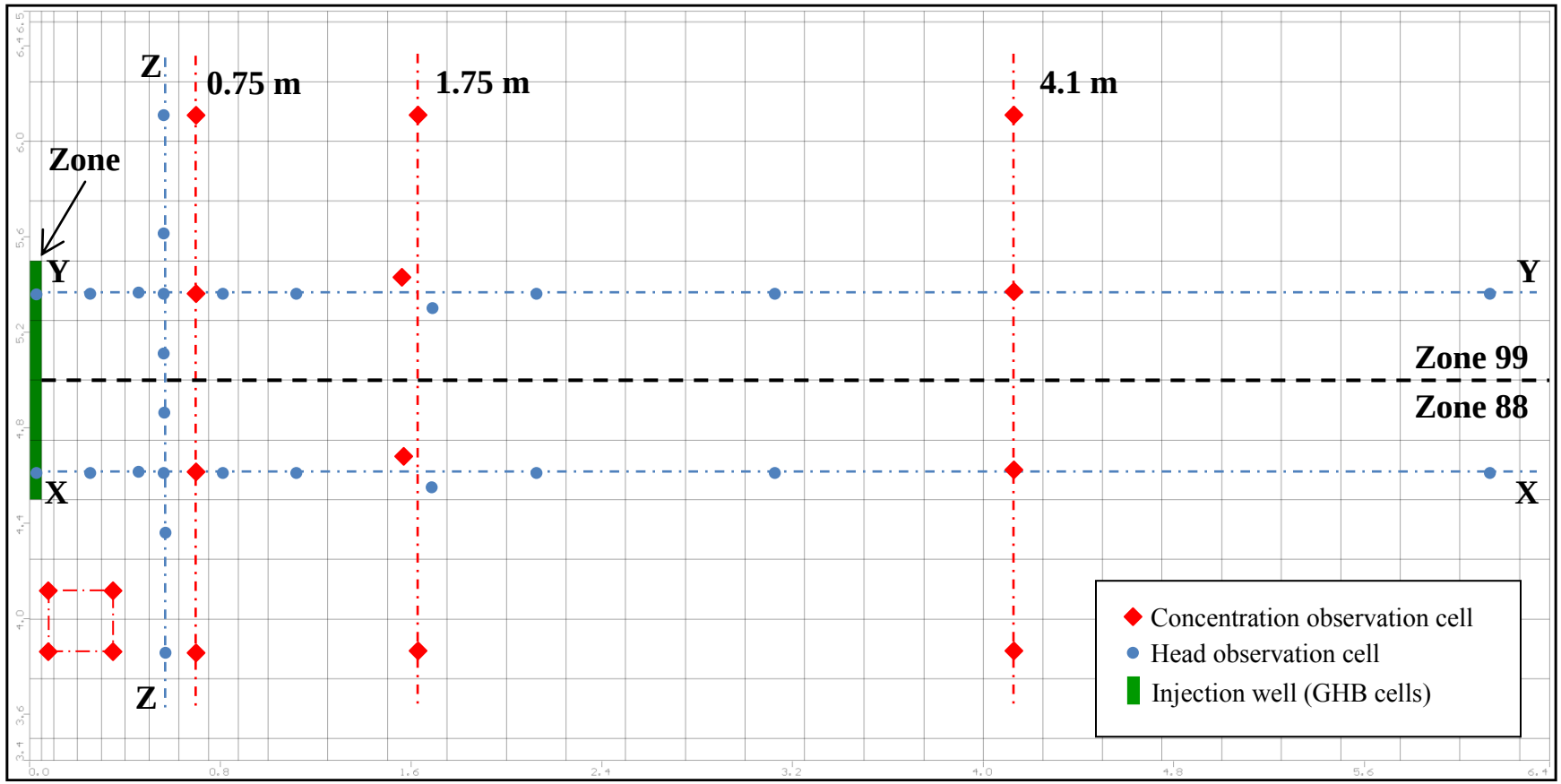

Figure 4.5 – 2D model domain depicting head and concentration observation cells.

Not shown: head observation point at column 140 along segment XX'

4.2.5 Three-Dimensional Model

Three-Dimensional (3D) modeling presented the opportunity to scale up the two-dimensional model and investigate the effects pressure pulsing may have had at a field-scale that were not detectable in field data. Simulating pressure pulsing in three dimensions was resource-intensive, requiring multiple days and very large amounts of hard disk space.

The 3D model domain had representative dimensions of length x width x height of 32.375 x 32.375 x 10 m. Discretization included 58 columns, 58 rows, and 38. The simulated injection well was assigned to eight cells at the centre of Column/Row 58 at one corner of the domain, at a height of 1.125 to 2.125 m above the model base. Layers were smallest at the base of the model and larger further upwards away from the injection well:

- 0.125 m layers 38 to 12 (0 to 3.25 m above model base)
- 0.25 m layers 11 to 6 (3.25 to 5.0 m above model base)
- 1.0 m layers to 1 (5.0 to 10.0 m above model base)

Column and row widths were set up symmetrically such that they were smallest near the injection well and grew progressively larger further away:

- 0.025 m Row/Column 58 (32.375 to 32.35 m)
- 0.1 m Row/Column 57 (32.35 to 32.25 m)
- 0.125 m Rows/Columns 56 to 31 (32.25 to 29.0 m)
- 1.0 m Rows/Columns 30 to 1 (29.0 to 0 m)

Two stages of modeling were conducted in the 3D domain (summarized in Table 4.2). The first stage was an iterative medium parameter estimation process to produce flow and transport behavior similar to the CFB Borden site. This required a multi-layer hydraulic conductivity field and multiple trial runs to assign hydraulic conductivity values that approached a match between hydraulic and solute transport measurements at the CFB Borden site and those produced by simulation. Only conventional injection was used. The second stage introduced pressure pulsing. Two pressure pulsing simulations were conducted. The first was a simulation of a pressure pulsing injection in a medium with properties similar to those at the CFB Borden field site. The second was only run to reach quasi steady-state medium pressurization, and involved a domain with higher overall hydraulic conductivity than the Borden site.

Table 4.2 – Summary of 3D model simulation sequence

Stage	Simulation ID	Domain ID	Pulsing	Remarks
1	3D-C	Borden	No	Iterative flow and transport data-matching
2	3D-P1	Borden	Yes	Complete Borden pressure pulsing injection simulation
	3D-P2	Modified Borden	Yes	Run to quasi-steady-state. Higher K than Borden

Porosity was set at 0.33 throughout the domain and longitudinal dispersivity was set at 0.1 m throughout the domain for all simulations. Initial heads were set to 10.0 m (referenced to bottom of model domain) throughout the model domain. All cells along column 1 and row 1, at the domain edges opposing the simulated injection well, were assigned as constant hydraulic head boundaries with a sustained value of 10.0 m. This model design simulated injection into a quartered, infinitely laterally extensive confined aquifer. Measurements of the injection flow rate must be scaled by a multiple of four to account for the no-flow boundaries imposed to quarter the model domain.

A simulation time of 3½ hours (210 min, 12,600 s) was used for conventional runs during Stage 1. This incorporated one stress period divided into 50 time steps. A simulation time of 2½ hours (150 min, 9,000 s) was used for the Stage 2 pulsing injection (simulation 3D-2). This incorporated 135,000 stress periods, with five stress periods simulating each complete pulsing cycle (refer to section 4.2.3). Time to quasi-steady-state was determined based on flow results for simulation 3D-2 and used to determine total simulation time for simulation 3D-3.

An injection concentration of 1.0 mg/L was assigned throughout all simulations. Initial concentrations of zero were assigned throughout the domain for all simulations. Solute transport was simulated by method of characteristics for advection and implicit finite difference for dispersion and sources/sinks.

Pressure pulsing was simulated by imposing a general head boundary condition on injection well cells. A 3Hz frequency was used, whereby a complete pulsing cycle occurs in 0.33 s. H_{min}, H_{max}, and H_{steady} were assigned 11.0, 22.5, and 18.5 m respectively. This represented a well head 1.0 m above the top of the ambient potentiometric surface, additional pump-supplied hydraulic head of 7.5 m, and accumulation of an additional 4.0 m hydraulic head associated with Sidewinder tool operation. These parameters are nearly identical to those used for 2D model simulation 1 (refer to section 4.2.4).

Pressure pulsing simulation was conducted using a processing stream that accommodated disk space requirements. Flow and transport modeling were conducted in sequence for a subset of the stress periods. This prevented flow output files required as transport and Zone Budget input (.FLO and .BGT files) from growing to unmanageable file sizes. At the end of each subset run final head and concentration values were written into input files as initial conditions for the subsequent run.

Post processing was conducted using a combination of proprietary and public domain software. A set of programs were written to extract head and concentration time series at cells of interest from Modflow and MT3D binary output files. Extracted data were used to generate head vs. time profiles and solute breakthrough curves. Cross section data were extracted from output files using the PostMT3D|Modflow (PM) program supplied in the MT3D distribution (documented by Zheng & Wang 1999). Surfer 7 (Golden Software 1999) was used to generate cross section plots from data files produced by PM. The Zone Budget program supplied with the Modflow 2005 software package was used to calculate flow rates between zones of interest. A series of batch files and scripts were written to automate the post-processing sequence. During the pressure pulsing simulation post-processing was conducted following each subset run.

Hydraulic head and concentration data were extracted at cells representative of well ports at the CFB Borden site. Node-to-node distances from the injection well were used to identify cells corresponding to multilevel sampling ports and hydraulic monitoring wells (

Table **4.3**). Lateral and vertical nodal distances to monitoring points in the model were all within a few centimeters of the distances determined by land survey at the CFB Borden site. Head values were also saved at a series of cells closer to the injection well, and a pair of cells adjacent to constant-head boundaries.

Zone Budget zones were assigned such that cells representing the injection well and each interpreted hydrostratigraphic layer were grouped. This allowed computation of flow into the formation from the injection well and across the contacts between layers.

Table 4.3 – 3D model representation of the CFB Borden monitoring network

Well Port	Relative distances at CFB Borden (horizontal, vertical*)	3D Model coordinates (Layers, Row, Column)	Representative 3D model distances (horizontal, vertical meters)
IWB	0, 0	22 – 29, 58, 58	0, 0
HWB1	1.04, -0.50	25, 53, 53	1.05, -0.44
HWB2	2.02, 0.03	20, 40, 40	2.09, 0.19
MLB1-1	1.05, 0.74	16, 53, 53	1.05, 0.69
MLB1-2	1.05, 0.24	20, 53, 53	1.05, 0.19
MLB1-3	1.05, -0.26	24, 53, 53	1.05, -0.31
MLB1-4	1.05, -0.76	28, 53, 53	1.05, -0.81
MLB1-5	1.05, -1.26	32, 53, 53	1.05, -1.31
MLB1-6	1.05, -1.76	36, 53, 53	1.05, -1.81

*Vertical distances reference to top of injection well screen (negative values indicate below)

Chapter 5 – Field Injection Results and Discussion

Data collected from the two field injection sites are summarized here. Comparisons are made between data collected for pairs of pressure pulsing and conventional injections. Analysis is focussed on differences related to pressurization of the formation and tracer breakthrough. Additional data is presented in Appendices B and C.

5.1 CFB Borden Injections

Four site-scale injections were conducted at CFB Borden (Table 5.1).

Table 5.1 – Parameters of the four CFB Borden injections

	Injection B-C1	**Injection B-P1**	**Injection B-C2**	**Injection B-P2**
Total Injected Volume	7475 L (1975 gallons)	7500 L (1980 gallons)	7100 L (1875 gallons)	7050 L (1860 gallons)
Duration	3h 20min	2h 21min	3h 32min	3h 17min
Tracer	Bromide	Rhodamine WT	Sulforhodamine B	Bromide
Mean injection concentration*	340 mg/L	50.7 ppb	50.9 ppb	384 mg/L
Pressure Pulsing? (Frequency)	NO	YES (3 Hz)	No	YES (3 Hz)

*Mean value of all samples collected from all tanks

5.1.1 Injection Hydraulics

Injections B-C1 and B-P1 constituted a conventional and pressure pulsing injection pair with a target flow rate of 51 L/min (13.5 gpm). A trend of increasing pressure was observed at the well head for Injection B-C1 (Figure 5.1). The pump was throttled down on three occasions (one not shown on Figure 5.1) to keep pressure values within the gauge range (gauge maximum of 100 kPa). At late injection times the well-head pressure was building up too quickly for throttling down the pump to be a pragmatic mitigation measure. Stepped decreases in flow rate correspond with pump down-throttling events. In contrast to Injection B-C1, during Injection B-P1 the target flow rate was sustained throughout and well-head pressure did not build up. The pressure gauge immediately upstream of the Sidewinder tool appeared

to reach peak pressures ranging 60 to 80 psi, minimum pressures of 0 psi, and steady pressures around 15 psi. The downstream gauge appeared to reach peak pressures of 15 to 20 psi, minimum pressures of 0 psi, and steady pressures around 12 psi.

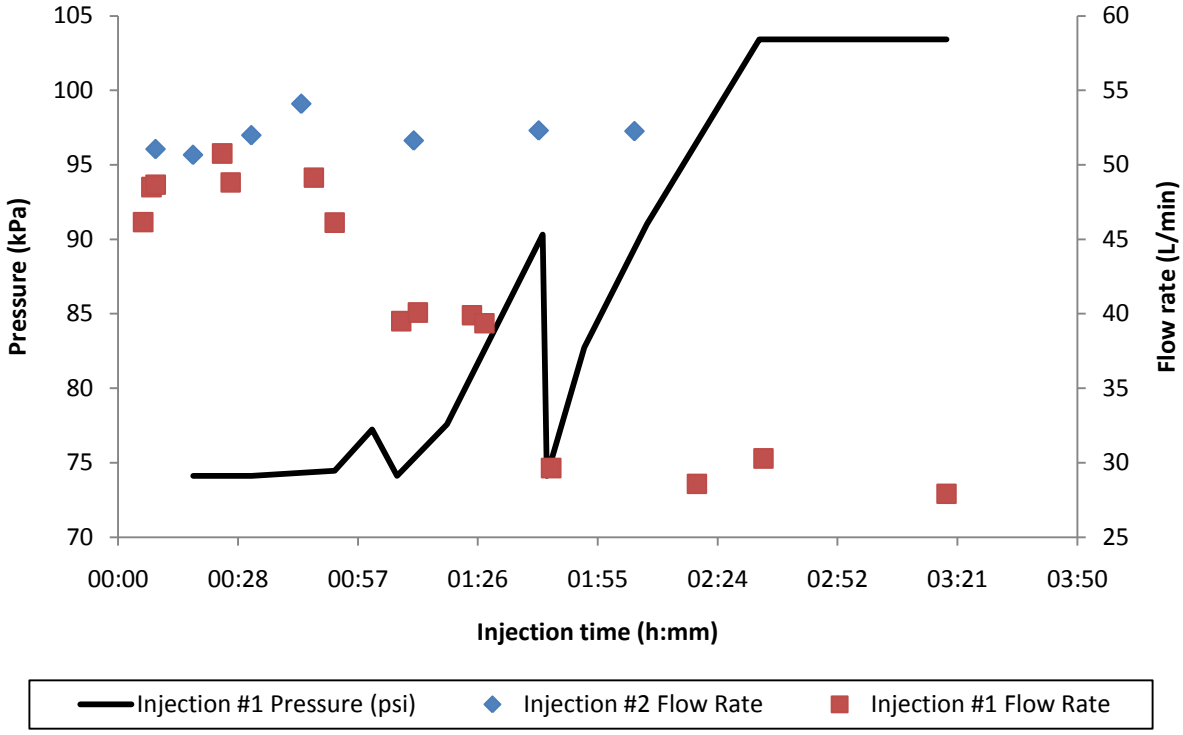

Figure 5.1 – Injection hydraulics for CFB Borden injections B-C1 and B-P1

Injections #3 and 4 constituted a conventional and pressure pulsing injection pair with a target flow rate of 34 L/min (9.0 GPM). Trends of increasing pressure and decreasing flow rate were observed at the well head for Injection B-C2 (Figure 5.2). During Injection B-P2 Sidewinder pressure gauge fluctuations were recorded using a hand-held video camera. Frame-by-frame inspection of gauge needle fluctuations allowed more thorough inspection of gauge needle movements than visual observation. The upstream gauge reached peak pressures ranging 60 to 70 psi, minimum pressures of 0 psi, and steady pressures of 10 to 11 psi. The downstream gauge reached peak maximum pressures of 12 to 16 psi, minimum pressures of 0 to 5 psi, and steady pressures of 10 to 11 psi. Maximum, minimum, and steady pressures were consistent throughout the injection.

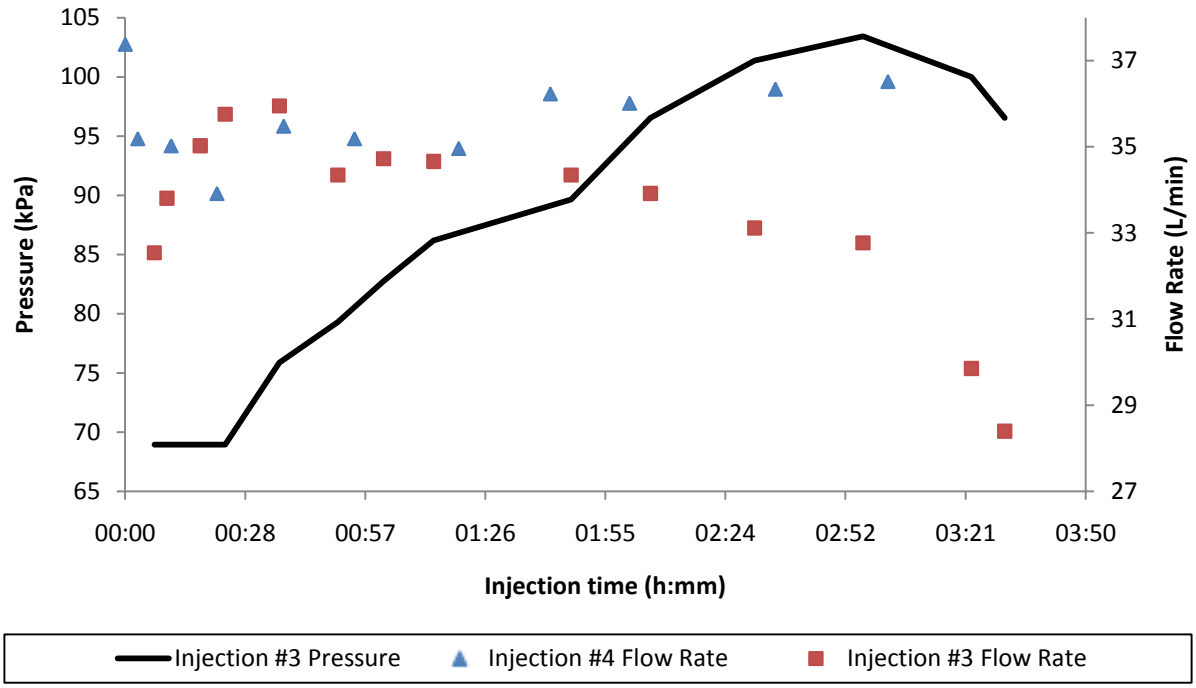

Figure 5.2 – Injection hydraulics for CFB Borden injections B-C2 and B-P2

5.1.2 Formation Pressurization

Formation pressurization was computed by subtracting the ambient water level prior to injection from water levels measured during the injection. This is similar to calculating drawdown for a pumping test, except positive values indicate pressurization as opposed to de-pressurization. Formation pressurization time series were created for monitoring wells HWB1 (Figure 5.3) and HWB2 (Refer to Appendix A).

Stepped decreases in pressurization for Injection B-C1 correspond with pump down-throttling events. The spike in down-hole pressure transducer data occurring mid-injection during injections #2 and 3 is a result of poor flow continuity arising during a switch of the water source from one holding tank to another. Changes in slope during Injection B-C1 and 3 appear to correspond with low water levels in tanks and may reflect air intake. During Injection B-P2 pressure transducers were set to record at 0.5 s intervals, and as such data storage was filled to capacity with 30 minutes of injection time remaining.

Overall formation pressurization was similar for paired pulsing and conventional injections. For example, formation pressurization recorded at HWB1 for injections #3 and 4 (target injection flow rate of 35 L/min) was in the range of 1.0 to 1.1 m.

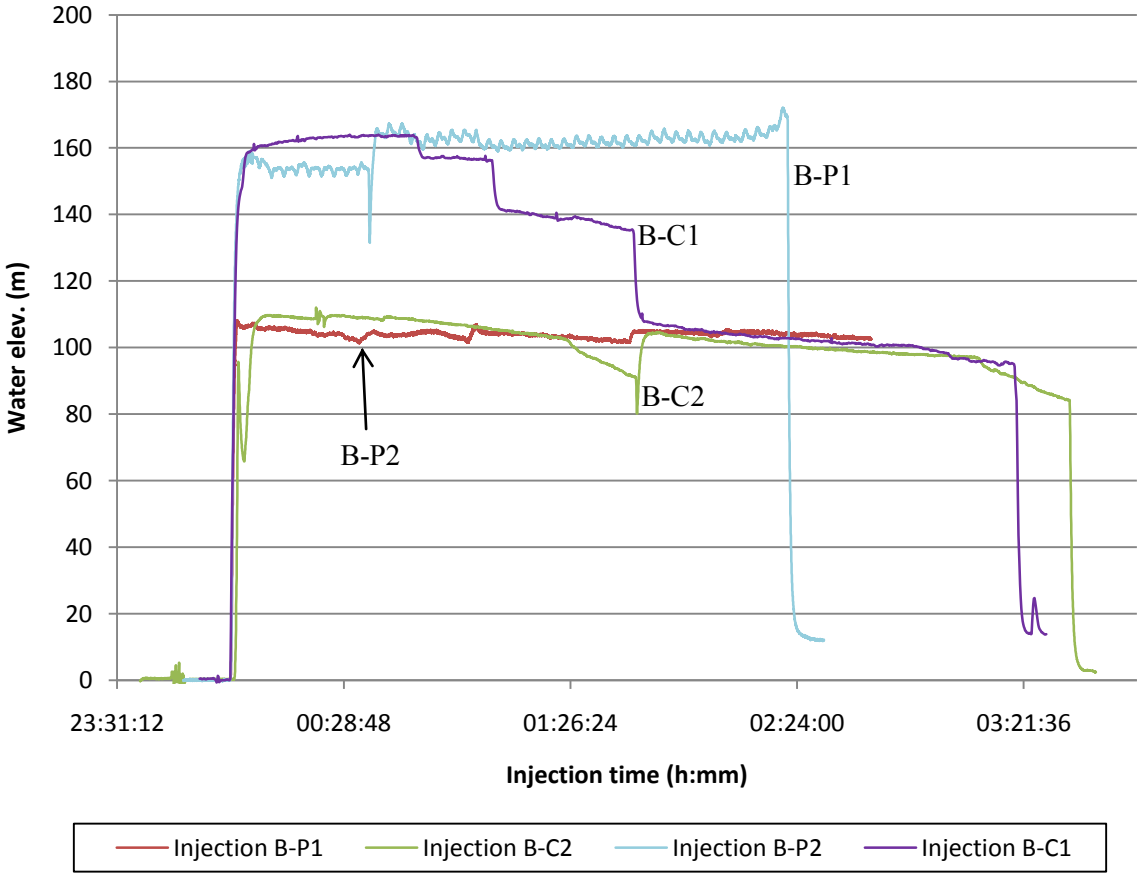

Figure 5.3 – Formation pressurization for all injections at CFB Borden as observed at HWB1. Refer to Appendix A for pressurization data at HWB2.

At late injection time both conventional injections recorded a trend of gradual pressure decrease in the formation. This was not the case for pulsing injections. It is possible that water elevation in the storage tanks was an influence. Lower water pressure upstream of the pump would translate into lower water pressure downstream of the pump. Slight pressure resurgence during Injection B-C2 after the spike marking the tank switch (injection time of approximately 1:45) suggests this. However water pressure monitoring at the well head (downstream of the pump) indicated a trend of pressure build-up for both conventional injections (refer to section 5.1.1). The combination of pressure build-up at the well head and decreasing formation pressure could be symptomatic of a growing well screen blockage. It appears that

both of these factors influenced formation pressurization over time for the conventional injections. Pressure pulsing appears to have alleviated well blockage.

Post-injection pressure for Injections #1 and 2 was around 0.15 m higher than pre-injection at both HWB1 and HWB2. Post-injection pressure returned to within 2 cm of pre-injection pressure for Injection B-C2. This is indicative of water mounding to accommodate the injected fluid. Injections #3 and #4 were conducted during the spring when the ambient water level was above natural ground surface at the site (a layer of coarse gravel 1 to 2 ft thick above ground surface acted as an access pad). Injections #1 and 2 were conducted during the fall when the natural water level was about 1.0 m below natural ground surface. During injections #3 and 4, water mounding reaching the surface would immediately dissipate because it would be allowed to flow freely. A water mound within the subsurface dissipates slowly after an injection, draining only laterally under the force of gravity (Payne et al 2008).

5.1.3 Solute Transport

Tracer breakthrough was observed at MLB1 ports 2, 3, 4, 5 and 6 for all injections. Initial tracer detection at port 2 occurred near the end of Injection B-C1 (Figure 5.4). Initial tracer detection at MLB1 port 1 was observed towards the end of injections #3 and 4 (Figure 5.5). No tracer concentrations above method detection limits were recorded for samples collected from any ports at MLB2 or MLB3 for any of the four injections.

RWT breakthrough curves exemplify incomplete two-step sigmodal shapes as described by Shiau et al (1993) (Figure 5.6). To isolate the low-sorption isomer the recorded plateau concentrations were treated as the injection concentration. This means, for example, that an arrival time for 50% of the injection concentration at a particular port would be taken to be the arrival time for 50% of the plateau concentration. The end result is a set of breakthrough curves with conservative solute transport behaviour.

Some SRB breakthrough curves appeared to take on a sub-injection concentration plateau form similar to those of RWT (Refer to Figure 5.5). However there is no documented laboratory evidence upon-which to explain this phenomenon. In fact, Kasanavia et al (1999) and Ghanem et al (2003) both documented conventional retarded breakthrough for SRB in column experiments. Hence no corrections were applied to the SRB breakthrough curves.

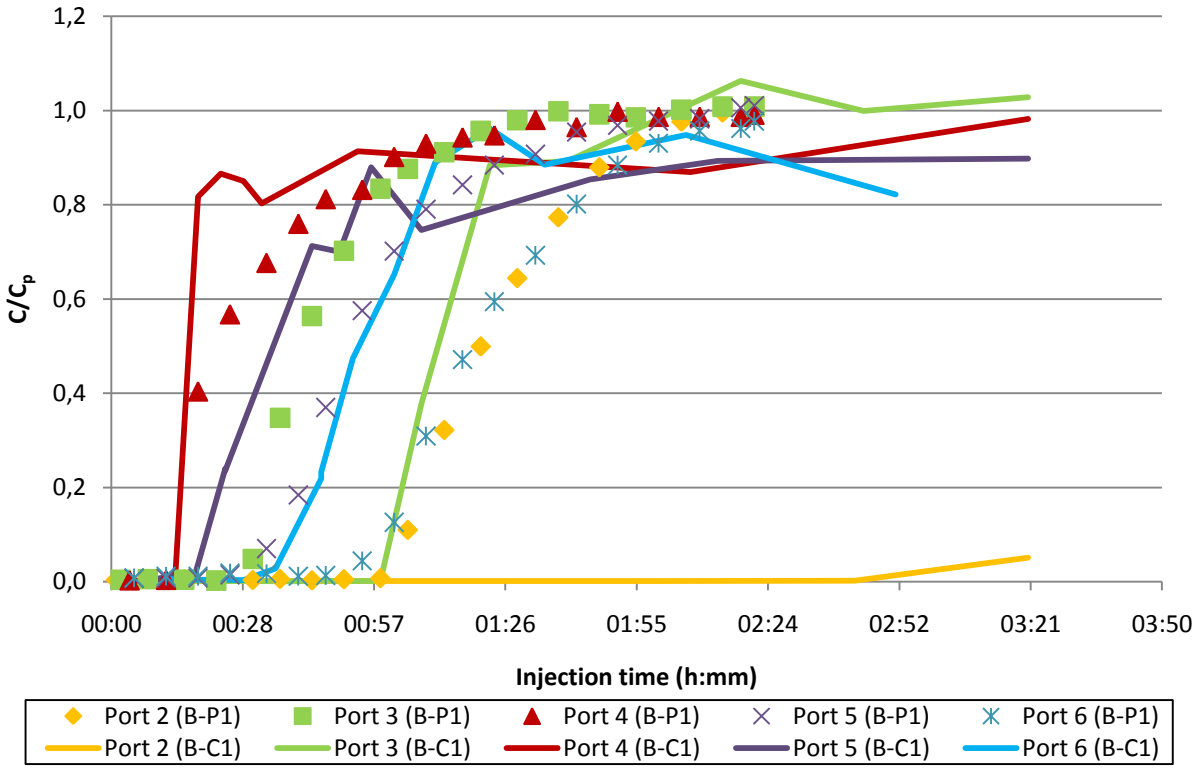

Figure 5.4 – Breakthrough curves for CFB Borden injections B-C1 and B-P1

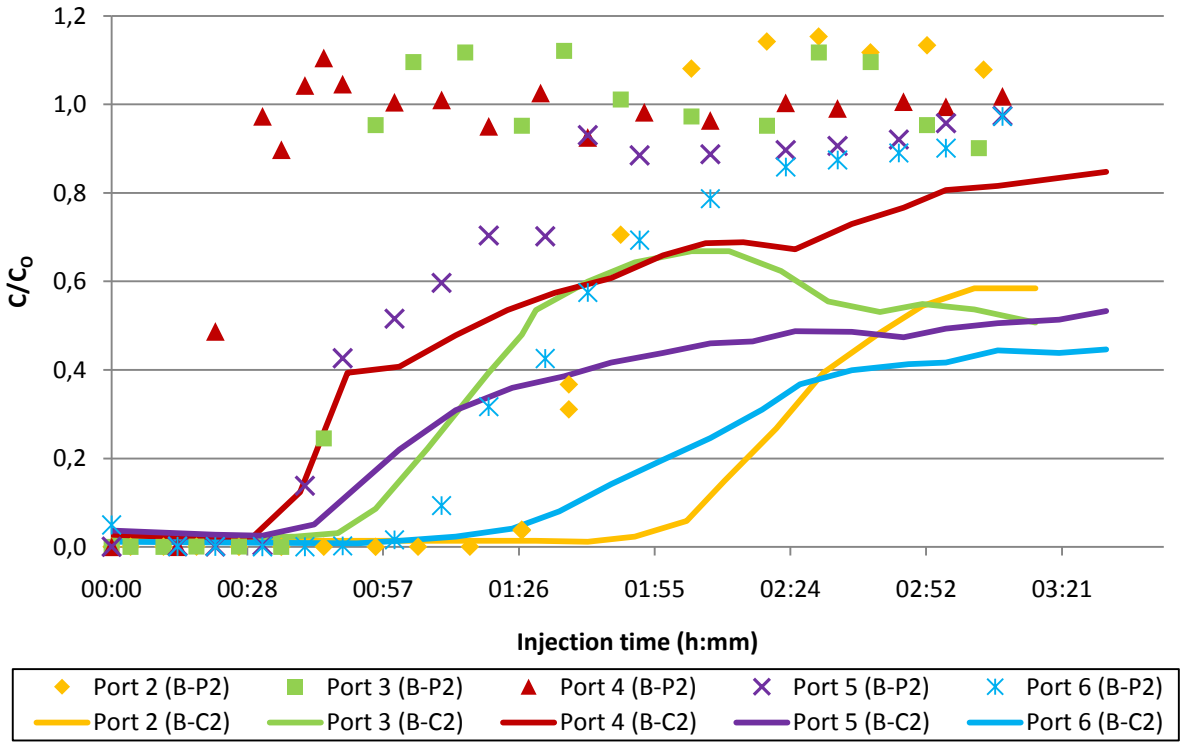

Figure 5.5 - Breakthrough curves for CFB Borden injections B-C2 and B-P2

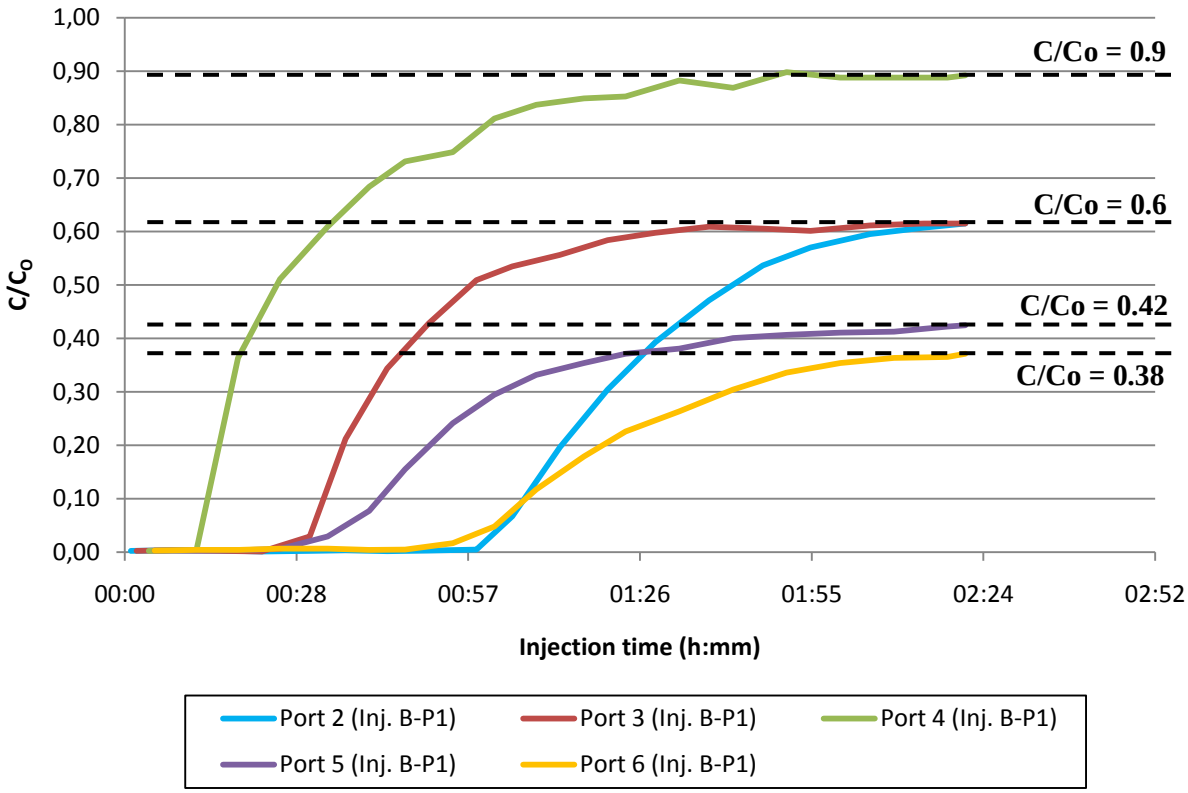

Figure 5.6 – Raw RWT breakthrough curves for CFB Borden injection B-P1 and interpreted plateau concentrations

The ideal set of tracer breakthrough curves would exemplify a tracer distribution as if the medium were perfectly homogeneous. This would include earliest arrival at MLB1 ports 3 and 4, which are approximately equal distances from the injection well. This would be followed by arrival (in order of earliest to latest arrival time) at ports 5, 3, 6, 2, and finally 1, based on distance from the well screen (Refer to section 3.1.2 for well screen and monitoring port locations).

Direct comparison of solute transport data among injections at CFB Borden was complicated by two issues that became apparent during data processing. First, Injection B-C1 appeared to have occurred during an intermediate stage of formation development. This resulted in tracer breakthrough that varied much more between MLB1 ports than the three other injections (as seen in Figure 5.7). Second, both fluorescent dye tracers (Injections B-P1 and B-C2) generated breakthrough curves that exemplified irregular sorption. The correction applied to RWT datasets did not entirely mitigate the effect of sorption on tracer arrival times.

Injection B-C1 displayed rapid breakthrough in the deeper half of the monitoring network with minimal dispersion. Injection B-P1 displayed a more ideal distribution of tracer than Injection B-C1. Dispersion may have been greater for Injection B-P1 than Injection B-C1, but sorption may also have played a role in the further delay between first arrival and advective arrival for Injection B-P1. When examining only low-concentration initial tracer arrival times, Injection B-C2 displayed a fairly ideal distribution of tracer (Figure 5.7), however it is difficult to compare this observation to Injection B-P2 due to the influence of sorption. Injection B-C2 first arrivals were followed by a relatively long delay to, and less ideal distribution of advective front arrivals. Injection B-P2 displayed a somewhat less ideal tracer distribution and less delay in advective front arrival than Injection B-P1. The impact of pressure pulsing on solute transport at the CFB Borden site was not clear due to the significant influence of sorption on fluorescent dye tracers. However it is noteworthy that the most ideal tracer distribution was recorded during injection B-P1, a pressure pulsing injection.

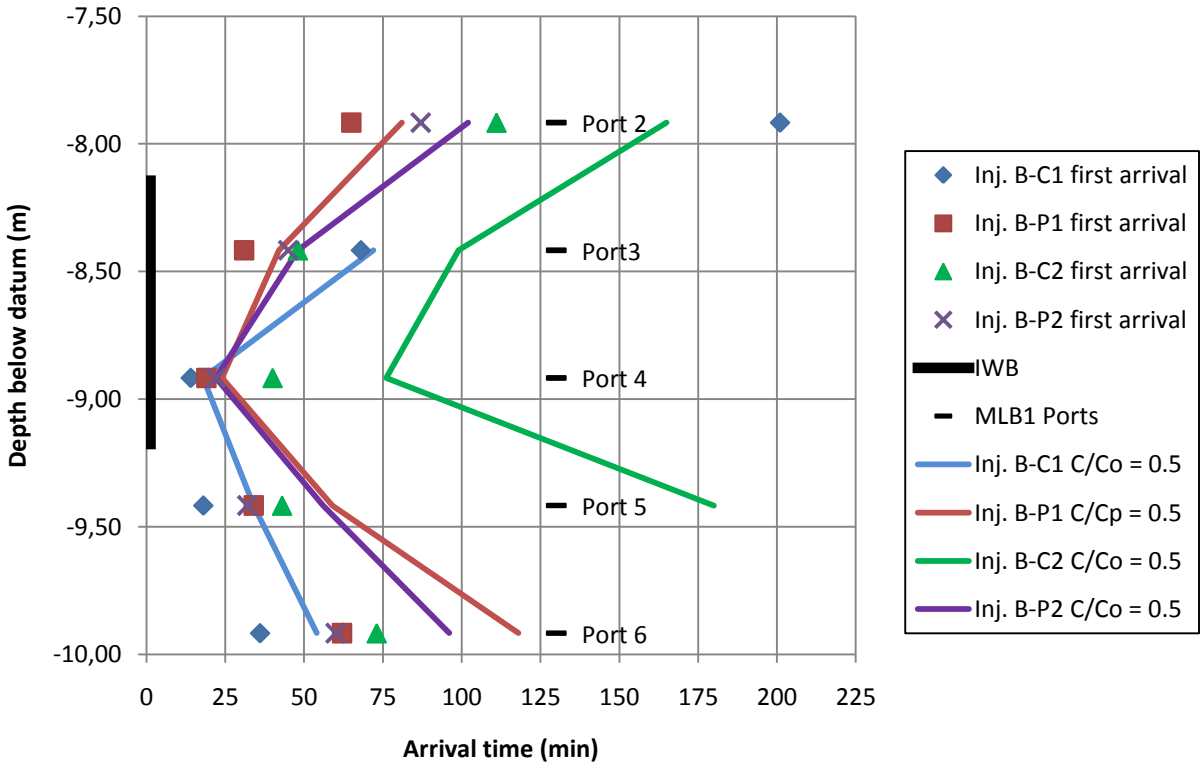

Figure 5.7 – First-detection and advective arrival times at MLB1 ports (1 m from IWB). MLB1 ports and IWB screened interval are identified for elevation reference. "First arrival" indicates first tracer detection above background levels. Times corresponding to C/Co = 0.5 are interpreted as advective front arrival. C/Cp refers to concentrations relative to the plateau concentration reached at that particular monitoring port for the RWT tracer

5.2 North Campus Injections

Three site-scale injections were conducted at the NCIS (Table 5.2).

Table 5.2 – Parameters of the four CFB Borden injections

	Injection NC-C1	**Injection NC-C2**	**Injection NC-P**
Total Injected Volume	3400 L (900 Gallons)	3390 L (900 Gallons)	3550 L (940 Gallons)
Duration	2h 49min	3h 18min	3h 20min
Approx. injection flow rate	20.0 L/min	18.9 L/min	17.6 L/min
Tracer	N/A	Bromide	Lithium / Chloride
Approx. injection concentration	N/A	100 ppm	127 / 687 ppm
Pressure Pulsing?	NO	NO	YES

5.2.1 Injection Hydraulics

Injection flow rates did not trend upward or downward with time for any of the NCIS injections. A trend of decreasing well-head pressure was observed for both conventional injections (Figure 5.8). Water pooling at surface was observed during all three injections, and identified as injected fluids due to the high measured tracer concentrations (refer to section 5.2.4). The first observation of water at the surface was documented during injection NC-C1 43 minutes after beginning the injection. This is interpreted as the time of formation failure initialization. A rapid loss of well-head pressure followed, which is symptomatic of a hydraulic fracturing event (Murdoch & Slack 2002). Channels leading to ground surface were distinguishable by rapid flowing water and conical deposition of fine sediments. The number and size of holes producing water at surface increased with time and repeated injection. Holes were initially distributed along the alignment between MLNC05 and HWNC1. During injections NC-C2 and NC-P additional holes were observed 0.5 to 1.0 m northeast of the injection well. The first appearance of water at surface during injections NC-C2 and NC-P was within a few minutes of injection commencement.

Pressure pulsing during injection NC-P was conducted with a range of frequencies. Frequency was increased at increments of around 1 Hz from 1.6 Hz (1 pulse/sec) to 6.0 Hz (3 pulses/sec) at 30 to 40 minute intervals from injection commencement. Different pulsing frequencies resulted in different Sidewinder upstream pressure gauge ranges (Table 5.3). The Sidewinder downstream pressure gauge broke soon after injection commencement. The low end of the pressure range at the upstream gauge is

indicative of pump-supplied pressure (H_{steady}). The high end is not a direct indication of pressure transmitted downstream of the tool (not H_{max}), but rather the accumulated pressure prior to release.

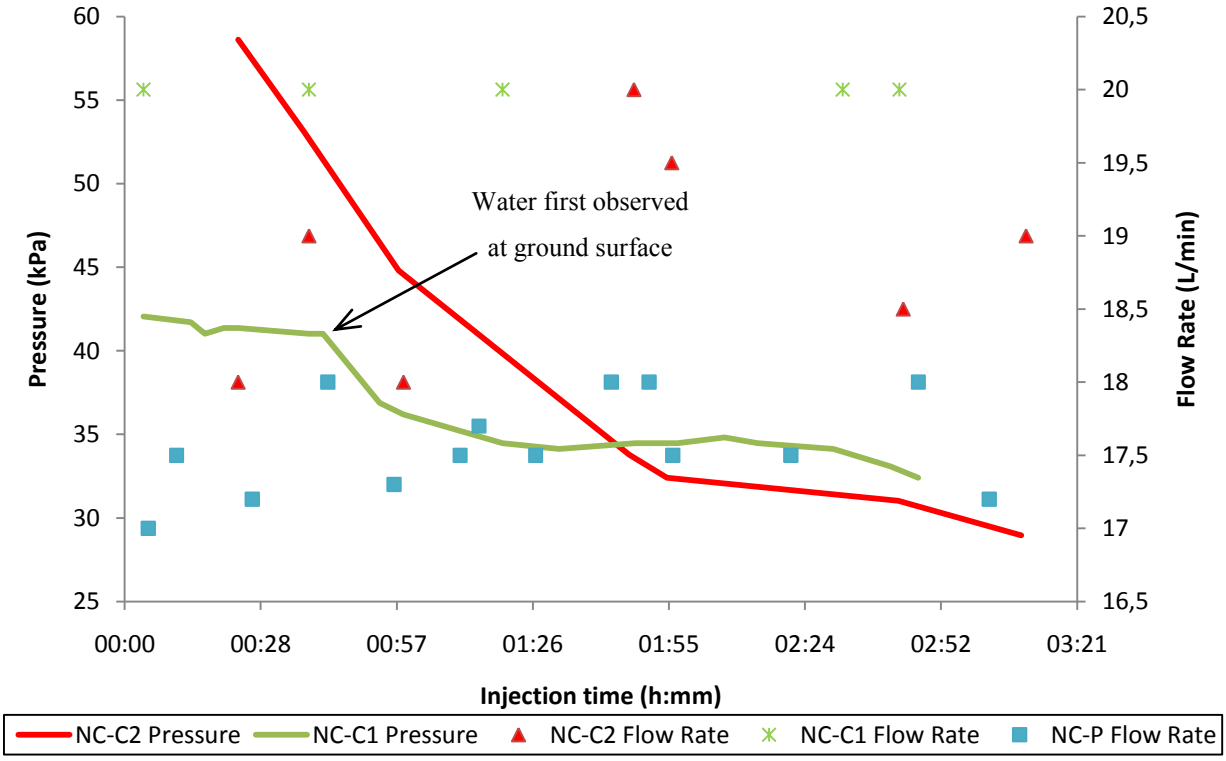

Figure 5.8 – Injection hydraulics for NCIS injections

Table 5.3 –Pressure ranges at the Sidewinder tool upstream gauge for injection NC-P

Injection time	Pulsing frequency (Hz)	Gauge Pressure Range (kPa)	
		Maximum*	H_{Steady}
0:00 to 0:41	1.6	276	48
0:42 to 1:12	2.7	207	41
1:13 to 1:53	3.7	179	38
1:53 to 2:30	4.9	199	41
2:30 to 3:20	6.0	179	Not determined

*Listed maximum pressure is highest observed for multiple consecutive pulses

Lower pulsing frequencies tended to produce a higher accumulated pressure more consistently. Higher pulsing frequencies tended to frequently produce pressure accumulations 5 to 10 psi lower than the maximum pressure listed in Table 5.3. The frequency with-which the maximum accumulated pressure sited in table 5.3 was reach appeared to decrease with increasing pulsing frequency. At pulsing frequencies of 4.9 and 6.0 Hz less than half of the pulsing cycles produced accumulated pressures exceeding 20 psi.

5.2.2 Single well response tests

Hydraulic conductivity values computed from single well response tests trended downward after successive injection (Table 5.4). This may be a result of incomplete sediment collapse after construction. Repeated injection would have encouraged consolidation and supplied fine sediment to fill voids. Hydraulic conductivity at the injection well decreased markedly following pressure pulsing. No change occurred to hydraulic conductivity measurements at monitoring wells after pressure pulsing, indicating that pressure pulsing did not augment formation development.

Table 5.4 – Hydraulic conductivity estimates derived from single well response test

Well	K (m/s) Bouwer-Rice			
	Before NC-C1	After NC-C1	After NC-C2	After NC-P
HWNC05	5.9E-06	3.9E-06	4.0E-06	4.0E-06
HWNC1	8.6E-07	4.8E-07	4.3E-07	4.1E-07
IWNC2	8.2E-07	1.1E-06	1.2E-06	7.0E-07

5.2.3 Formation Pressurization

Formation pressurization was computed by subtracting the ambient water level prior to injection from water levels measured during the injection (Figure 5.9). Similar overall pressurization magnitudes were recorded at both wells for each injection. Waveform patterns appear in HWNC05 data for injections NC-C2 and NC-P, with amplitudes ranging 5 to 10 cm and wavelength around 10 to 20 minutes. This is interpreted to be associated with sampling events at MLNC05. MLNC05 port 10 likely influenced the recorded drawdown most due to the large purge volume required (port 10 is the 1.25 cm ID multilevel center stock).

Formation pressurization did not decrease alongside decreasing injection pressure during injections NC-C1 and NC-C2. However there is a distinct contrast in the pressurization curve at HWNC05 before and after formation failure initialization. Development of pathways to ground surface appears to have had a leaky boundary effect on pressurization. Further pressure build-up is curtailed when the pressurized zone reaches high-conductivity pathways to surface. Pressure pulsing did not have a discernable impact on the influence of preferential flow to surface on formation pressurization.

Post-injection pressure was monitored for a period of time approximately equivalent to the duration of injections. Datasets for all three injections recorded post-injection pressures 7 to 10 cm higher than pre-injection at both HWNC05 and HWNC1. This is indicative of water mounding to accommodate the injected fluid. Slow dissipation of residual pressurization is identified and expected for lateral drainage of a residual mound (Payne et al 2008).

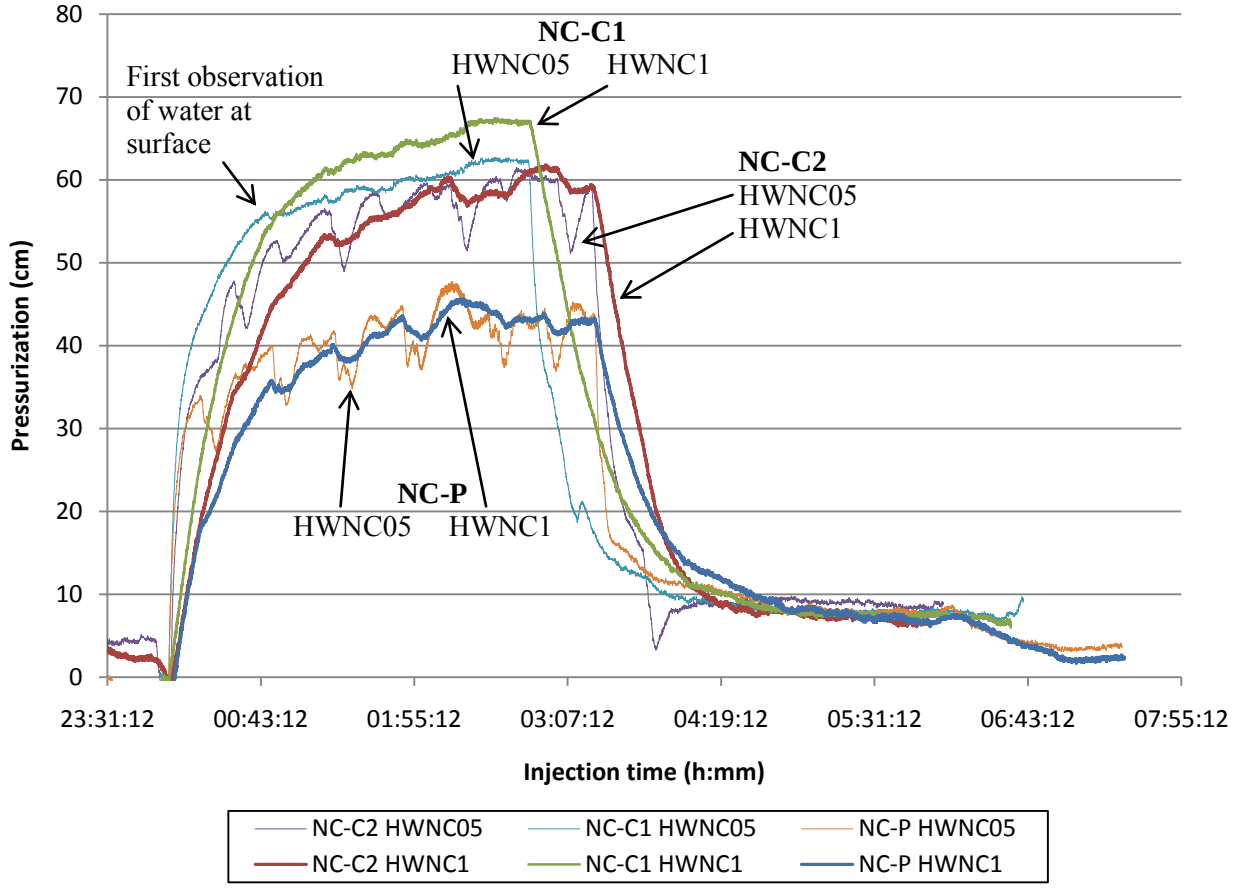

Figure 5.9 – Pressurization data for the three NCIS injections

5.2.4 Solute Transport

All water samples collected from ground surface pooled fluid during both tracer injections contained concentrations of tracer ions similar to injection concentrations. In contrast, samples collected from multilevel sampling ports containing measured concentrations above background levels were sparse for both injections. This indicated that the majority of injected water was flowing through preferred pathways leading to ground surface.

Concentration contour plots were created to illustrate the spatial and temporal distribution of tracer detection within the monitoring network for the two tracer injections (Figure 5.10). Inverse Distance to a Power gridding method was used (Golden Software, 1999). A high power weighting was used to minimize the effect of values far away from any particular grid node during interpolation. Discretization included 10 vertical rows at 0.35 m elevation intervals corresponding to the 10 ports at each multilevel well, and 10 horizontal columns corresponding to 20 minutes injection time intervals.

During injection NC-C2 bromide was detected at MLNC05 ports 2 and 3, and at MLNC1 ports 7, 8, and 9. First detections were during the last hour of injection. A concentration that could constitute arrival of an advective front (C/C_O of 0.50) was only measured at MLNC1-8. Port 1 was dry at both MLNC05 and MLNC1 throughout the injection and could not be sampled.

During injection NC-P low lithium concentrations were detected at MLNC05 ports 5 and 6 at early time and were sustained at low levels throughout. Elevated chloride concentrations were also measured at MLNC05 ports 7, 8, and 9 at 150 to 180 minutes into the injection. Lithium was detected at MLNC1 ports 7, 8, and 9, with first arrival approximately 120 minutes into the injection. Chloride concentrations reflected those for lithium at MLNC1, with additional elevated levels measured at port 10. Ports 1 and 2 were dry at both MLNC05 and MLNC1 throughout the injection and could not be sampled.

Injection NC-P tracer concentration results do not follow the conventions of solute transport behaviour in a stable porous medium. In particular, the decreasing tracer concentrations observed towards the end of the injection would not be expected to occur. This is likely a result of ongoing uncontrolled formation failure. Pressure pulsing may have affected the fracture growth pattern, inducing collapse during periods of low injection pressure. There was insufficient positive detection of tracer during injection NC-C2 to ascertain whether pressure pulsing affected fracture growth patterns.

Two factors may account for discrepancies between chloride and lithium measurements during injection NC-P. First, it is possible that lithium underwent measurable sorption, and therefore only came into contact with monitoring points along highly advective pathways. While there are no data indicating sorption, it has been documented in the literature at near-neutral pH sites (Bencala et al 1984). Second, background chloride concentrations were variable, ranging approximately 35 to 150 mg/L. With an average measured injection concentration of 687 mg/L this translates into relative concentrations as high as 0.18 being attributable to background variability.

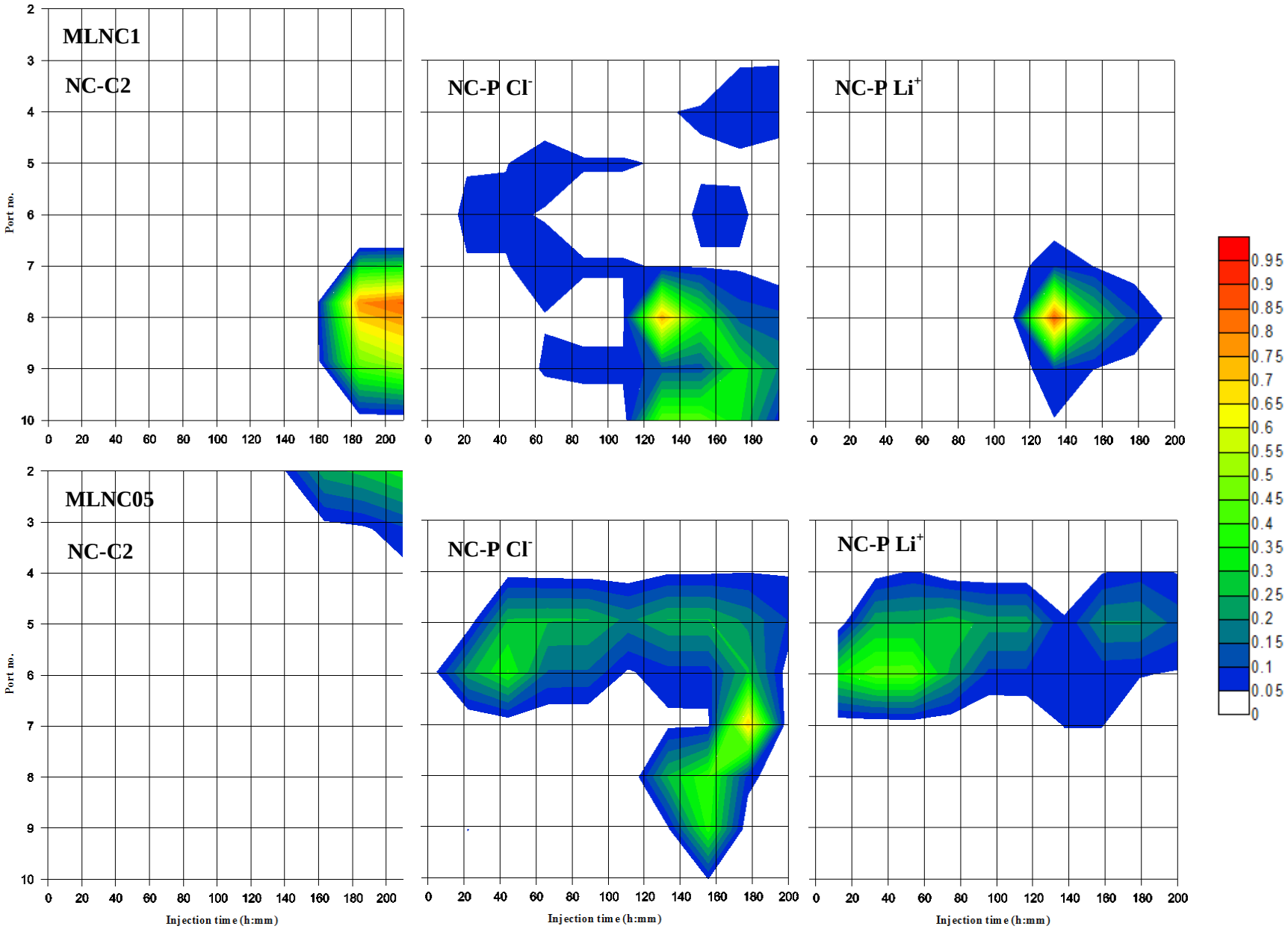

Figure 5.10 – Solute transport results at the North Campus Injection Site

Subsurface conditions at the North Campus site were not ideal for a solute transport comparison. However formation failure occurs at contaminated sites and often becomes a reality that must be managed. Pressure pulsing did not overcome the advective pathways to ground surface created by formation failure. Tracer concentration measurements reflect a somewhat more ideal tracer distribution in the target zone during the pressure pulsing injection (NC-P) than the conventional injection (NC-C2). However it is not possible to ascertain that this was a direct result of pressure pulsing.

5.3 Normalized Formation Pressurization

To investigate the effect of pressure pulsing on formation pressurization the pressure data were normalized by the injection flow rate. NCIS pressurization data were normalized to the mean injection flow rate computed for the duration of the injection (Figure 5.11). Borden data were normalized based on the flow rate time series (Figure 5.12). Flow rates were collected at 15 to 20 minute intervals during field injections. An individual flow rate measurement was assumed to represent the flow rate up to half the duration of the interval before and after that measurement. This assumption produced normalized pressurization time series with a blocky appearance.

$$\widetilde{H} = \frac{H(t) - H_O}{Q} \quad \textbf{(3)}$$

Where $\widetilde{H}$ is the normalized formation pressure, $H(t)$ is the pressure transducer measurement, H_O is the ambient pre-injection pressure, and Q is the flow rate, as measured by the flowmeter at the well-head.

The contrast between normalized pressurization datasets for conventional and pressure pulsing injections is particularly large at the North Campus site. Ongoing development of high-permeability pathways to surface may have played a role here. Injection NC-P occurred last in the sequence of injections at North Campus.

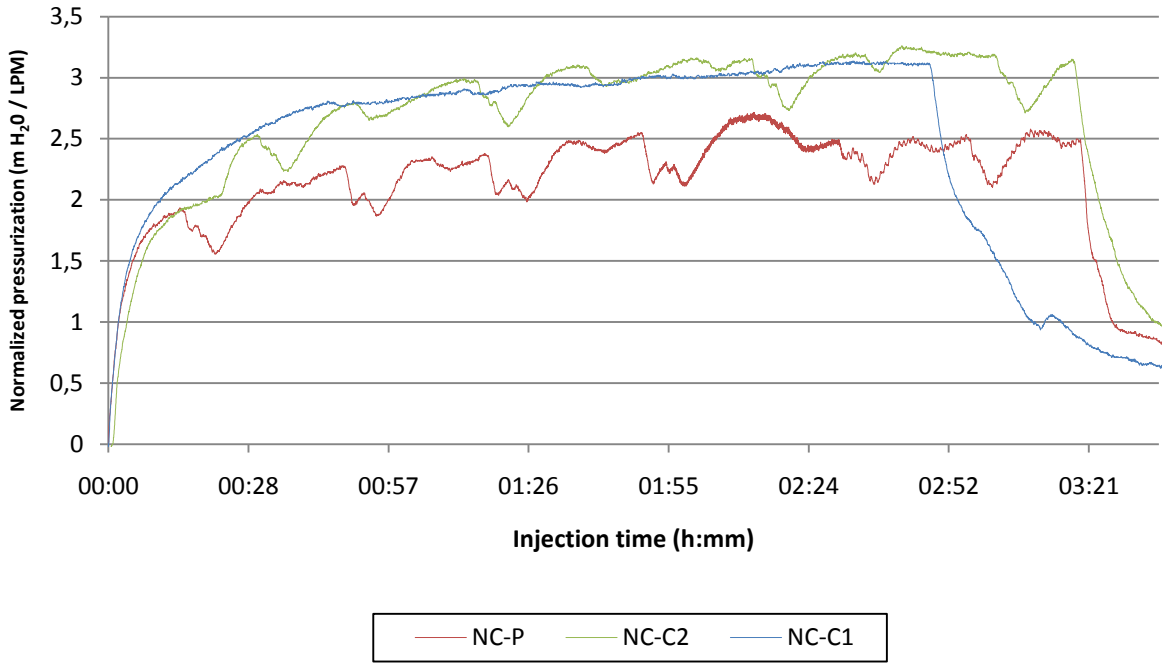

Figure 5.11 - NCIS formation pressurization time series at HWNC05 normalized to injection flow rate. Refer to Appendix B for normalized injection flow rate time series at HWNC1.

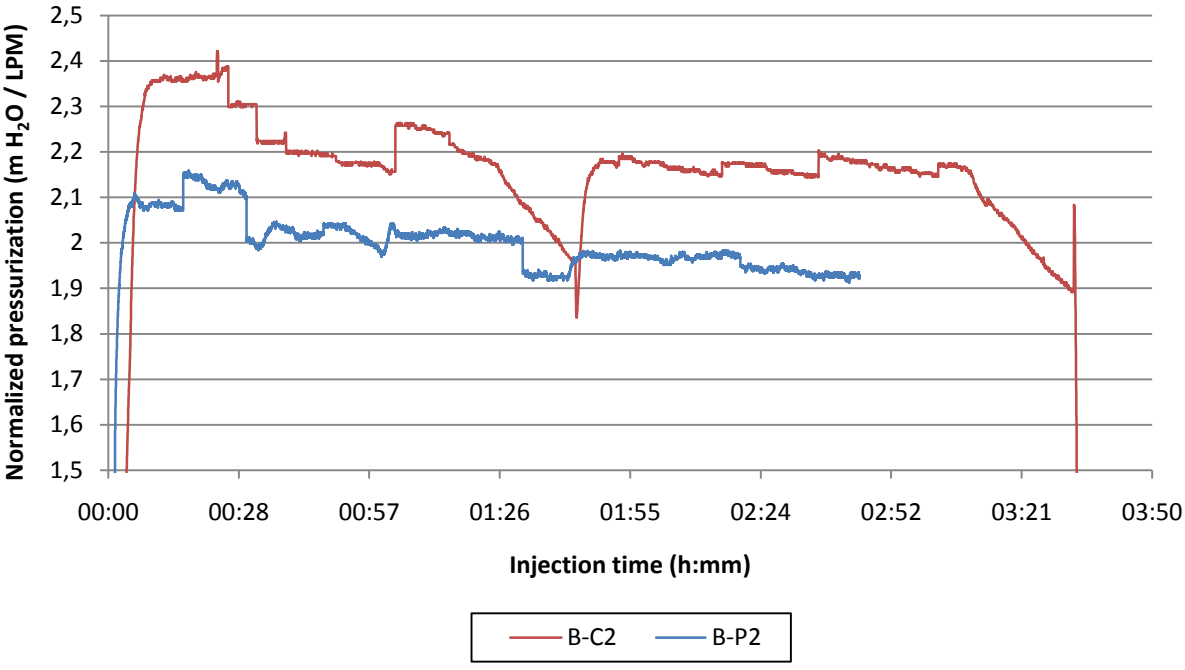

Figure 5.12 – CFB Borden formation pressurization at HWB2 normalized to injection flow rate. Refer to Appendix A for normalized injection flow rate time series at HWB1.

5.4 Consideration for Injection Pressure Limits and Formation Failure

High injection pressures pose a risk of inducing hydraulic fracturing or liquefaction (Payne et al 2008). When uncontrolled and unintended these failure mechanisms can lead to development of very high permeability channels that reduce sweep efficiency, and short-circuiting of injected fluids to ground surface (ITRC 2005). Short-circuiting occurred at the North Campus site, resulting in a large portion of the injected tracer migrating away from the target delivery zone (Refer to section 5.2).

According to Payne et al (2008) an examination of horizontal and vertical effective stresses at the depth of the top of the injection well screen can be used to determine the maximum injection pressure that prevents formation failure.

$$\Delta\sigma_{uf} = \sigma'_{vi}(1 - sin\varphi)/2 \quad \textbf{(4)}$$

Where $\Delta\sigma_{uf}$ is the increase in pore pressure to failure, σ'_{vi} is vertical effective stress at ambient conditions, and φ is the internal friction angle of the soil. To determine the maximum injection pressure the height of the water column above ambient conditions must be accounted for in addition to gauge pressure at the well head. Maximum injection pressures for the CFB Borden and North Campus injection sites were calculated for a range of internal friction angles and typical depth to ambient water table observed at the respective sites (Table 5.5).

Table 5.5 – Calculated safe injection pressures at the North Campus and CFB Borden injection sites. Ranges for angle of internal friction were determined based on range of soil types (Perloff 1976).

Injection Site	Top of well screen (mbg)	Water Table (mbg)	φ (degrees)	$\Delta\sigma_{uf}$ (m H2O)	Max. safe gauge pressure (psi)	Range of gauge pressures used (psi)
North Campus	4.0	3.5	23	2.2	0	5 - 10
			32	1.7	0	
CFB Borden	7.5	1.0	25	2.6	1.5	10 - 15
			38	1.7	0.3	

Based on equation (4) the injection pressures sustained at both sites were considerably greater than that which would risk inducing formation failure. In fact, even gravity feed from a tank at ground surface would have exceeded maximum injection pressure at the NCIS. This underscores a conflict between budgetary constraints and effective amendment delivery that undoubtedly exists at many contaminated sites.

While injection pressures exceeding the formation failure criterion are likely commonplace in industry, it is important to account for the impact of the Sidewinder tool when planning injections. Pulses exceeded pump-supplied pressure downstream of the tool by up to a factor of 1.5 at the CFB Borden site. This factor may be greater for lower pulsing frequencies and higher pump-supplied pressures. A step-pressurization approach would be a prudent measure to ensure injection pressure constraints are not exceeded at unfamiliar injection sites. High-resolution, real-time pressure monitoring downstream of the Sidewinder tool would be an asset under such circumstances.

Chapter 6 – Numerical Modeling Results and Discussion

Results of the two- and three-dimensional numerical modeling exercises are summarized here. Quality control data indicating the accuracy with-which simulations represented the environment of interest are discussed. Detailed hydraulics and solute transport analyses focussed on the near-well medium are presented. Included in the analyses are a series of formation pressurization and solute breakthrough curve comparisons that tie the modeling and field experiments together.

6.1 Two-dimensional Model

A selection of model results are presented in Appendix D. Results are presented in five formats:

1. **Hydraulic head time series profiles at cells of interest:** Head time series were extracted from output files for the duration of the last two pulsing cycles where simulations involved pressure pulsing (totaling last 10 stress periods of the simulation). Time series plots present head values over a full pulsing cycle from H_{steady} before a pulse to H_{steady} after a pulse. Head time series were extracted for the complete duration of the simulation where injection was conventional. Cells of interest are grouped into line segments AA', BB', and CC' such that data for all cells of interest along a particular line segment are presented together (line segment layouts are described in section 4.2.4).

2. **Hydraulic head contour maps:** Head contour maps illustrate the distribution of head in the medium at a particular time. Maps were generated for each time step in the last complete pulsing cycle of simulations involving pressure pulsing (totalling 30 map images representing each time step of the last five stress periods of the simulation). A consistent set of contouring parameters were used for all head contour maps of a given pulsing simulation. Animations were generated by creating a slideshow of a complete set of contour maps in sequence. Maps were generated for the last individual time step for simulations involving conventional injection. Contour map extents were limited to a few meters laterally and vertically around the simulated injection well to optimize ease of examination in the section of the domain affected by pressurization.

3. **Solute breakthrough curves:** Concentration time series were extracted from output files for the full duration of all simulations at 50 second intervals. They are presented grouped by their representative distances from the injection well (0.75, 2.0 and 4.0 m).

4. **Solute concentration contour maps:** Concentration contour maps illustrate the spatial distribution of solute concentrations in the medium at a particular time. Maps were generated at times of 300 s and 1800 s for all simulations. Contour map extents were limited to a few meters laterally and vertically around the simulated injection well to optimize ease of examination. Plume extents did not exceed 5 m laterally from the injection well in any simulation.

5. **Zone Budget flow rate time series:** Flow between prescribed zones were extracted from the Zone Budget output listing file and tabulated to create time series. Average flow rates over complete pulsing cycles were determined by computing net volume transfers and dividing by cycle duration.

6.1.1 Quality Control Indicators

Quality control data indicated modeling artefacts were within acceptable ranges. Head increases at the domain edge opposite the injection well were less than 0.1 m (less than 0.01%) throughout all simulations. This reflects accurate representation of a laterally continuous formation. Head waveforms at the injection well and throughout the formation showed minimal change between consecutive pulsing cycles at late injection time (less than 10^{-4} m at all cycle phases for all pulsing simulations). Therefore treatment of the head solution as a quasi-steady-state system at late injection time is valid. Head values were identical for all cells representing the injection well at all inspection times. This indicates accurate simulation of pipe hydraulics. Average head at the injection well for pulsing simulations matched the injection pressure assigned for paired conventional injections within 0.1 m. Tabulated quality control data sets are presented in Appendix D.

6.1.2 Parametric investigation of the mixing zone phenomenon

Pressure pulsing simulations produced a complex cycling hydraulic head distribution near the injection well (e.g., Figure 6.1). This resulted in a zone characterised by a hydraulic gradient that is temporally and spatially variable in direction and magnitude. This phenomenon occurs for two reasons.

First, the constant rapid fluctuations in boundary pressure at the injection well put the medium near the well into a constant state of disequilibrium. This disequilibrium is driven by a pressure response diffusing radially out into the medium from the well head every time the boundary pressure changes. Second, layers of differing hydraulic diffusivity ($\alpha = K/S_S$) respond to rapid changes in boundary pressure at different rates (greater hydraulic diffusivity is associated with a more rapid response). The response to a pressure pulse travels faster and further in the higher diffusivity layer.

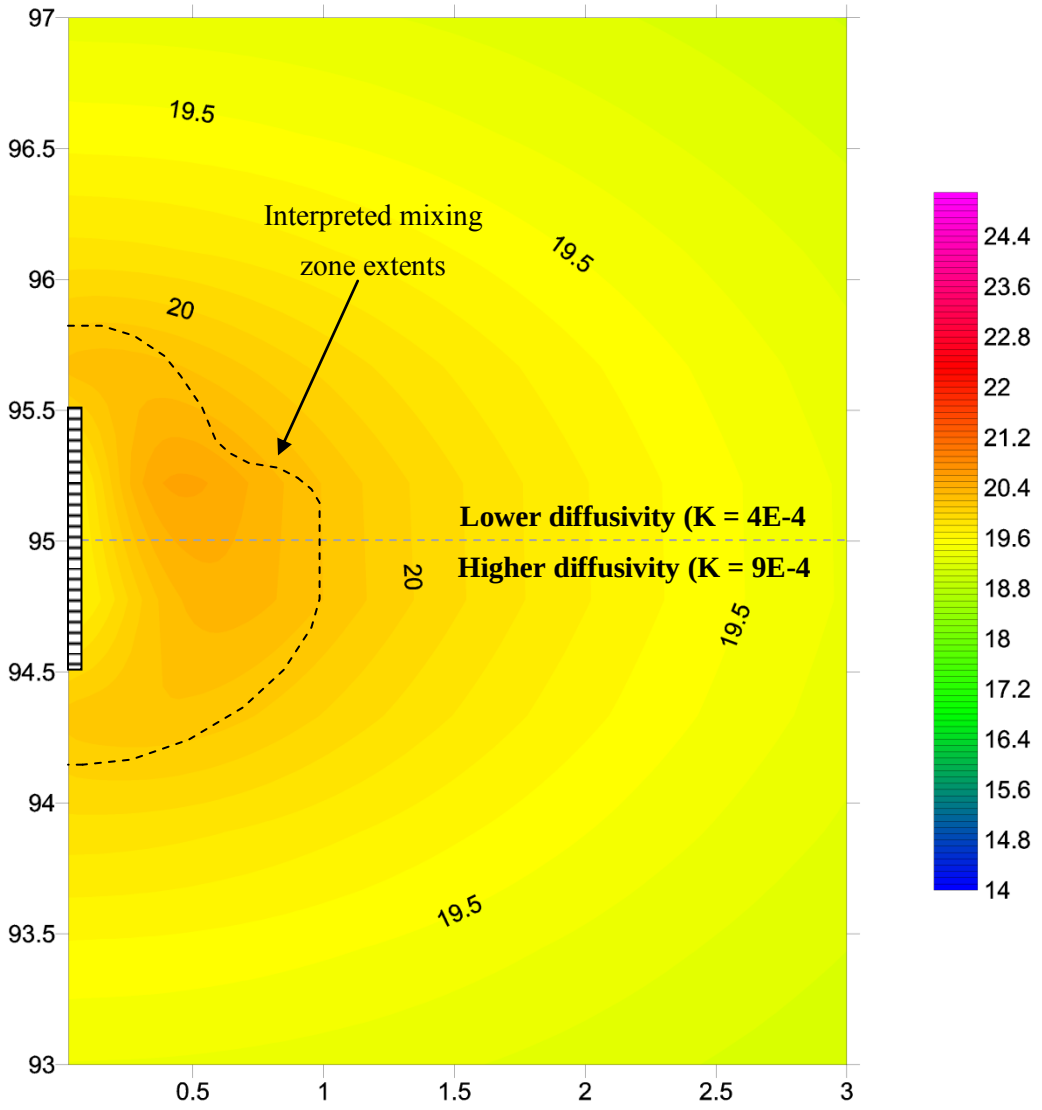

Figure 6.1 – Head contour map for Sim. 1 at stress period 26993 time step 5 (pulse cycle stress period 3). At this stage pressure is recovering in the well in conjunction with a gradient reversal in the medium nearby. Different response rates of the two layers to rapid fluctuations in pressure at the well result in a complex head distribution and flow field.

Pressure distribution in the medium once the system reaches a quasi-steady-state may be generalized into three stages as governed by the five stress periods of a pressure pulsing cycle (refer to section 4.2.3):

During pressure pulsing Stress Period 1: Pressure distribution in the medium approaches that of the equivalent conventional injection simulation.

During pressure pulsing Stress Periods 2 and 3: The rapid onset of low pressure at the well during stress period 2 introduces a gradient reversal in the medium. The distance to-which this gradient reversal extends expands in time and varies from one simulation to the next. This would be analogous to a propagating pressure wave trough. For simulations in domains A and C the higher α layer responds more rapidly than the lower, resulting in development of a pressure difference between the two layers favouring flow towards the higher diffusivity layer. As stress period 3 progresses the pressure distribution in the lower diffusivity layer catches up with that of the higher diffusivity layer and the transverse gradient decreases in magnitude.

During pressure pulsing stress periods 4 and 5: The onset of high pressure at the well during stress period 4 rapidly restores pressure in the near-well medium, replacing the gradient reversal with a growing high-pressure zone immediately around the well. This would be analogous to a propagating pressure wave crest. A forward gradient is sustained through stress periods 4 and 5, with greater magnitude than a conventional injection at H_{Steady} would present. For simulations in domains A and C pressure in the higher diffusivity layer increases more rapidly and extensively. This results in development of a transverse gradient favouring flow towards the lower diffusivity layer. As stress period 5 progresses the lower diffusivity layer pressurizes and this transverse gradient decreases in magnitude.

Transient flow inducing hydraulic gradients from high permeability preferred flow paths to adjacent lower-permeability zones has been demonstrated and discussed by a number of authors (Bauer et al 2009; Luo et al 2007, Rolle et al 2009, Weeks & Sposito 1998, Zhang et al 2009). Zhang et al (2009) also demonstrated up to three-fold increases in mixing at the laboratory scale when three injection wells were used to inject and extract in an oscillatory pattern. This was characterized by a smaller plume radius, indicating greater effective porosity, and attributed to increased interfacial surface area for diffusion. Effects were greatest when applied in a layered heterogeneous medium, but mixing was also increased by

up to two-fold in a homogeneous medium. These results suggest that the complex flow field observed near the injection well in the 2D model may be interpreted as an advective mixing zone.

The spatial extents of the mixing zone were interpreted for each 2D pressure pulsing simulation (Table 6.1). Three criteria were used to evaluate mixing zone extents, including the following:

(1) Maximum extents of flow reversal, as determined by inspection of hydraulic head waveform plots for cells near the injection well.
(2) Maximum pressure wave penetration with amplitude of at least 0.1 m hydraulic head. Determined by inspection of hydraulic head waveform plots and contour map animations
(3) Bending of equipotential lines by at least 10 degrees over a pulsing cycle. Determined by inspection of hydraulic head contour map animations.

Table 6.1 – Interpreted mixing zone extents for 2D pressure pulsing simulations

Simulation	Mixing zone extents (m)	
	Low α layer	High α layer
1. Baseline: 3Hz pulsing in domain (A)	0.6	1.0
2. 3Hz pulsing in domain (B)	0.7	0.7
3. 3Hz pulsing in domain (C)	0.6	1.45
4. 3Hz pulsing in domain (D)	0	0.8
5. 4Hz pulsing in domain (A)	0.6	0.85
6. 2Hz pulsing in domain (A)	0.75	1.1
7. High-Amplitude 3Hz pulsing in domain (A)	0.6	1.0
13. High-Amplitude 3Hz pulsing in domain (C)	0.6	1.4
15. 4Hz pulsing in domain (C)	0.5	1.15
16. 2Hz pulsing in domain (C)	0.65	1.5
17. 3Hz pulsing in domain (E)	0.1	0.2

The primary factor that affects mixing zone extents is the hydraulic diffusivity of the medium. A higher diffusivity medium responds more rapidly to sudden pressure fluctuations and thus the pressure wave propagates more rapidly. It follows that greater heterogeneity is characterized by greater mixing. Transverse gradients that develop between the high-diffusivity layers and adjacent low-diffusivity layers are greater in magnitude and duration when the difference in diffusivity between the two layers is greater. The mixing zone in Domain E was much smaller than that in other domains. Hydraulic conductivities less than 10^{-5} m/s appear to be too small to generate a mixing zone that is extensive enough for practical application.

Lower frequency pulsing lead to a somewhat more extensive mixing zone. Lower frequency pulsing involved a longer recovery period from low pressure (pressure pulsing stress period 3) and longer sustenance at H_{max} (pulsing stress period 4). This allowed responses in the medium to extend further before a change in boundary pressure. Lower frequency pulsing may also be an opportunity to achieve a greater H_{max} using a Sidewinder tool, because the accumulation period is longer (although this was not considered for the model). A greater H_{max} could act to increase the magnitude of the forward hydraulic gradient and consequential transverse hydraulic gradient into the lower diffusivity layer.

Higher amplitude pulsing did not have a distinguishable effect on mixing zone extents. It did, however, increase the magnitude of all temporary gradients. The net effect is increased total flows along these gradients during each cycle, thereby increasing the mixing effect.

Pulsing in Domain D did not produce a discernable pressure wave signal in the low-diffusivity layer located below the injection well. The pressure wave signal adjacent to the low-diffusivity layer was already considerably dampened due to distance from the boundary condition. Response in the low-diffusivity layer was also very slow due to the low assigned hydraulic conductivity. It is possible that lower frequency pulsing could produce a discernable pressure wave response in this layer and extend significant mixing gradients into it.

Zone budget results reflected the mixing zone identified in the pressure data. Time series plots of flow rate and cumulative volume at late simulation time were created for Simulations 1 (Figure 6.2) and 3 (Appendix D), and their paired conventional injection simulations.

Flows across the contact between the two hydrostratigraphic layers always had a net direction into the lower conductivity layer from the higher. Pressure pulsing produced marginally lower net flows into the lower diffusivity layer than conventional injections (true for both domains A and C). Mixing gradients in close proximity to the well had no effect to increase or decrease net flow into the lower dffusivity layer near the well. They did, however, produce considerable repetitive fluxes across the boundary in both directions.

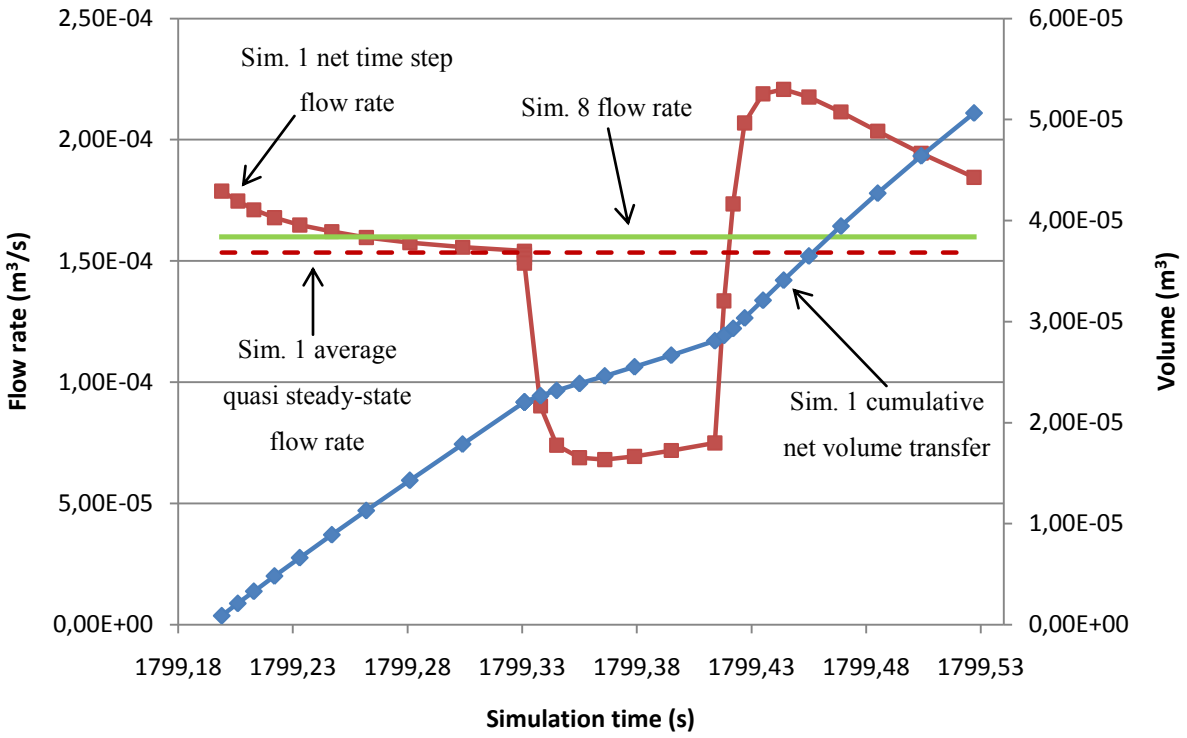

Figure 6.2 – Water movement across contact between upper and lower hydrostratigraphic layers for 2D model Sim. 1 (3 Hz pulsing domain A) and Sim. 8 (conventional domain A).
One complete pulsing cycle shown. Positive indicates flow into upper layer (lower K).

While these results do not show a net increase of water flux into the lower-diffusivity layer associated with pressure pulsing, they do demonstrate the utility of transience as a means of inducing flow in directions that cannot occur once a system reaches a steady state. As an injection progresses pressure increases more rapidly further from the source in higher conductivity zones. This gives rise to a temporary hydraulic gradient into the lower conductivity zones. When the system reaches a steady state this gradient reduces to zero. The opposite is also true: a low-pressure boundary condition would induce a temporary gradient from lower-diffusivity zones into higher. The nature of pressure pulsing is such that gradients in both directions (from high α layers into low α layers and the reverse) occur. Thus it is unlikely that the mixing zone phenomenon presents an opportunity to achieve a more equal rate of injected fluid advancement in layers of differing permeability.

The spatial distribution of flow leaving the injection well was compared between pulsing and non-pulsing simulations (Table 6.2). Flows leaving the injection well during pulsing simulations were determined by summation of net flows over a complete pulsing cycle. Pulsing did not have an effect on

flow into the low K layer from the borehole in domain A. A slightly greater flow into the low K layer was recorded for the pulsing simulation in domain C.

Table 6.2 – Net flow into low K layer from borehole relative to total inflow

Simulation	Flow into Low K layer as a percentage of total inflow (%)
1 – 3Hz pulsing domain A	30.7%
3 – 3Hz pulsing domain C	11.7%
8 – No Pulsing domain A	30.7%
10 – No Pulsing domain C	10.1%

Time series of flow from the injection well over a pulsing cycle were plotted for Simulations 1 (Figure 6.3) and 3 (refer to Appendix D). Both show a similar evolution of cumulative volume transfer and flow rate. The recovery from H_{min} is marked by flow into the well bore. This is predominantly a model anomaly, as discussed in section 4.2.3. The vast majority of net inflow occurs while the pulsing cycle is at H_{max} and recovering back to H_{steady}.

A fundamental requirement for the simulated mixing phenomenon is the period of flow reversal towards the injection well during each pulsing cycle. The movement of water back towards the injection well is allowed to occur in large part because water is artificially removed from the borehole cells to establish H_{min}. Zone Budget data indicated that water volumes removed from the system during each pulsing cycle to establish H_{min} amounted to as much as 12% (varied from one simulation to the next) of the total fluid added to the system over the same pulsing cycle. In reality no water would be removed from the system and this reversal would likely be very short-lived. Depressurization of the higher-conductivity layer occurs, in part, because water is allowed to flow back into the well. This depressurization in turn drives the complex transverse hydraulic mixing gradients. The magnitudes of mixing gradients in reality are likely lower than predicted here, not-withstanding scaling up to three dimensions.

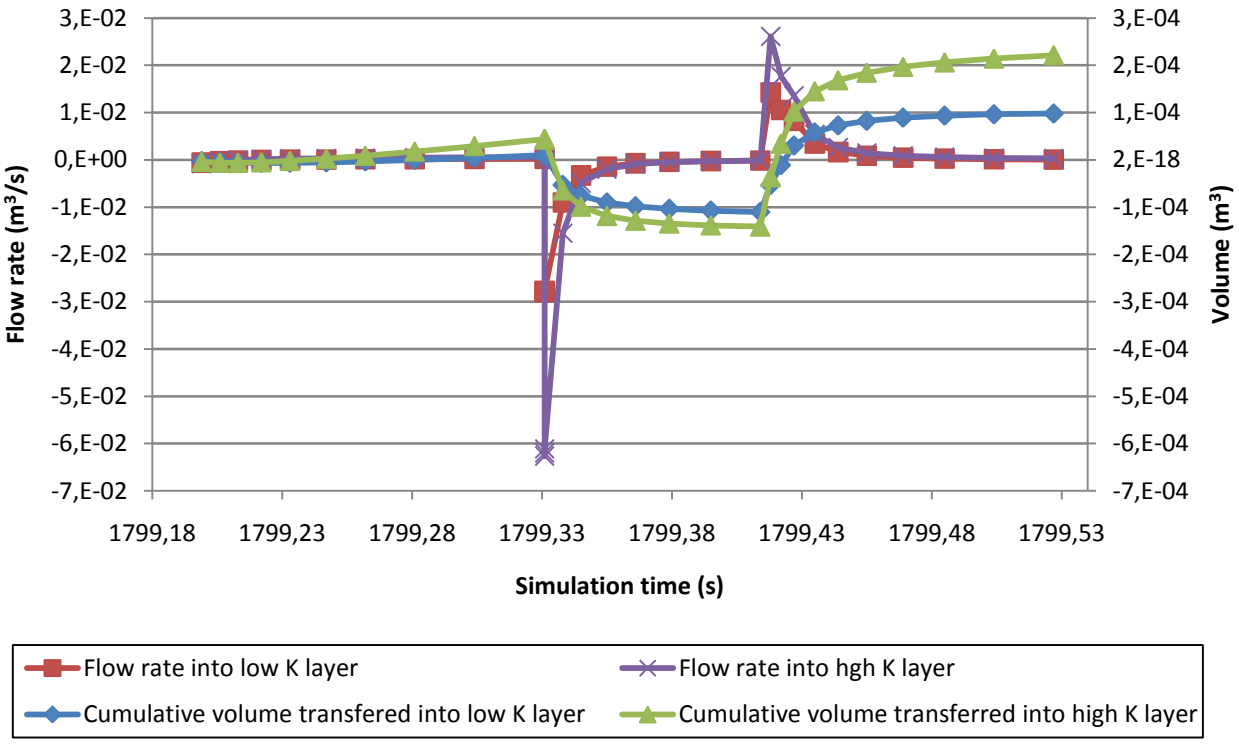

Figure 6.3 – Time series of flow from the injection well into the two K-field layers in domain A. One complete pulsing cycle shown for Simulation 1. Positive values indicate flow into the formation; negative values indicate flow into the well.

6.1.3 Effects of pressure pulsing on solute transport

Plotting breakthrough curves from pulsing and conventional injection simulations together (e.g., Figure 6.4) revealed only minor differences. Refer to Appendix D for the complete set of breakthrough curve comparison plots.

Solute arrival time differences at monitoring points appeared to be most sensitive to domain parameters. In particular, arrival was earlier in the low-diffusivity layer when pressure pulsing was introduced in domain C (as shown in Figure 6.4). Differences were not significant at any monitoring point in domain A (low heterogeneity), B (homogeneous), or D (underlying aquitard). Variations in pulsing parameters (amplitude and frequency) did not have a distinguishable effect. Earlier arrival in a low-hydraulic diffusivity layer reflects somewhat greater flow into this layer from the injection well, as identified in section 6.1.2.

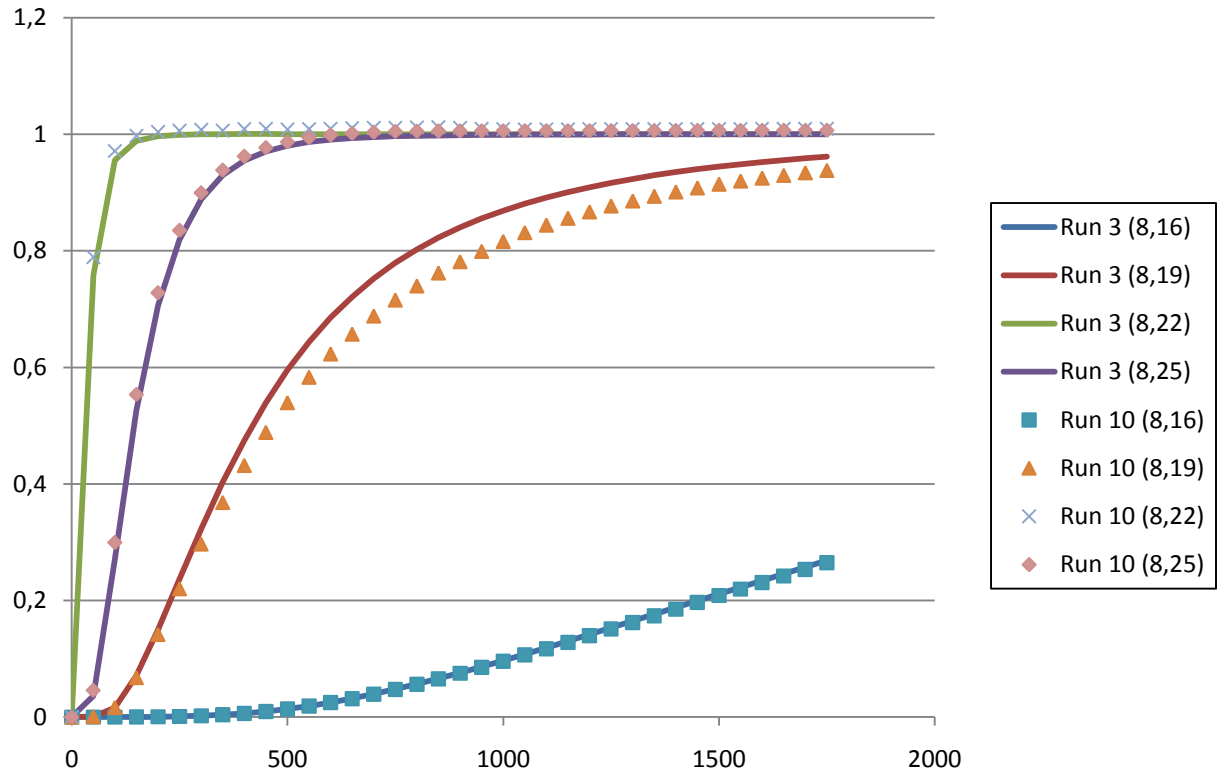

Figure 6.4 – Breakthrough curves 0.75 m from source for Simulations 3 (3 Hz pulsing – Domain C) and 10 (conventional injection – domain C)

Concentration difference contour maps were generated at simulation times of 300 s (e.g., Figure 6.5) and 1800 s (e.g., Figure 6.6) using the grid math package available in the Surfer 7 program. All difference maps followed a standard whereby the conventional injection simulation concentration map was subtracted from the pressure pulsing map, such that positive values always indicate a higher concentration for the pulsing simulation. Differences in these grids are normalized to the injection concentration such that values indicate differences relative to injection concentration. These are not relative difference plots in the sense that the subtraction is not normalized to the concentration in one of the input concentration grids. Therefore it is useful to cross-reference the original concentration contour maps when analysing the difference maps. Refer to Appendix D for the complete set of concentration difference contour maps.

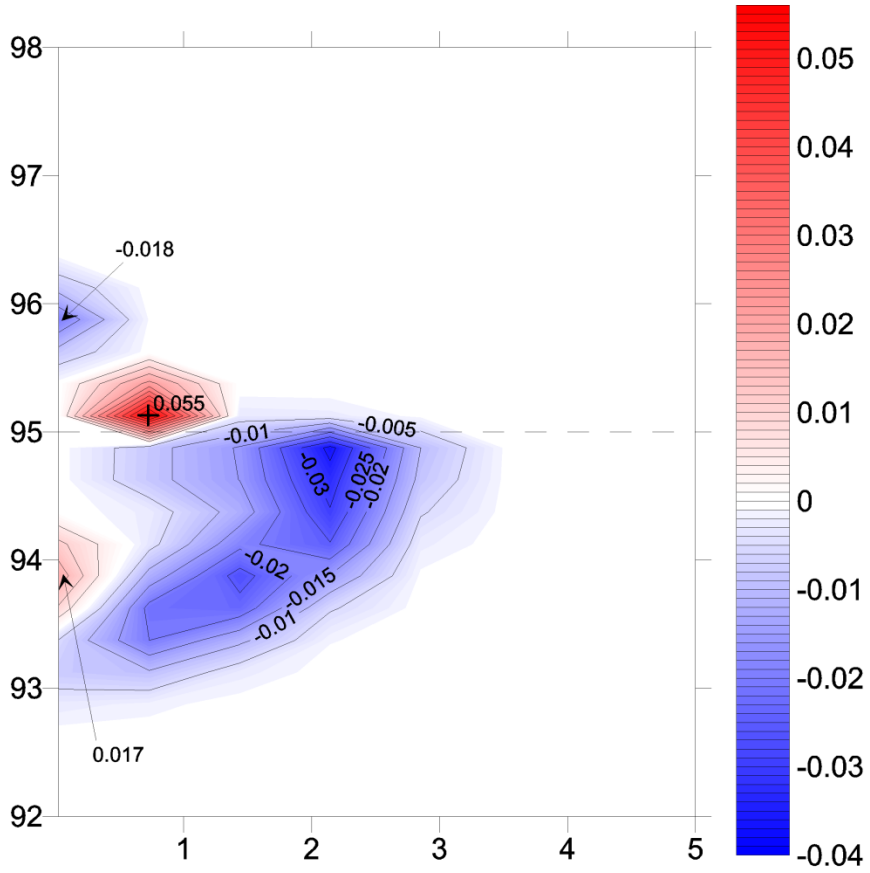

Figure 6.5 – Concentration difference contour map: Sim. 3 (pulsing) – Sim. 10 (conventional) t = 300 s
Positive values indicate higher concentration for the pulsing injection. Values are fractions of injection concentration (e.g. 0.01 = 1% injection concentration)

There are two trends common among concentration difference plots at 300 s simulation time. First, the advancing concentration front is characterised by higher concentrations (varying as high as 7%) for the conventional injections. For heterogeneous domains this is confined to the higher-diffusivity layer. Peak differences align approximately with the advective front of both plumes. This is symptomatic of a plume that has advanced slightly further in the conventional injection simulation. Second, the pulsing injections tended to record higher concentrations in the lower diffusivity layer lateral to the injection well (ranging 0 to 5.5%). This is symptomatic of a plume that has advanced slightly further in the pressure pulsing simulation. For domain C it also corresponds with the finding of additional fluid entry into the lower diffusivity layer from the injection well, as indicated in section 6.1.2.

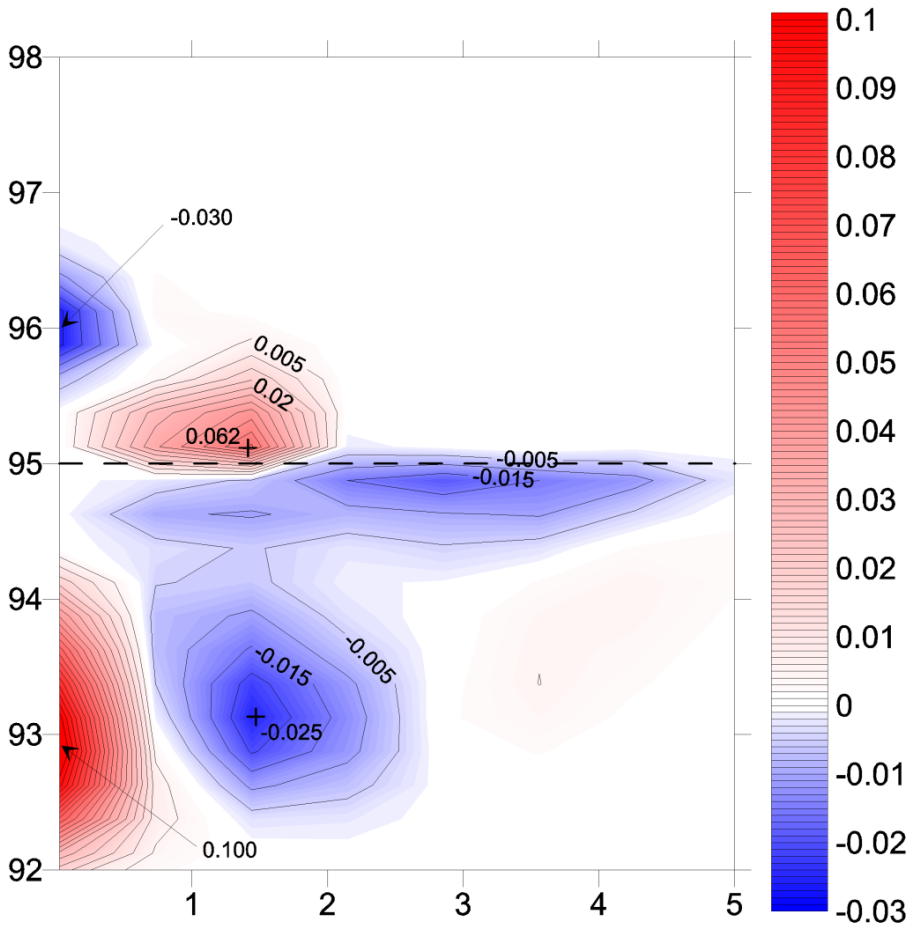

Figure 6.6 – Concentration difference contour map: Sim. 3 – Sim. 10 t = 1800 s

Difference plots generated at 1800 s simulation time captured similar trends to those at 300 s. Concentrations were somewhat higher in the low-diffusivity layer for the pulsing simulations in domains A and C. This difference was more spatially extensive and of greater magnitude at 1800 s than at 300 s. Concentrations were somewhat higher in the high-diffusivity layer for conventional injection simulations. This difference was more spatially extensive but not greater magnitude at 1800 s. The appearance of differences vertically above and below the injection well (ranging as high as 10% injection concentration below) was a development at later simulation time. An investigation comparing multiple transport solution methods and solution tolerance factors indicated this to be, at least in part, an artefact of the 3rd order TVD transport engine. In domains A and C the particularly high pulsing simulation concentrations below the well may also be a function of mixing currents favouring flow towards this point (Figure 6.7). A similar mixing current favours flow above the well but is in a less conductive zone. It may also be dominated by the reversal gradient cycling water back towards the well and preventing solute transport into this area.

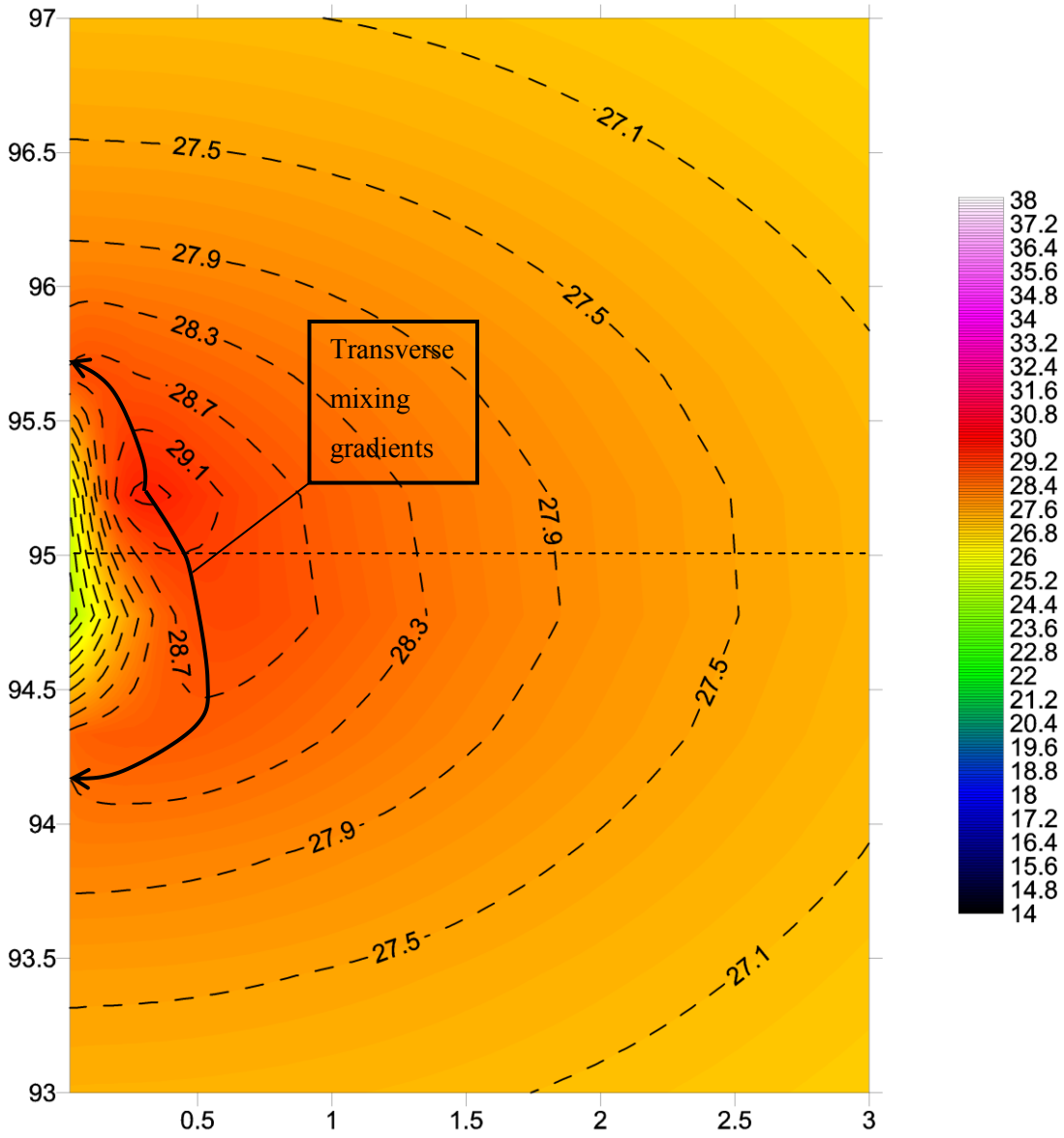

Figure 6.7 – Head contour map (Sim. 13) demonstrating transverse mixing currents favouring flow towards the domain boundary above and below the injection well.

Concentration differences between pulsing and conventional injection simulations were consistently below a level which would suggest potential for considerable solute transport differences in a field trial.

6.2 Three-dimensional Model

Complete sets of model results for all simulations are presented in Appendix E. Results are presented in five formats:

- Head time series profiles at simulated HWB1 and 2 ports and additional cells of interest
- Contour maps of head distribution near the simulated borehole
- Solute breakthrough curves at simulated MLB1 ports
- Contour maps of solute concentrations near the simulated borehole
- Zone budget flow rate time series

Presentation formats followed conventions used for the 2D model (Refer to section 6.1). Head and concentration data were extracted at the end of each subset run (every 67 seconds).

6.2.1 Stage 1 Benchmarking Results: Development of Two 3D Conductivity Fields

Three distinct hydrostratigraphic layers were used to generate flow and transport results similar to those collected at the CFB Borden site (

Table 6.3). Steady-state hydraulic head was within 10 cm of target for HWB1, but off by nearly 60 cm for HWB2 (Figure 6.8). Breakthrough of advective fronts were within 15 minutes of target for each monitoring point at MLB1 (Figure 6.9). The discrepancy at HWB2 demonstrates that heterogeneity at the CFB Borden site has a lateral component that was not accounted for in the model domain. HWB2 may have had a greater hydraulic connection with the injection well than solute transport data at similar elevations would indicate. Final stage-1 benchmarking results correspond with Simulation 3D-C (conventional injection in Borden domain). Results for Simulation 3D-C include one head and one concentration contour map generated at the last time step along row 58 (refer to Appendix E), head time series profiles at cells of interest for the full duration of the simulation (shown in Figure 6.8), and solute breakthrough curves at simulated MLB1 ports for the duration of the simulation (shown in Figure 6.9).

Table 6.3 – 3D model Borden domain parameters.

Three hydrostratigraphic layers were built in to the 3D model to simulate flow and transport behaviour observed at the CFB Borden site. This was the result of stage 1 modeling.

Hydrostratigraphic layer	Rep. elevation range (m) *	Domain layer range	K_H (m/s) ◊	K_V (m/s)	α_H (m^2/s)
Upper	1.5 to 10.0	1 to 26	2E-5	6.7E-6	0.02
Middle	0.75 to 1.5	27 to 32	6E-5	4E-5	0.06
Lower	0 to 0.75	33 to 38	3E-4	1E-4	0.3

*Elevations relative to bottom of model domain (2.125 m below top of inj. well screen)
◊ $K_y = K_x$ was assumed throughout the benchmarking process

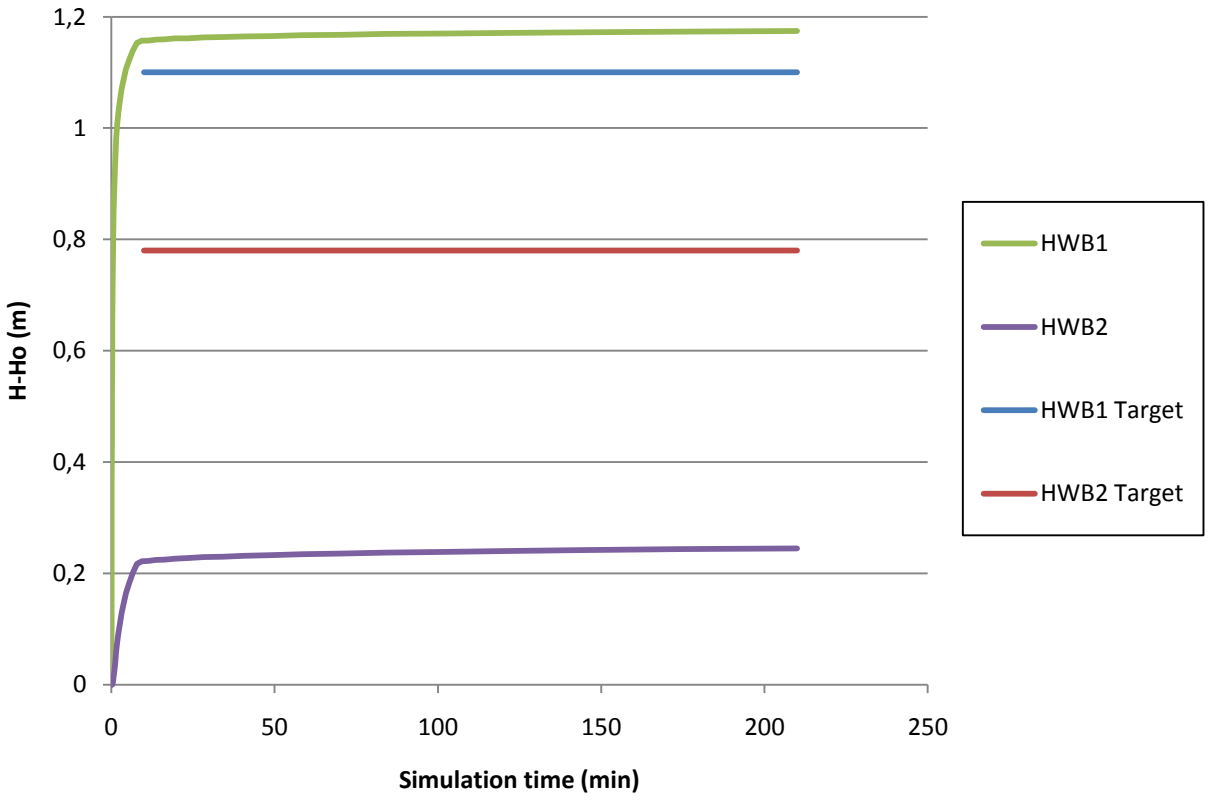

Figure 6.8 – Simulation 3D-C hydraulic head data for simulated hydraulic monitoring wells HWB1 and HWB2

The Modified Borden Domain was built based on the Borden domain. Changes were made to the middle hydrostratigraphic layer only (Table 6.4). Horizontal hydraulic conductivity was increased by an order of magnitude, and vertical conductivity increased to 2E-4 m/s.

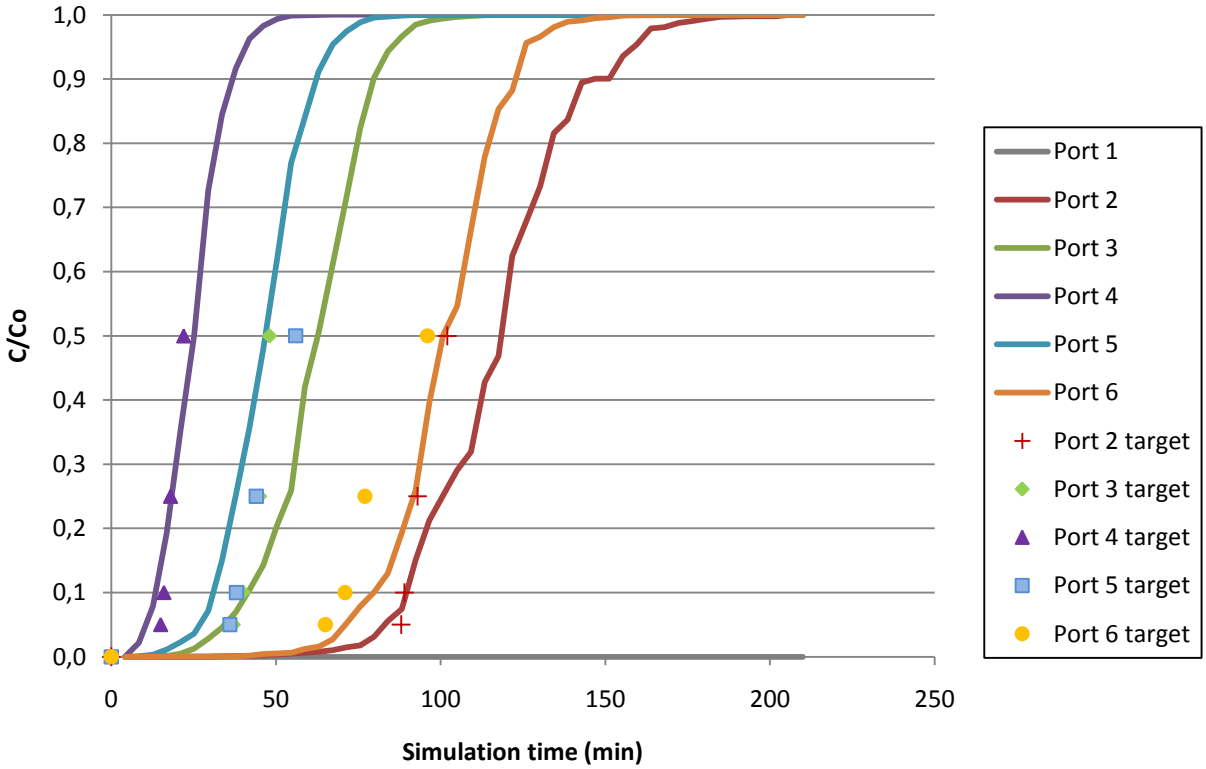

Figure 6.9 – Simulation 3D-C breakthrough curves and target arrival times for the simulated MLB1 multilevel well cluster

Table 6.4 – 3D model Modified Borden Domain parameters

Hydrostratigraphic layer	Rep. elevation range (m) *	Domain layer range	K_H (m/s) ◊	K_V (m/s)	α_H (m^2/s)
Upper	1.5 to 10.0	1 to 26	2E-5	6.7E-6	0.02
Middle	0.75 to 1.5	27 to 32	6E-4	2E-4	0.6
Lower	0 to 0.75	33 to 38	3E-4	1E-4	0.3

*Elevations relative to bottom of model domain (2.125 m below top of inj. well screen)
◊ $K_y = K_x$ was assumed throughout the benchmarking process

6.2.2 Quality Control Indicators

Quality control data indicated modeling artefacts were within acceptable ranges. Head increases near the domain edges opposite the injection well (adjacent to constant head boundaries simulating lateral continuity) were 0.005 m (0.0005%) or less throughout all simulations. This reflects accurate representation of a laterally continuous formation. Hydraulic head values differed by 2E-5 m or less for all cells representing the injection well at all inspection times. This indicates accurate simulation of pipe hydraulics. Artificial water withdrawal at the GHB amounted to approximately 11% of the total volume of water injected. The net pressure pulsing quasi-steady-state injection flow rate was within 0.1 L/min of conventional. Average pulsing cycle pressure at the well head differed from the assigned conventional injection pressure by 0.1 m or less. Quality control data sets are presented in Appendix E.

6.2.3 Mixing Zone Phenomenon in 3D

Pressure pulsing in the Borden domain (Simulation 3D-P1) produced a discernable mixing zone up to 0.2 m from the injection well (Figure 6.10). Greatest extents of the mixing zone were in the middle hydrostratigraphic layer and along its contact with the upper layer (refer to Simulation 3D-P1 pressure pulsing head contour map series, Appendix E). Hydraulic diffusivities in the 3D Borden domain were similar to those used in 2D domain E. Pulsing in the 2D domain E produced a mixing zone with maximum extents of 0.2 m in the higher-diffusivity layer ($\alpha = 0.06$).

Pressure pulsing in the 3D Modified Borden Domain (Simulation 3D-P2) produced a discernable mixing zone up to 0.7 m from the injection well in the middle hydrostratigraphic layer, and along its contact with the upper layer (Figure 6.11, also refer to Simulation 3D-P2 pressure pulsing head contour map series in Appendix E). Hydraulic diffusivity in the middle stratigraphic layer of the Modified Borden Domain is similar to that of the high-diffusivity layer in the 2D domain A. Pulsing in 2D domain A produced a mixing zone with maximum extents of 1.0 m in the high-diffusivity layer. Therefore there is evidence to suggest a reduction in mixing zone extents when the third spatial dimension is introduced. However the 30% reduction in extents identified by comparing Simulations 3D-P2 and 2D-1 does not eliminate the possibility of enhancing mixing at the scale of injections at contaminated sites.

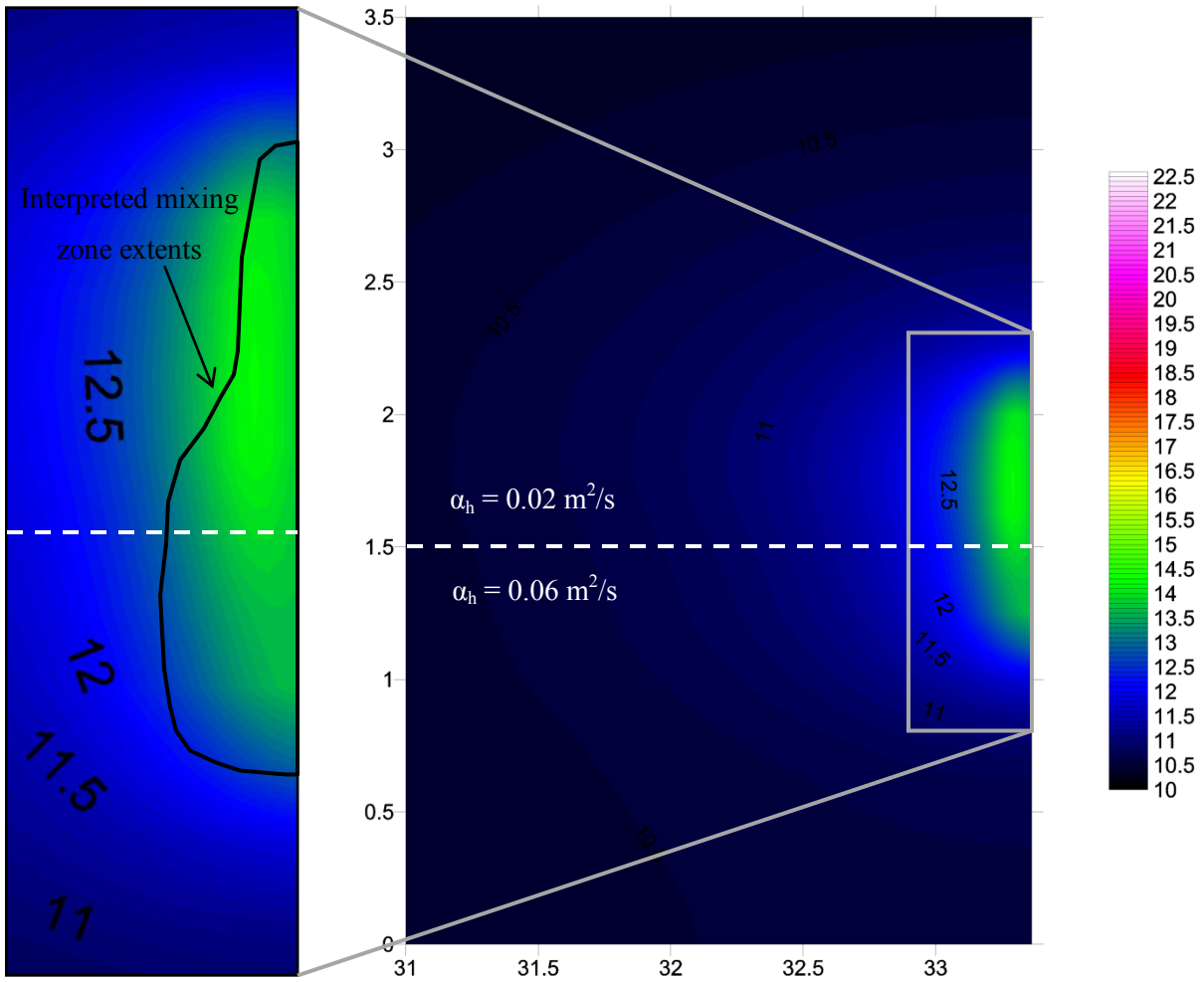

Figure 6.10 – Simulation 3D-P1: interpreted mixing zone extents. Overlaid on head contour map for stress period 134 998 time step 7.

Overall pressurization of the medium was less extensive in the 3D domain for both pulsing and conventional injection simulations relative to the 2D domain. For example, the equipotential line representing 2.0 m pressurization relative to initial conditions ranged 0.5 to 1.0 m from the injection well in 150-minute 3D simulations, and was approximately 50 m away in 30-minute 2D simulations. This is a result of flow scaling. When the third spatial dimension is introduced the amount of flow required to propagate pressurization into the medium is greater. This may have been a contributing factor in reduced mixing zone extents.

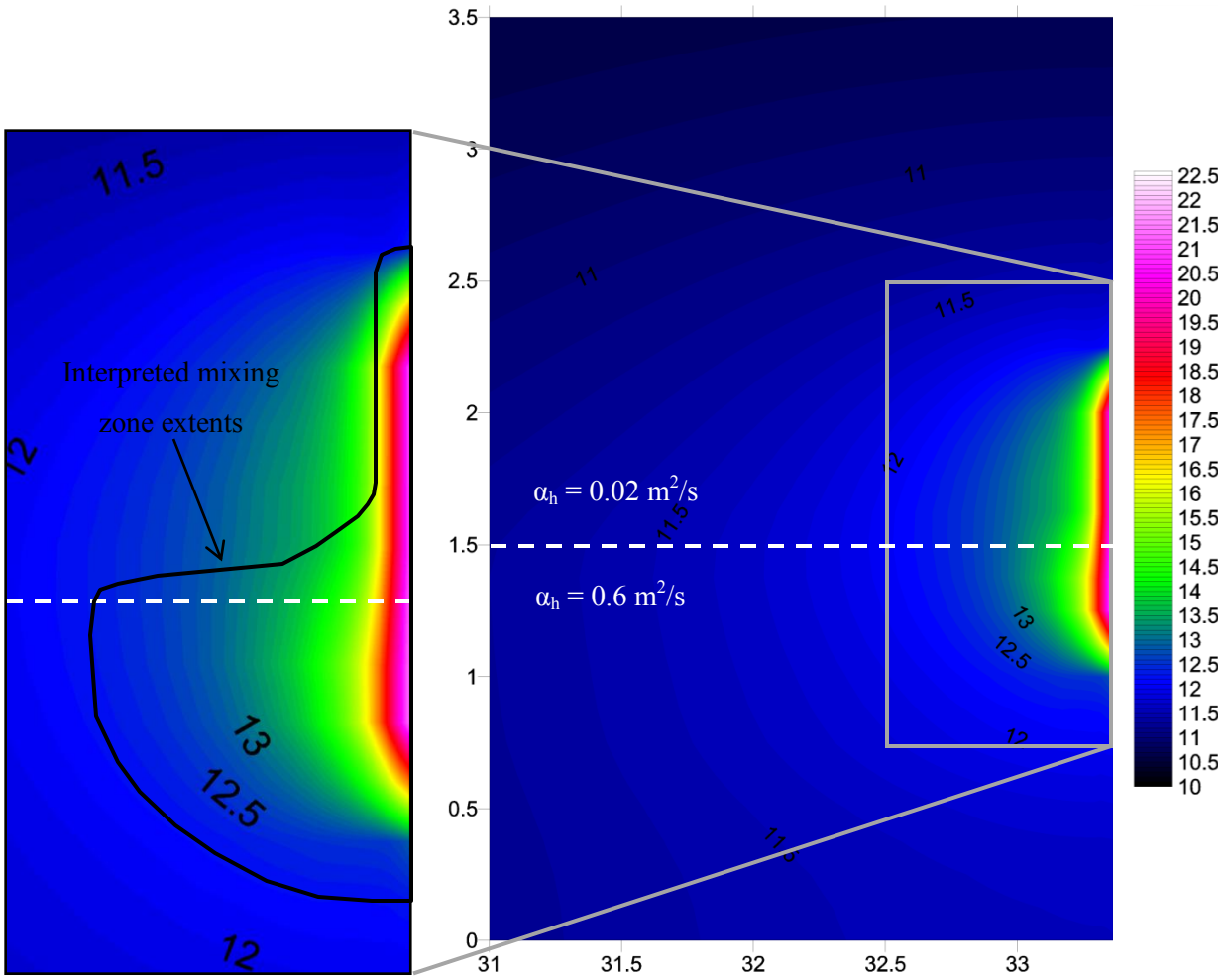

Figure 6.11 – Simulation 3D-P2: interpreted mixing zone extents. Showing head contour map for stress period 15 999 time step 6.

6.2.4 Medium Pressurization

Late time medium pressurization was distinguishably greater for Simulation 3D-P1 than for Simulation 3D-C (Figure 6.12). Pressurization at early simulation time is similar. Approximately 10 minutes into the conventional simulation medium pressurization levels off rapidly (Figure 6.13). Pressurization continues after this time for the pressure pulsing simulation. Steady-state hydraulics are reached less rapidly in the pressure pulsing simulation.

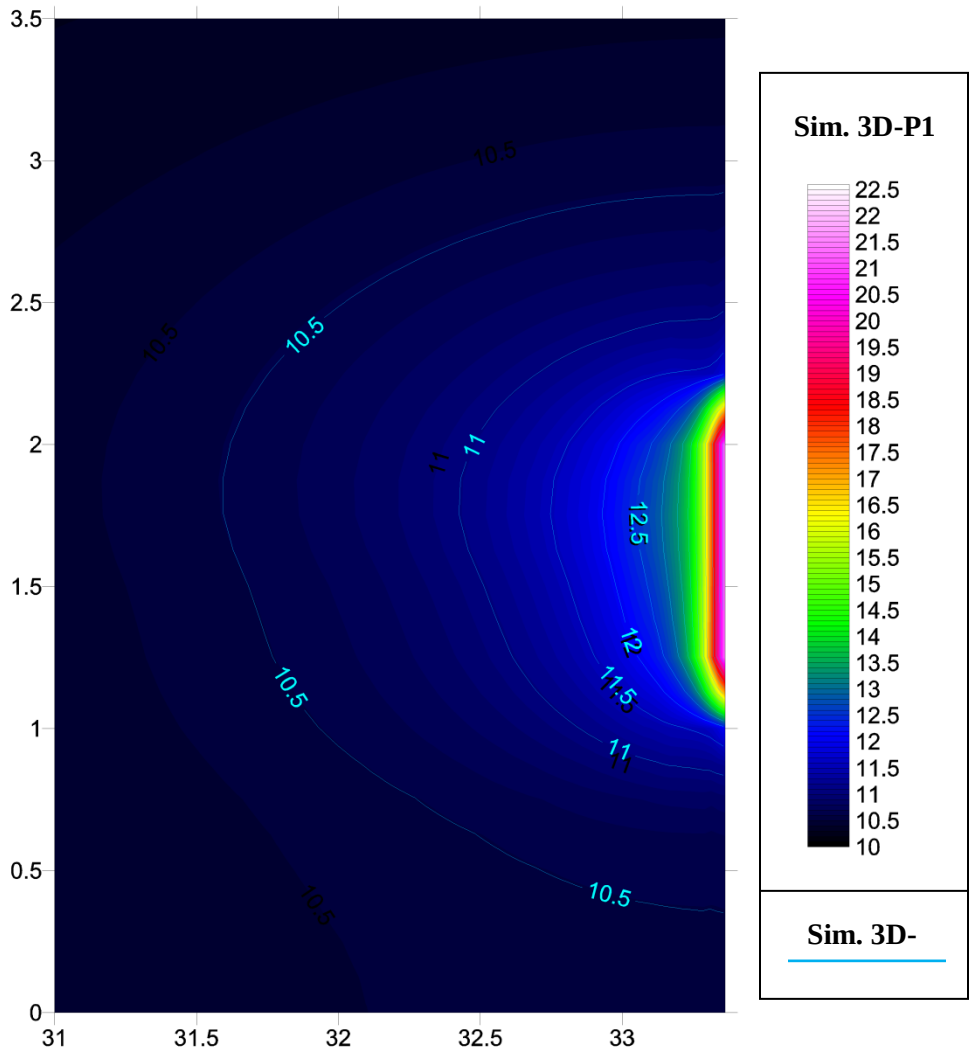

Figure 6.12 – Head contour maps at 150 min for simulations 3D-P1 (Colour contours) and 3D-C (light blue line contours)

Quality control data indicated that average pressure at the injection well for Simulation 3D-P1 is within 0.1% of that for 3D-C throughout the injection. Flow rate data indicated discrepancies of 1% or less throughout (refer to section 6.2.2 and Appendix E for Quality control data and results). Therefore the additional pressurization cannot be attributed to a difference in average injection parameters.

An occurrence similar to the synergetic pressure build up described by Wang (1999) may account for the additional pressurization cause by pressure pulsing. If pressurization in the medium near the well arising from a pressure pulse does not dissipate as quickly as it rises there will be a net pressure build-up. Consequently, greater pressure will be passed along further into the formation. Pressure near the well during a pressure pulsing event is in a constant state of flux, therefore the increased pressurization effect

is not sustained near the well. However repetitive brief moments of rapid pressurization with slow decay could transfer greater pressure further into the medium than possible during conventional injection.

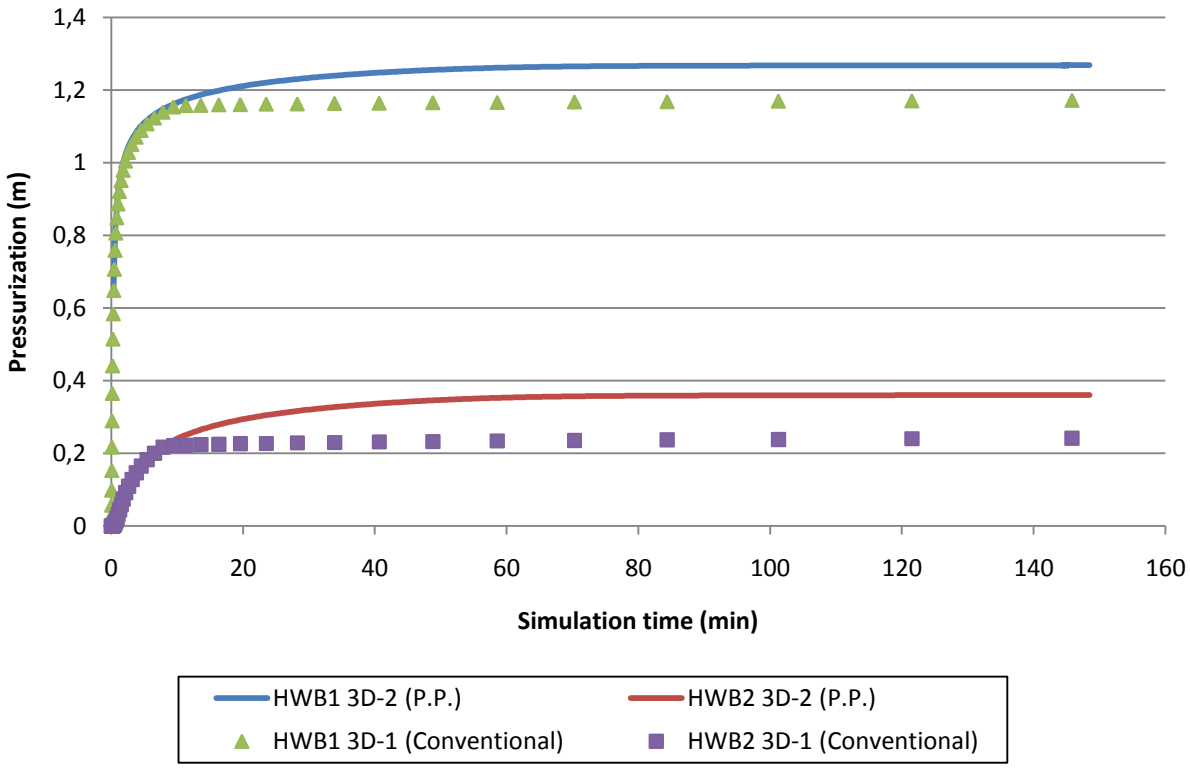

Figure 6.13 – Pressurization data at HWB1 and HWB2 for Simulation 3D-P1

Normalized pressurization data from both field sites disagree with the trend observed in the 3D model (Refer to section 5.3). For a given flow rate, pressure pulsing produced a somewhat lower formation pressure. However, unlike the model, neither field site is an ideal aquifer. It is likely that a number of assumptions inherent in the model do not hold at these field sites. For example, neither site constitutes a confined aquifer.

6.2.4 Solute Transport

Breakthrough curves generated at simulated MLB1 ports demonstrated similar tracer arrival times for simulations 3D-1 and 3D-2 (Figure 6.14). Simulation 3D-2 (pressure pulsing) produced breakthrough curves exemplifying greater smearing of the advective front, indicating greater dispersion. Advective front arrival times were not distinguishably different between the two simulations at any particular port.

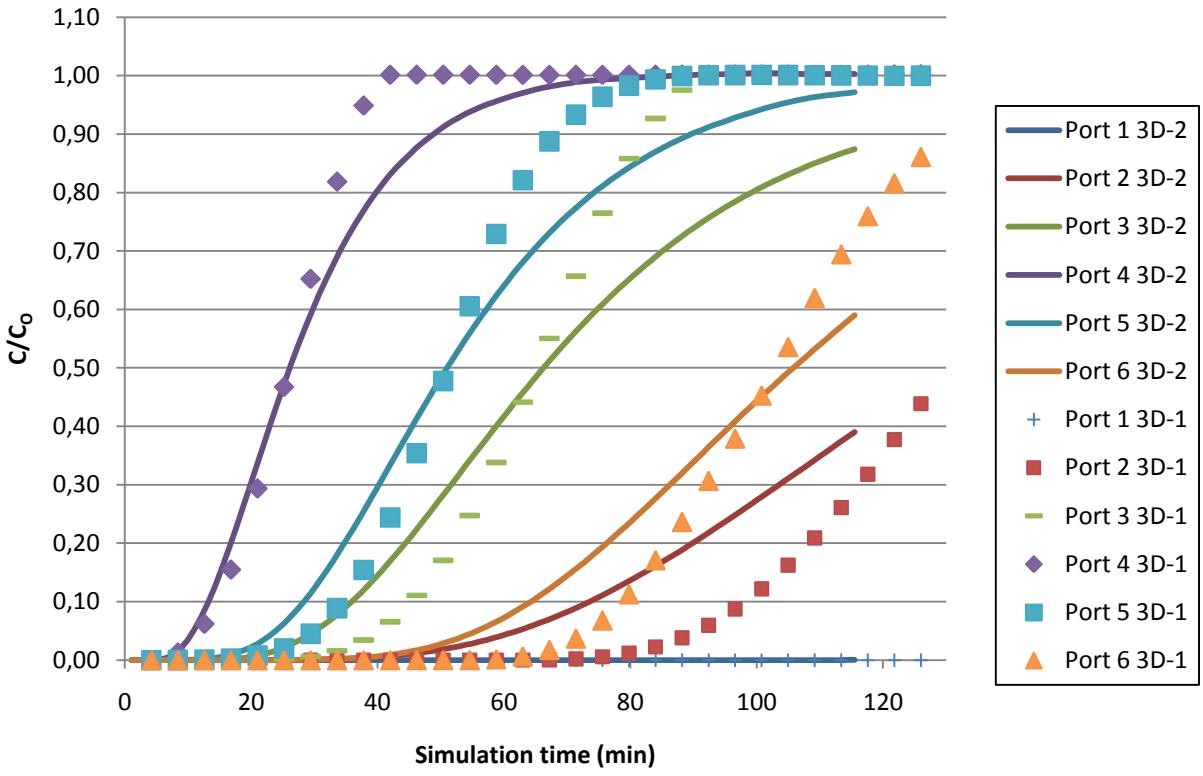

Figure 6.14 – 3D model simulated breakthrough curves at MLB1

A comparison of tracer concentration cross-section contour maps (Figure 6.15) demonstrates that pressure pulsing enhanced dispersion throughout the plume of injected tracer. A wider distribution of contours along the advancing plume front indicates greater dispersion for simulation 3D-2 (Figure 6.15a). A concentration difference contour map (Figure 6.15b) displaying a dipole trend along the plume front, with higher 3D-2 concentrations followed by higher 3D-1 concentrations, is also symptomatic of greater dispersion for simulation 3D-2. Contour maps reveal no distinguishable difference in spatial distribution of the advective front.

Dispersion enhancement arising from pressure pulsing is interpreted to be associated with the mixing zone phenomenon. Temporary reverse and augmented forward gradients are responsible for the observed enhancement within the constraints of a finite difference solute transport model. Transverse gradients, expected to augment transverse dispersion, would not impact smearing of the front for a plume emanating from an injection well.

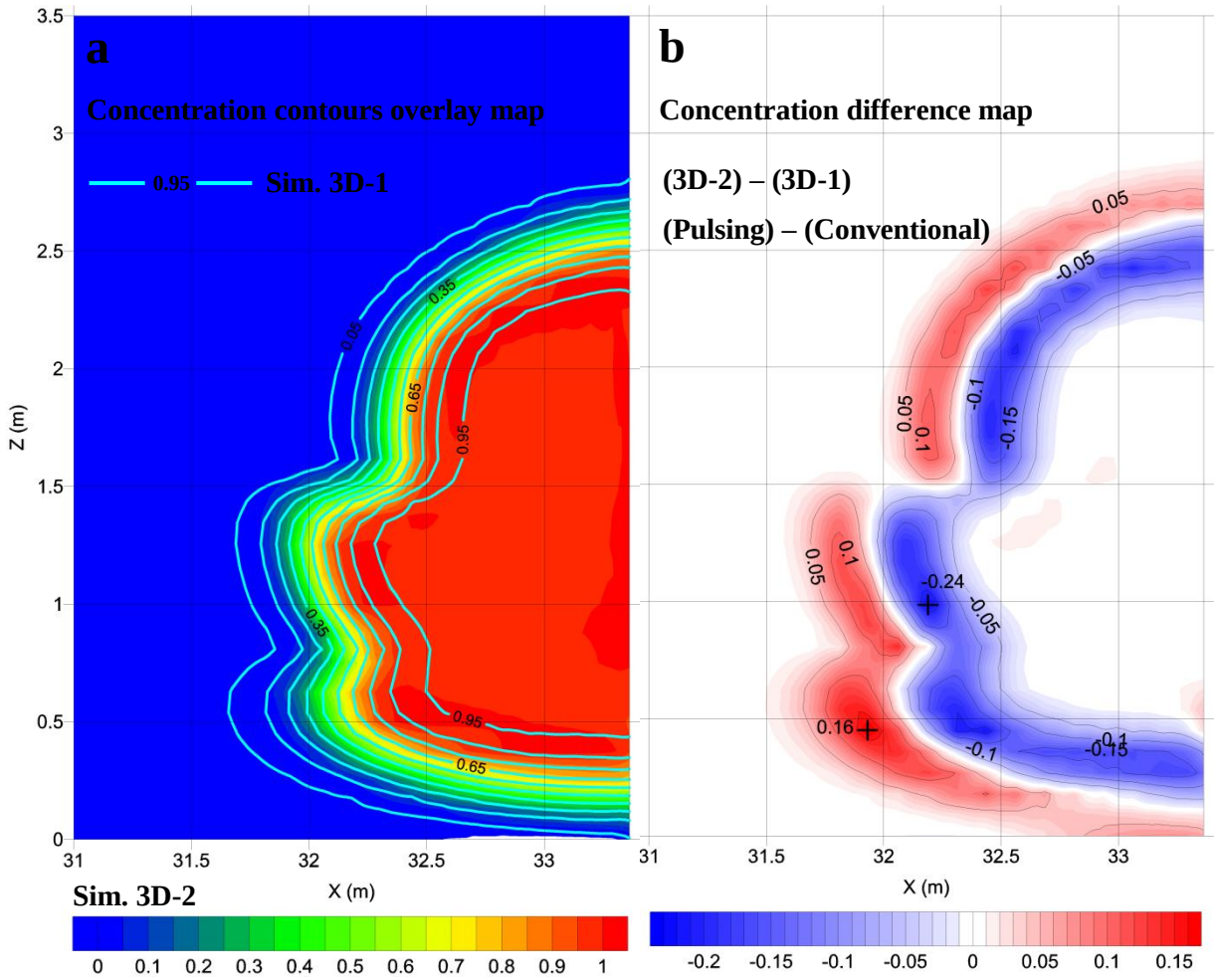

Figure 6.15 – Cross-sectional contour maps illustrating 3D model solute transport results. Presented as an overlay of results for simulations 3D-1 and 3D-2 (a) and concentration differences (b). Positive values in b indicate higher pressure pulsing concentrations.

Current understanding of subsurface solute transport, arising from the growing global database of site-scale tracer tests, places diffusion from mobile to immobile porosity as a dominating component of longitudinal hydrodynamic dispersion (Payne et al 2008). This implies that dispersion has a temporal consideration that is not fully accounted for in the advection-dispersion equation (which is inherent in the MT3DMS code). Therefore it is likely that the dispersion enhancement observed in 3D modeling exercises overestimates that which would occur at a real site. However hydraulic mixing has been shown to have the effect of increasing the interfacial surface area exposed for diffusion (Zhang et al. 2009). Therefore the observed dispersion enhancement is symptomatic of the potential for pressure pulsing to augment access to immobile porosity.

The dispersion enhancement demonstrated in the 3D modeling exercise is not distinguishable in field solute transport data. Transport at the North Campus site was controlled by highly advective pathways to surface. Transport data at the CFB Borden site was influenced too greatly by reaction with the medium and formation development to distinguish effects of dispersion. However, comparing breakthrough curves for injections B-C1 and B-P1 (refer to section 5.1.3), it is clear that any dispersion enhancement resulting from pressure pulsing is small. A much slower pulsing frequency could be used to sustain mixing gradients, thereby increasing exposure time for diffusion into immobile porosity.

6.3 Well Design Considerations

Field injections demonstrated the need for careful consideration of pump-supplied pressure exceedances that occur when pressure pulsing is used during injection (Refer to section 5.4). The modeling exercise demonstrated the additional need to consider the effects of flow reversal when designing injection wells.

The occurrence of flow back in to the well necessitates the use of a filter pack designed with consideration for inflow. Often injection wells are designed under the assumption that flow will only be out through the well screen (Payne et al. 2008). In the event that backflow occurs in such a well there is a risk of transporting fine soil particles into the well through the well screen, thereby degrading the well's performance.

Chapter 7 – Conclusions and Recommendations

7.1 Conclusions

Pressure pulsing simulation results reveal that repeated sudden onset of injection cessation produces brief periods of gradient reversal near the injection well and the development of a mixing zone around the injection well. The spatial extents of this mixing zone are highly dependent upon the hydraulic diffusivity of the medium. Greater heterogeneity in combination with presence of high hydraulic diffusivity pathways maximized the extent of the mixing zone and the magnitude of transverse and reversal hydraulic gradients. Lower pulsing frequency and higher pulsing amplitude favoured a more significant mixing zone, though these effects were secondary to geologic properties.

Solute transport simulation results demonstrated augmentation of dispersion arising from the mixing zone phenomenon. This demonstrates an opportunity to augment diffusive mass fluxes of injected amendments into immobile porosity.

Use of the pressure pulsing tool did not manifest into changes in tracer breakthrough at either field research site that could be clearly deciphered above noise arising from formation development and sorption. Formation development around the injection well at CFB Borden was incomplete until a full scale injection had been conducted, and development improved distribution of injected aqueous amendments. The impact of repeated injection on formation development at the North Campus site was unclear due to the development of preferred flow pathways to ground surface early during the first injection. Maximum modelled injection pressures prescribed by the geotechnical properties of overburden stress, and internal angle of friction were exceeded at both field sites. Fluorescent dyes sorbed considerably. Sorption rendered Sulforhodamine B unsuitable as a conservative groundwater tracer. The impact of sorption on Rhodamine WT analysis was mitigated greatly by isolating data associated with the low-sorption isomer.

Formation pressurization at field sites was lower during pressure pulsing for a given injection flow rate. The 3D model results contradicted field observations, demonstrating greater pressurization and slower stabilization. This discrepancy may be a function of the assumptions used to build the model domain.

Both numerical and field results demonstrated that gradient reversals associated with pressure pulsing can act to prevent well blockage during injection.

7.2 Recommendations

Experimental findings revealed a few opportunities for additional research, including the following:

(1) **Investigation of lower frequency pressure pulsing**. There is evidence to suggest that a lower pulsing frequency allows responses to pressure changes at the injection well to penetrate further into the formation. Lower frequency pulsing also sustains mixing gradients longer, which could increase diffusive fluxes into immobile porosity. It may be of interest to investigate the effects of modulating boundary pressure at lower frequencies beyond the range investigated during this research.

(2) **Investigate prospect of a pressure pulsing instrument designed to allow back-flow.** Integrating free back-flow into the pressure pulsing cycle would expedite pressure depletion in high-hydraulic-diffusivity zones during the no-flow period. This would increase mixing zone extents and transverse gradient magnitudes. This functionality presents an opportunity to enhance the effectiveness of pressure pulsing as a tool that promotes a more uniform delivery of reagents around an injection well.

(3) **Groundwater flow and solute transport data collected from additional injections at additional field sites.** The complexity of natural subsurface media greatly limits the control achievable for field-based research. Documentation of multiple injections in multiple geologic environments would be required to ascertain the effects of pressure pulsing. An emphasis on solute transport data acquisition with high temporal resolution is recommended.

References

Alexander, M. (2009). Evaluation of Traditional Hydrogeologic Characterization Approaches n a Highly Heterogeneous Glaciofluvial Aquifer/Aquitard System. Master's Thesis, Department of Earth Science, University of Waterloo, Waterloo, ON

Bauer, R.D.; Rolle, M.; Bauer, S; Eberhardt, C.; Grathwohl, P.; Kolditz, O.; Meckenstock, R.U.; Griebler, C. (2009). Enhanced Biodegradation by Hydraulic Heterogeneities in Petroleum Hydrocarbon Plumes. J Contaminant Hydrology 105: 56-68

Bencala, K.E.; Kennedy, V.C.; Zellweger, G.W.; Jackman, A.P.; Avanzino, R.J. (1984). Interactions of Solutes and Streambed Sediment 1. An Experimental Analysis of Cation and Anion Transport in a Mountain Stream. Water Resour Res 20(12): 1797-1803

Biot, M.A. (1956). Theory of Propagation of Waves in a Fluid-Saturated Porous Solid I. Low-Frequency Range. J. Of the Acoustical Society of America 28 (2): 168-178.

Bouwer, H.; Rice, R.C. (1976). A Slug Test Method for Determining Hydraulic Conductivity of Unconfined Aquifers with Completely or Partially Penetrating Wells. Water Resource Research 12(3): 423-428

Brough, M. J.; Martin, R. J.; Al-Tabbaa A. (1998). In situ subsurface active bioFilm barriers. Ground Engineering, 31(3): 32.

Butler, J.J.; Healey, J.M.; McCall, G.W.; Garnett, E.J.; Loheide, S.P. (2002). Hydraulic Tests with Direct-Push Equipment. Ground Water 40(1): 25-36

Cable, A.S.; Dorey, M.P.; Goodyear, S.G.; Jayasekera, A.J. (2001). Pulse Injection Technology for IOR. In proceedings of 11th European Symposium on Improved Oil Recovery – Amsterdam, The Netherlands

Chang, P.; Abranovic, D.; Gilbertsen, J.; Brown, R.A. (2007). Biodegradation of Petroleum Hydrocarbons under Nitrate-Reducing Conditions: Bench and Field Results. In proceedings of 9th International In Situ and On-Site Bioremediation Symposium pp. 150-157

Christiansen, C.M.; Riis, C.; Christensen, S.B.; Broholm, M.M.; Christensen, A.G.; Klint, K.E.; Wood, J.S.A.; Bauer-Gauttwein, P.; Bjerg, P.L. (2008). Characterisation and Quantification of Pneumatic Fracturing at a Clay Till Site. Environ. Sci. Tech. 42: 570-576

Darwish, M.I.M.; McCray, J.E.; Currie, P.K.; Zitha, P.L.J. (2003). Polymer-Enhanced DNAPL Flushing from Low-Permeability Media: An Experimental Study. Groundwater Monitoring and Remediation 23(2): 92-101

Davidson, B.C.; Spanos, T.J.T.; Dusseault. M.B. (1999). Laboratory Experiments on Pressure Pulse Flow Enhancement in Porous Media. Proceedings of the CIM Regina Technical Meeting, Oct. 1999.

Davis, W.M.; Wise, M.B.; Furey, J.S.; Thompson, C.V. (1998). Rapid Detection of Volatile Organic Compounds in Groundwater by In Situ Purge and Direct-Sampling Ion-Trap Mass Spectrometry. Field Analytical Chemistry and Technology 2(2): 89-96

Day, S.R..; Ryan, C.R. (1995). Containment, stabilization, and treatment of contaminated soils using in situ soil mixing. American Society of Civil Engineers, in proceedings of Geoenvironment 2000 (Geotechnical Special Publication no. 46): Characterisation, Containment, Remediation, and Performance in Environmental Geotechnics.

de la Cruz, V.; Sahay, P.N.; Spanos, T.J.T. (1993). Thermodynamics of Porous Media. Proceedings: Mathematical and Physical Sciences 443(1917): 247-255.

de la Cruz, V.; Spanos, T.J.T. (1985). Seismic Wave Propagation in a Porous Medium. Geophysics 50(10): 1556-1565

de la Cruz, V.; Spanos, T.J.T. (1989). Thermomechanical Coupling during Seismic Wave Propagation in a Porous Medium. Journal of Geophysical Research. 94(B1): 637-642

Frank, U.; Barkley, N. (1995). Remediation of low-permeability subsurface formations by fracturing enhancement of soil vapour extraction. J. Hazardous Materials 40: 191-201

Franson, M.A.H. (1998). Standard Methods for the Examination of Water and Wastewater 20th Ed. American Public Health Association, Washington, D.C.

Frind, E.O.; Molson, J.W.; Schirmer, M.; Guiguer, N. (1999). Dissolution and mass transfer of multiple organcs under field conditions: The Borden emplaced source. Water Resour. Res. 35: 683-694

Gassman, F. (1951). Uber die elastizitat poroser medien: Ver der Natur. Gesellschaft 96, 1-23.

Geilikman, M.B.; Spanos, T.J.T.; Nyland, E. (1993). Porosity Diffusion in Fluid-Saturated Media. Tectonophysics, 217: 111-115.

Grotenhuis, J.T.C.; Rjnaars, H.H.H.M. (2011). Dealing with Contaminated Sites Chapter 21: In Situ Remediation Technologies. Springer Science+Business Media: Dordrecht

Harbough, A.W. (2005). MODFLOW-2005, The U.S. Geological Survey Modular Ground-Water Model-the Ground-Water Flow Process. U.S. Geological Survey, Reston, VA

Harvey, J.W.; Bencala, K.E. (1993). The Effect of Streambed Topography on Surface-Subsurface Water Exchange in Mountain Catchments. Water Resour Res 29(1): 89-98

Hubbert, M.K. (1940). The Theory of Ground-water Motion. Journal of Geology 48(8): 785-944

Interstate Technology and Regulatory Council Chemical Oxidation Team, The (2005). Technical and Regulatory Guidance for In Situ Chemical Oxidation of Contaminated Soil and Groundwater (2nd Ed). Interstate Technology and Regulatory Council

Karrow, P.F. (1979). Quaternary Geology of the University of Waterloo Campus. Department of Earth Sciences, University of Waterloo, Waterloo, ON

Kent, B.; Bianchi Mosquera, G.G. (2001). Remediaton of NAPL-contaminated Aquifers: is the Cure Worth the Cost? Journal of Envronmental Science and Health. A36(8): 1559-1569

Lambert, J.M.; Tianxiao, Y.; Thomson, N.R.; Barker, J.F.(2009). Pulsed Sparging of a Residual Fuel Source Emplaced at CFB Borden. In Proceedings of The Annual International Conference on Soils, Sediments, Water and Energy 14, Article 5

Lunn, S.R.D.; Kueper, B.H. (1999). Manipulation of Density and Viscocity for the Optimization of DNAPL recovery by Alcohol Flooding. Journal of Contaminant Hydrology 38: 427-445

Luo, J.; Wu, Wei-Min; Carley, J.; Ruan, C.; Gu, B.; Jardine, P.M.; Criddle, C.S.; Kitanidis, P.K. (2007). Hydraulic Performance Analysis of a Multiple Injection-Extraction Well System. J Hydrology 336: 294-302

Martel, K.E.; Martel, R.; Lefebvre, R.; Gelinas, P.J. (1998). Laboratory Study of Polymer Solutions Used for Mobility Control During In Situ NAPL Recovery. Groundwater Monitoring and Remediation 18(3): 103-113

McCray, J.E.; Munakata-Marr, J.; Silva, J.A.K.; Davenport, S.; Smith, M.M. (2010). Multi-scale Experiments to Evaluate Mobility Control Methods for Enhancing the Sweep Efficiency of Injected Subsurface Remediation Amendments. Final Report to Department of Defence Strategic Environmental Research and Development Program. Colorado School of Mines, Golden, CO

McKay, D.M.; Freyberg, D.L.; Roberts, P.V. (1986). A Natural Gradient Experiment on Solute Transport in a Sand Aquifer 1. Approach and Overview of Plume Movement. Water Resour Res 22: 2017-2029

Mocanu, M.C. (2007). Behaviour of Oxygenates and Aromatic Hydrocarbons in Groundwater from Gasoline Residuals. Master's Thesis, Department of Earth Science, University of Waterloo, Waterloo, ON

Morrison, W.E. (1998). Hydrogeological Controls on Flow and Fate of PCE DNAPL in a Fractured and Layered Clayey Aquitard: A Borden Experiment. Master's Thesis, Department of Earth Science, University of Waterloo, Waterloo, ON

Murdoch, L.C.; Slack, W.W. (2002). Forms of Hydraulic Fractures in Shallow Fine-Grained Formations. J. Geotech & Geoenviro Eng. 126(6): 479-487

National Research Council of the National Academies (2005). Contamination in the Subsurface: Source Zone Assessment and Remediation. Washington, DC: The National Academies Press

Neville, C.J.; Tonkin, M.J. (2004). Modelling Multiaquifer Wells with Modflow. Groundwater 42(6): 910-919

Nichols, H.F.; Lazar, B.J., Rabah, N.M.; Lippencott, R.J.; Hicks, P.; Carlson, B. (2009). Optimization of In-Situ Injection and Bioremediation Design at a Brownfield Site. In proceedings of Tenth International In Situ and On-Site Bioremediation Symposium. Baltimore, MD, May 2009

Nikolaevskiy, V.N.; Lopukhov, G.P.; Liao, Y.; Economides, M.J. (1996). Residual Oil Reservoir Recovery with Seismic Vibrations. SPE Production and Facilities, May 1996.

Oostrom, M.; Wietsman, T.W.; Covert, M.A.; Vermeul, V.R. (2007). Zero-Valent Iron Emplacement in Permeable Porous Media Using Polymer Additions. Groundwater Monitoring and Remediation 27(1): 122-130

Parker, B.L.; Gillham, R.W. (1994). Diffusive disappearance of immiscible-phase organic liquids in fractured geologic media. Ground water 32(5): 805-820

Payne, F.C.; Quinnan, J.A.; Potter, S.T. (2008). Remediation Hydraulics. CRC Press: Boca Raton, FL

Reilly, T.E.; Franke, O.L..; Bennett, G.D. (1989). Bias in Groundwater Samples Caused by Wellbore Flow. J Hydraulic Engineering 115(2): 270-276

Rolle, M.; Eberhardt, C.; Chiogna, G.; Cirpka, O.A.; Grathwohl, P. (2009). Enhancement of Dilution and Transverse Reactive Mixing in Porous Media: Experiments and Model-based Interpretation. J Contaminant Hydology 110: 130-142

Saenton, S.; Illangasekare, T.H..; Soga, K.; Saba, T.A. (2002). Effects of Source Zone Heternogeniety on Surfactant-Enhanced NAPL Dissolution and Resulting Remediation End-Points. J. Contam. Hydrol. 59: 27-44

Samaroo, M. (1999). Pressure Puse Enhancement: Report on the First Reservoir Scale Experiment Conducted by PE-Tech in Section 36 of Wascana Energy Inc.'s Morgan Field Lease. Master's Thesis, Department of Earth Science, University of Waterloo, Waterloo, ON

Schulmesiter, M.K.; Butler, J.J.; Healey, J.M.; Zheng, L.; Wysocki, D.A.; McCall, G.W. (2003). Direct-Push Electrical Conductivity Logging for High-Resolution Hydrostratigraphic Characterisation. Groundwater Monitoring & Remediation 23(3): 52-62

Schuring, J.R.; Chan, P.C.; Boland, T.M. (1995). Using Pneumatic Fracturing for In-Situ Remediation of Contaminated Sites. Remediation Journal 5(2): 77-90.

Sebol, L.A. (2000). Determination of Groundwater Age using CFC's in Three Shallow Aquifers in Southern Ontario. Ph.D. Thesis, Department of Earth Science, University of Waterloo, Waterloo, ON

Siegrist, R.L.; Lowe, K.S.; Murdoch, L.C.; Case, T.L.; Pickering, D.A. (1999). In Situ Oxidation by Fracture Emplaced Reactive Solids. J. Enviro. Eng. 125(5): 429-440

Spanos, T.J.T. (2009). Seismic Wave Propagation in Composite Elastic Media. Transp. Porous Med. 79: 135-148

Sudicky, E.A.; Cherry, J.A.; Frind, E.O. (1983). Migration of Contaminants in Groundwater at a Landfill: A Case Study 4. A Natural Gradient Dispersion Test. Journal of Hydrology 63: 81-108

Sudicky, E.A. (1986). A Natural Gradient Experiment on Solute Transport in a Sand Aquifer: Spatial Variability of Hydraulic Conductivity and its Role in the Dispersion Process. Water Resour Res 22(13): 2069-2082

Thomson, N.R.; Fraser, M.J.; Lamarche, C.; Barker, J.F.; Forsey, S.P. (2008). Rebound of a Coal Tar Creosote Plume Following Partial Source Zone Treatment with Permanganate. Journal of Contaminant Hydrology 102: 154-171

Univesity of Waterloo (2011). Directions and Map. Retrieved July 7 2011 from: <http://uwaterloo.ca/map>. University of Waterloo, Waterloo, ON

Waller, R.M.; Thomas, H.E.; Vorhis, R.C. (1965) Effects of the Good Friday Earthquake on Water Supplies. J. Am. Waterworks Assoc. 57(2): 123-131.

Wavefront Reservoir Technologies Ltd. Canada Patent 2663703 (2009)

Wang, J. (1999). Flow Rate Enhancement Under Liquid Pressure Pulsing. Master's Thesis, Department of Civil Engineering, University of Waterloo, Waterloo, ON

Weeks, S.W.; Sposito, G. (1998). Mixing and Stretching Efficiency in Steady and Unsteady Groundwater Flows. Water Resour Res 34(12): 3315-3322

Woynillowicz, A.C. (2000). Pressure Pulsing for Aquifer Remediation. Undergraduate Thesis, Department of Civil Engineering, University of Waterloo, Waterloo, ON

Wrenn, B.A.; Suidan, M.T.; Strohmeier, K.L.; Eberhart, B.L.; Wilson, G.J.; Venosa, A.D. (1997). Nutrient Transport during Bioremediation of Contaminated BeachesL Evolution with Lithium as a Conservative Tracer. Water Resour Res 31(3): 1997

Yeskis, D.; Zavala, B. (2002). Ground-Water Sampling Guidelines for Superfund and RCRA Project Managers. United States Environmental Protection Agency, Washington, D.C.

Zschuppe, R.P. (2001). Pulse Flow Enhancement in Two-Phase Media. Master's Thesis, Department of Earth Science, University of Waterloo, Waterloo, ON

Zhang, P.; Devries, S.L.; Dathe, A.; Bagtzoglou, A.C. (2009). Enhanced Mixing and Plume Containment in Porous Media under Time-Dependent Oscillatory Flow. Envron Sci Technol 43: 6283-6288

Zheng, C.; Wang, P.P. (1999). MT3DMS: A Modular Three-Dimensional Multispecies Transport Model for Simulation of Advection, Dispersion, and Chemical Reactions of Contaminants in Groundwater Systems; Documentatio and User's Guide. U.S. Army Corps of Engineers, Washington, D.C.

Zhong, L.; Szecsody, J.; Oostrom, M.; Truex, M.; Shen, X.; Li, X. (2011). Enhanced Remedial Amendment Delivery to subsurface using shear thinning fluid and aqueous foam. Journal of Hazardous Materials 191: 249-257

Appendix A – Supplemental CFB Borden Injection Information

Holding tanks used to store tracer solution at surface (total 7500 L capacity)

Injection site showing injection set-up with Sidewinder® tool

Multilevel well-head, including adaptor tubing used to connect syringes

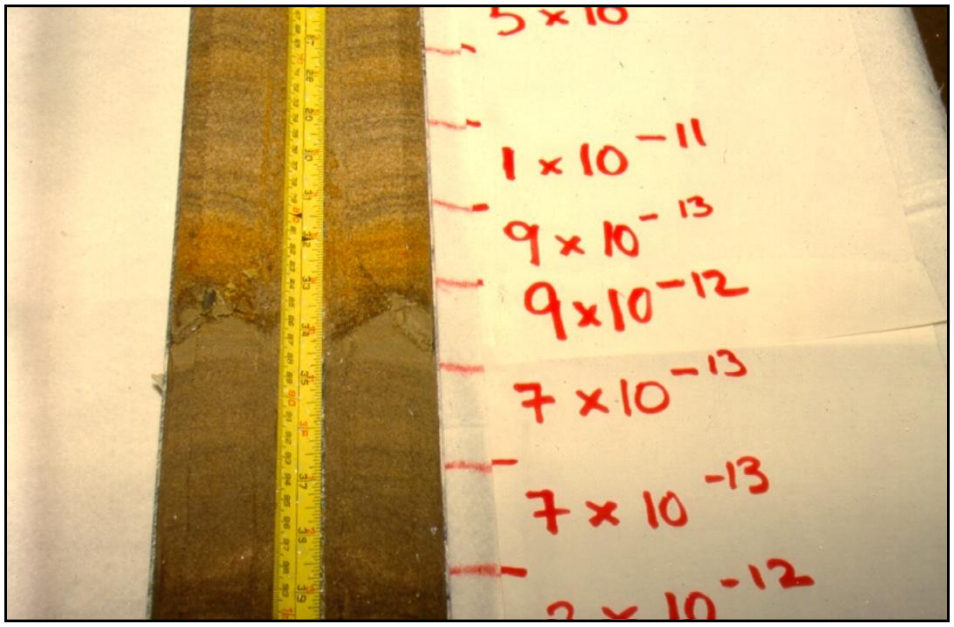

Core recovered from the CFB Borden site exemplifying laminated fine sand

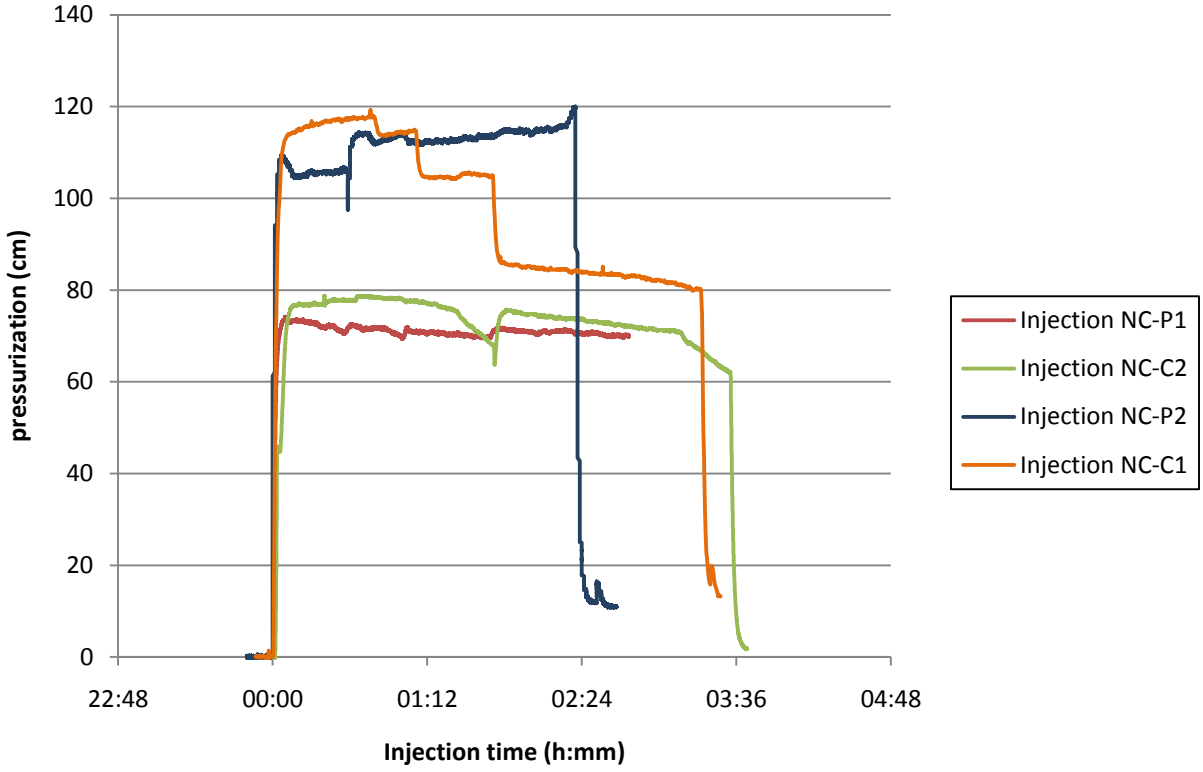

HWB2 formation pressurization time series

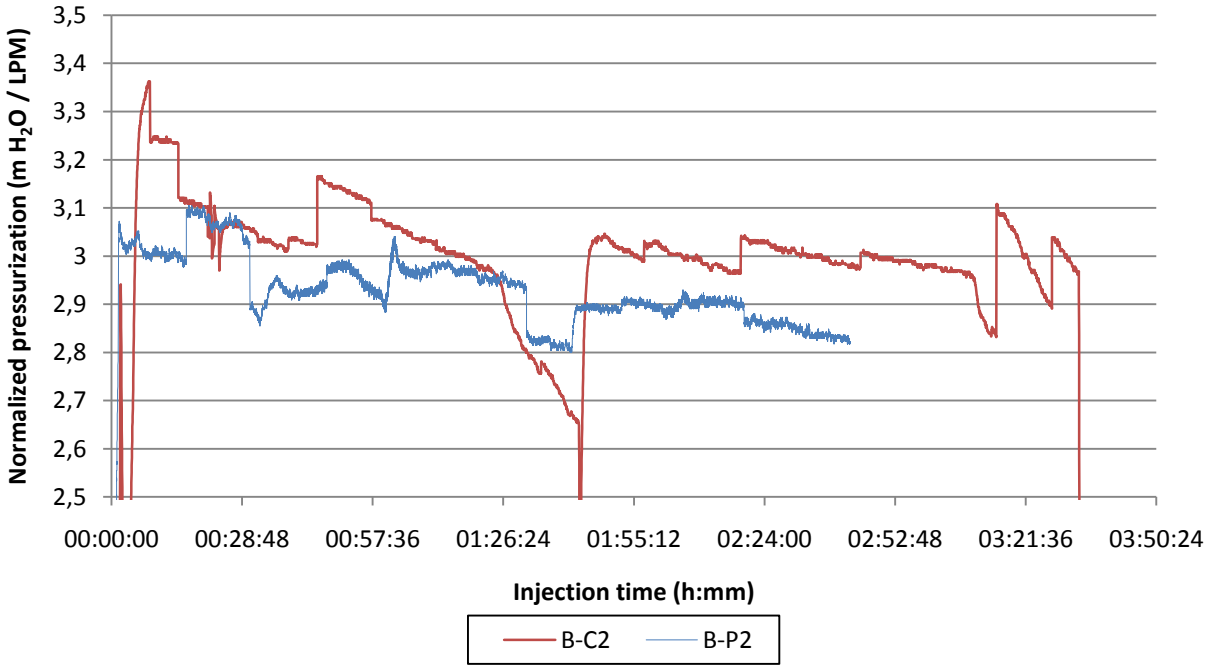

HWB1 formation pressurization time series for injections B-C2 and B-P2 normalized to injection flow rate

Appendix B – Supplemental North Campus Injection Information

Water pooling at ground surface during injection

Holding tanks used to store tracer solution at ground surface (3250 L capacity)

North Campus Injection site wells (looking north)

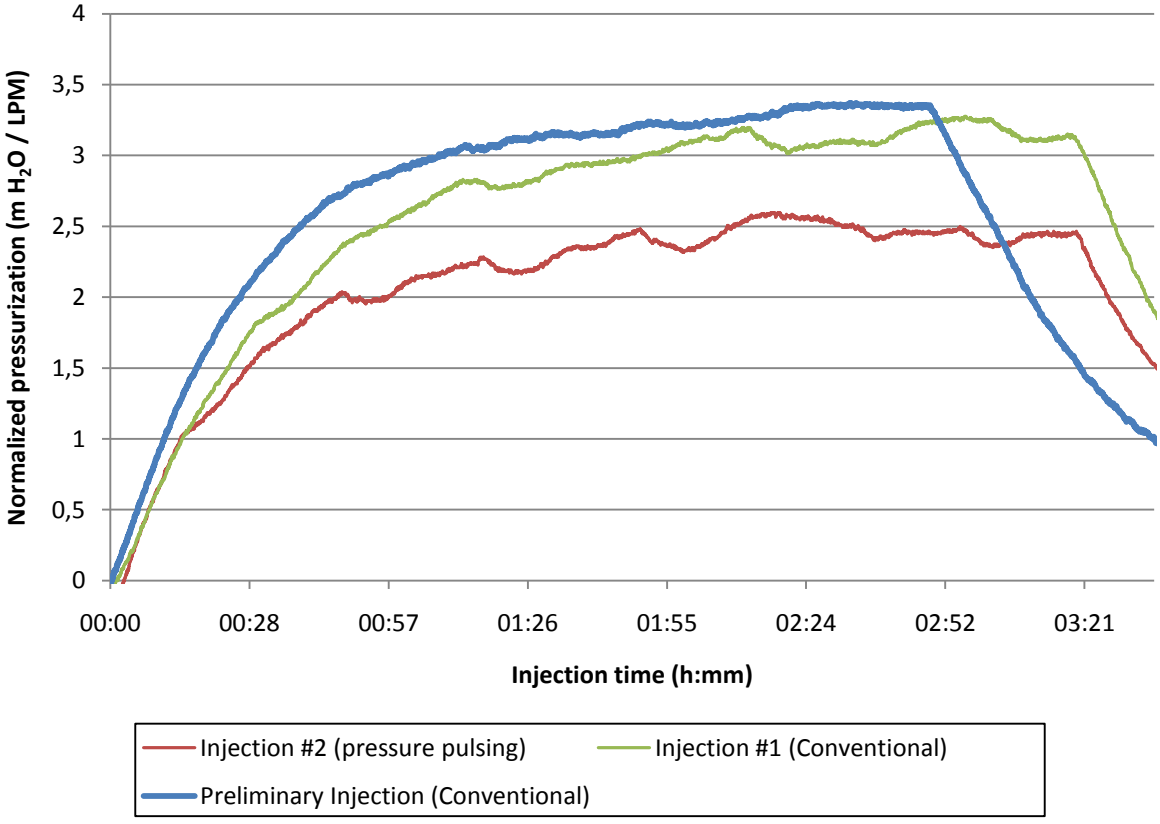

HWNC1 formation pressurization time series normalized to injection flow rate

Injection NC-C2 tabulated bromide relative concentrations

MLNC1				MLNC05			
Port	Inj. Time		C/Co	Port	Inj. Time		C/Co
	h:mm	min			h:mm	min	
2	3:15	196	0.00	10	3:46	227	0.02
2	1:00	60	0.00	10	1:21	81	0.00
2	2:25	146	0.00	10	2:17	138	0.00
3	2:26	147	0.00	10	0:00	0	0.00
3	0:42	42	0.00	10	3:07	188	0.01
3	3:16	197	0.00	10	0:35	35	0.00
4	2:27	148	0.00	9	2:14	135	0.00
4	3:17	198	0.00	9	1:18	78	0.00
4	0:45	45	0.00	9	2:17	138	0.00
5	3:21	202	0.00	9	0:33	33	0.00
5	2:31	152	0.00	9	3:07	188	0.00
5	1:45	106	0.00	9	0:00	0	0.00
5	0:46	46	0.00	8	3:43	224	0.00
6	0:49	49	0.00	8	0:00	0	0.00
6	2:32	153	0.00	8	3:03	184	0.00
6	3:22	203	0.00	8	0:32	32	0.00
7	0:49	49	0.00	8	2:14	135	0.00
7	2:32	153	0.00	8	1:17	77	0.00
7	3:23	204	0.00	7	2:13	134	0.00
8	0:53	53	0.00	7	0:29	29	0.00
8	2:36	157	0.00	7	2:59	180	0.00
8	3:27	208	0.86	7	1:14	74	0.00
9	0:52	52	0.00	7	0:00	0	0.00
9	2:37	158	0.00	7	3:40	221	0.00
9	3:28	209	0.58	6	2:09	130	0.00
10	2:42	163	0.00	6	2:58	179	0.00
10	0:55	55	0.00	6	3:40	221	0.00
10	2:01	122	0.00	6	0:29	29	0.00
10	3:30	211	0.00	6	1:14	74	0.00
MLNC05				5	2:58	179	0.00
Port	Inj. Time		C/Co	5	2:09	130	0.00
	h:mm	min		5	1:11	71	0.00
3	2:53	174	0.02	5	0:20	20	0.00
3	3:35	216	0.10	5	3:39	220	0.00
3	2:05	126	0.00	4	2:08	129	0.01
2	2:52	173	0.25	4	2:54	175	0.01
2	1:06	66	0.01	4	1:10	70	0.01
2	2:05	126	0.01	4	2:20	140	0.01
2	0:17	17	0.01	4	3:36	217	0.01
2	3:34	215	0.34	3	1:06	66	0.00
Surface	1:57	117	0.87				

Injection NC-P tabulated lithium relative concentrations

MLNC05				MLNC1			
Port	Inj. Time		Conc.	Port	Inj. Time		Conc.
	h:mm	min			h:mm	min	
10	0:21	21	0.00	10	0:39	39	0.00
10	0:54	54	0.00	10	1:09	69	0.01
10	1:57	117	0.00	10	1:44	104	0.00
10	2:36	156	0.00	10	2:23	143	0.05
10	3:00	180	0.01	10	2:50	170	0.00
10	3:24	204	0.02	10	3:15	195	0.01
9	0:18	18	0.00	3	0:27	27	0.00
9	0:52	52	0.00	3	0:59	59	0.01
9	1:22	82	0.00	3	2:12	132	0.01
9	1:55	115	0.00	3	2:39	159	0.00
9	2:34	154	0.00	3	3:05	185	0.00
9	2:59	179	0.00	4	0:27	27	0.00
9	3:23	203	0.00	4	0:45	45	0.00
8	0:18	18	0.00	4	1:00	60	0.01
8	0:52	52	0.00	4	2:13	133	0.00
8	1:21	81	0.00	4	2:40	160	0.00
8	1:53	113	0.00	4	3:06	186	0.04
8	2:33	153	0.00	5	0:29	29	0.01
8	2:58	178	0.00	5	1:00	60	0.00
8	3:22	202	0.00	5	2:13	133	0.00
7	0:17	17	0.00	5	2:41	161	0.00
7	0:51	51	0.01	5	3:07	187	0.02
7	1:20	80	0.00	6	0:33	33	0.00
7	1:52	112	0.00	6	1:03	63	0.00
7	2:31	151	0.05	6	2:17	137	0.00
7	2:58	178	0.00	6	2:44	164	0.05
7	3:22	202	0.00	6	3:10	190	0.00
6	0:13	13	0.34	7	0:34	34	0.00
6	0:47	47	0.43	7	1:04	64	0.00
6	1:16	76	0.24	7	1:37	97	0.00
6	1:46	106	0.09	7	2:18	138	0.04
6	2:28	148	0.06	7	2:45	165	0.00
6	2:55	175	0.05	7	3:12	192	0.00
6	3:19	199	0.04	8	0:35	35	0.00
5	0:13	13	0.00	8	1:05	65	0.02
5	0:46	46	0.24	8	1:38	98	0.00
5	1:15	75	0.29	8	2:18	138	0.98
5	1:45	105	0.23	8	2:45	165	0.23
5	2:55	175	0.21	8	3:12	192	0.02

MLNC05				MLNC1			
Port	Inj. Time		Conc.	Port	Inj. Time		Conc.
	h:mm	min			h:mm	min	
5	3:19	199	0.13	9	0:38	38	0.00
4	0:12	12	0.00	9	1:08	68	0.01
4	1:14	74	0.00	9	1:40	100	0.00
4	1:45	105	0.00	9	2:22	142	0.00
4	2:27	147	0.04	9	2:48	168	0.01
4	3:18	198	0.05	9	3:15	195	0.05
Surface	1:39	99	0.79	Surface	1:19	79	1.03
Surface	2:23	143	0.95	Surface	2:39	159	1.08
Surface	3:09	189	1.07	Surface	2:02	122	1.05
Surface	0:50	50	0.92				

Injection NC-P tabulated chloride relative concentrations

MLNC1				MLNC05			
Port	Inj. Time		Conc.	Port	Inj. Time		Conc.
	h:mm	min			min	h:mm	
10	0:39	39	0.00	10	21	0:21	0.00
10	1:09	69	-0.01	10	54	0:54	0.05
10	1:41	101	0.01	10	85	1:25	0.03
10	2:23	143	0.44	10	117	1:57	0.03
10	2:50	170	0.31	10	156	2:36	0.03
10	3:15	195	0.07	10	180	3:00	0.04
3	0:27	27	0.01	10	204	3:24	0.03
3	0:59	59	-0.02	9	0	0:00	0.00
3	1:31	91	-0.02	9	18	0:18	0.05
3	2:12	132	0.02	9	52	0:52	-0.01
3	2:39	159	-0.01	9	115	1:55	0.01
3	3:05	185	0.05	9	154	2:34	0.37
3	0:00	0	0.00	9	179	2:59	0.00
4	0:28	28	0.00	9	203	3:23	-0.02
4	1:00	60	-0.01	8	0	0:00	0.00
4	1:32	92	0.00	8	18	0:18	-0.01
4	2:13	133	0.05	8	52	0:52	-0.02
4	2:40	160	0.06	8	81	1:21	-0.02
4	3:06	186	0.09	8	113	1:53	-0.02
4	0:00	0	0.00	8	153	2:33	0.40
5	0:29	29	0.04	8	178	2:58	0.08
5	1:00	60	0.09	8	202	3:22	-0.02
5	1:33	93	0.06	7	0	0:00	0.00
5	2:13	133	0.05	7	17	0:17	-0.02
5	2:41	161	0.04	7	51	0:51	0.01

MLNC1				MLNC05			
Port	Inj. Time		Conc.	Port	Inj. Time		Conc.
	h:mm	min			min	h:mm	
5	3:07	187	0.01	7	80	1:20	-0.01
5	0:00	0	0.00	7	112	1:52	-0.01
6	0:33	33	0.06	7	151	2:31	0.04
6	1:03	63	0.04	7	178	2:58	0.70
6	1:35	95	0.02	7	202	3:22	-0.02
6	2:17	137	0.01	6	0	0:00	0.00
6	2:44	164	0.06	6	13	0:13	0.23
6	3:10	190	-0.03	6	47	0:47	0.36
6	0:00	0	0.00	6	76	1:16	0.15
7	0:34	34	0.04	6	106	1:46	0.04
7	1:04	64	0.09	6	148	2:28	0.08
7	1:37	97	0.06	6	175	2:55	0.26
7	2:18	138	0.05	6	199	3:19	0.02
7	2:45	165	0.04	5	0	0:00	0.00
7	3:12	192	0.01	5	13	0:13	0.00
7	0:00	0	0.00	5	46	0:46	0.25
8	0:35	35	0.01	5	75	1:15	0.26
8	1:05	65	0.05	5	105	1:45	0.19
8	1:38	98	0.03	5	148	2:28	0.25
8	2:18	138	0.74	5	175	2:55	0.18
8	2:45	165	0.13	5	199	3:19	0.10
8	0:00	0	0.00	4	0	0:00	0.00
9	0:38	38	0.00	4	12	0:12	0.01
9	1:08	68	0.06	4	45	0:45	0.00
9	1:40	100	0.07	4	74	1:14	-0.01
9	2:22	142	0.12	4	105	1:45	-0.01
9	2:48	168	0.33	4	147	2:27	0.02
9	3:15	195	0.19	4	174	2:54	0.03
9	0:00	0	0.00	4	198	3:18	0.04
Surface	0:50	50	0.74	Surface	143	2:23	0.96
Surface	1:19	79	0.76	Surface	159	2:39	0.92
Surface	1:39	99	0.87	Surface	189	3:09	1.54
Surface	2:02	122	0.93				

Appendix C – Sidewinder Tool Operational Protocol

PRIMAWAVE SIDEWINDER FIELD ASSEMBLY

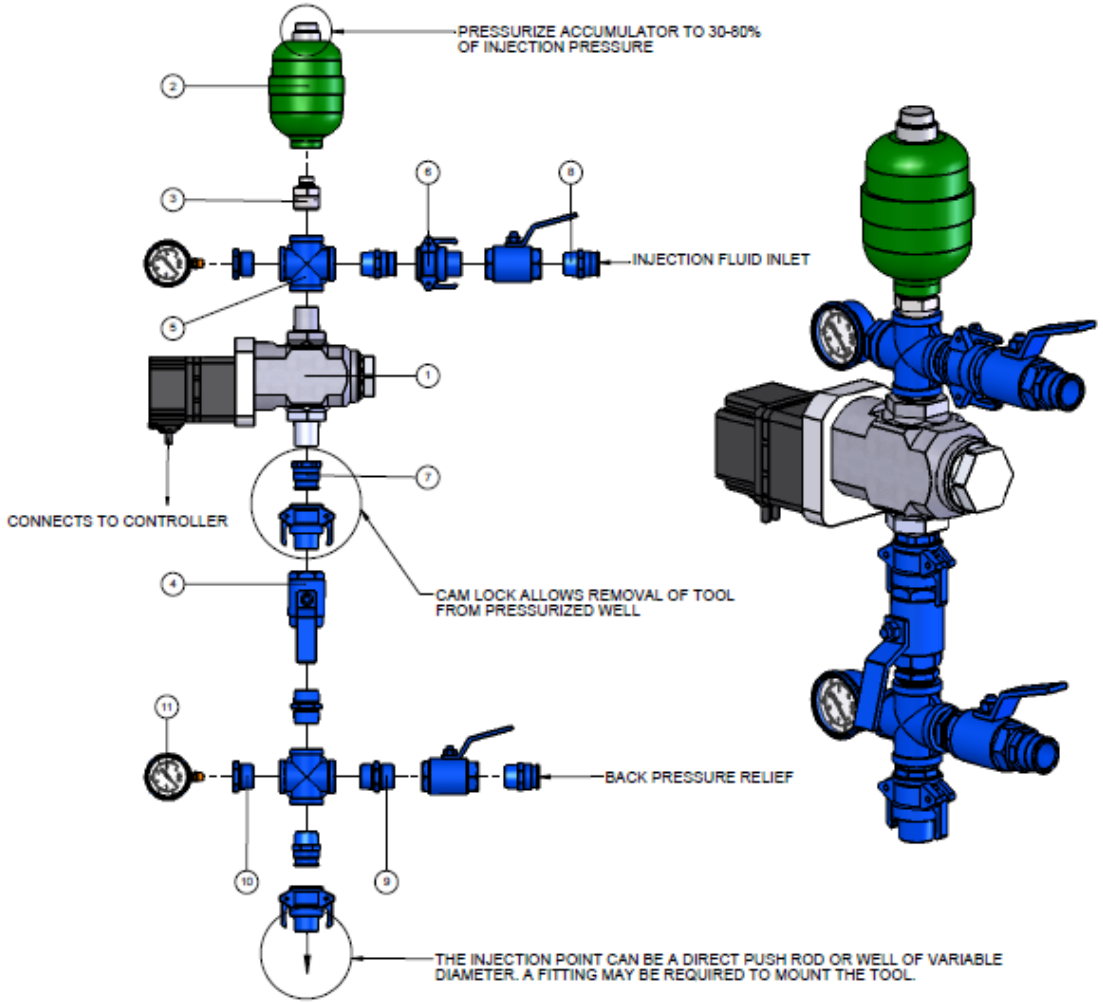

ITEM	PART	QTY	DESCRIPTION	
1	1038WT-000	1	SIDEWINDER TOOL	WAVEFRONT SUPPLIED
2	ACCUMULATOR	1	ACCUMULATOR	WAVEFRONT SUPPLIED
3	ACCUMULATOR REDUCER	1	3/4"-ORB x 1" NPT 316 SS	WAVEFRONT SUPPLIED
4	BALL VALVE	3	1" 316 SS BALL VALVE	CUSTOMER SUPPLIED
5	CROSS	2	1" CROSS	CUSTOMER SUPPLIED
6	FEMALE CAM LOCK	3	1" - MNPT - 316 SS FEMALE CAM LOCK	CUSTOMER SUPPLIED
7	MALE CAM LOCK (FEMALE THREAD)	1	1" - FNPT - 316 SS Male Cam Lock	CUSTOMER SUPPLIED
8	MALE CAM LOCK (MALE THREAD)	4	1" - MNPT - 316 SS Male Cam Lock	CUSTOMER SUPPLIED
9	NIPPLE	2	1" DOUBLE NIPPLE 316 SS	CUSTOMER SUPPLIED
10	PRESSURE GAUGE BUSHING	2	1/4" NPT X 1" NPT BUSHING 316 SS	CUSTOMER SUPPLIED
11	PRESSURE GAUGE	2	PRESSURE RANGE AS REQUIRED	CUSTOMER SUPPLIED

1. SIDEWINDER POWER REQUIREMENTS: AC, 110V, 60HZ
2. TO ENSURE PRIMAWAVE EFFICIENCY, PUMP CAPABILITIES SHOULD BE MAXIMIZED FOR SITE CONDITIONS.
3. A BYPASS TO AUTOMATICALLY LIMIT PUMP PRESSURES IS RECOMMENDED.
4. PRIMAWAVE TOOLS MUST BE MOUNTED DIRECTLY ON THE WELL.
5. THE WELL SHOULD BE SEALED AND NO AIR GAP SHOULD EXIST UNDER THE TOOL
6. CAM-LOCK TIE-BACKS SHOULD BE USED TO PREVENT ACCIDENTAL RELEASE.

WAVEFRONT
#100, 17608 - 103 Ave
Edmonton, AB T5S 1J9
Tel: 780-486-2222
Fax: 780-484-7177

B	SCALE: NTS	SHEET: 1 OF 1	DRAWING NUMBER: FIELD ASSEMBLY	REV: 0

WAVEFRONT

Hornet Tool Operating Instructions

Startup Sequence

1. Connect all cables & tighten all fittings
2. Turn on power switch
   - >> Power switch is illuminated red
   - >> Display panel shows zero
   - >> <*mtr*> and <*r/min*> illuminated solid green
3. Start pump or water flow and check DP gauge
4. Adjust pump or water flow to obtain 15psi DP
5. Press <*Run*> button
   - >> Display panel shows current motor speed in rpm
   - >> This is the last preset motor rpm used/stored
6. Press <*Mode*> button
   - >> <*mtr*> indicator flashes green
7. Press and hold either the ↑ or the ↓ button, as required, until desired motor speed is reached (Range is 80 – 2000 rpm)
   - >> Display panel shows current motor speed
8. Press the <*Set*> button
   - >> <*mtr*> becomes solid green
   - >> Display panel shows the new preset motor speed

Shutdown Sequence

1. Press <*Stop*> button
2. Turn off pump or water flow
3. Turn off power switch

If Alarm Condition Present

1. Turn off power switch

Please Read Operations Manual before Use!!

Wavefront Reservoir Technologies Ltd.
Suite 100, 17608 – 103 Avenue N.W.
Edmonton, AB, T5S 1J9
Telephone: 780 486 2222 Fax: 780 484 7177
Web Address: http://www.onthewavefront.com

RPM Guidelines

K (cm/sec)	RPM
3.87E-03	80
3.78E-03	80
3.68E-03	80
3.58E-03	80
3.48E-03	80
3.39E-03	80
3.29E-03	80
3.19E-03	80
3.10E-03	80
3.00E-03	80
2.90E-03	80
2.81E-03	80
2.71E-03	80
2.61E-03	80
2.52E-03	80
2.42E-03	80
2.32E-03	80
2.23E-03	80
2.13E-03	80
2.03E-03	82
1.94E-03	86
1.84E-03	90
1.74E-03	95
1.65E-03	101
1.55E-03	107
1.45E-03	114
1.36E-03	122
1.26E-03	132
1.16E-03	143
1.06E-03	156
9.68E-04	171

K (cm/sec)	RPM
8.71E-04	190
7.74E-04	214
6.78E-04	245
5.81E-04	286
4.84E-04	343
3.87E-04	429
2.90E-04	571
1.94E-04	857
9.68E-05	89
8.71E-05	99
7.74E-05	112
6.78E-05	127
5.81E-05	149
4.84E-05	178
3.87E-05	223
2.90E-05	297
1.94E-05	446
9.68E-06	892
8.71E-06	991
7.74E-06	1,115
6.78E-06	1,275
5.81E-06	1,487
4.84E-06	1,785
3.87E-06	2,231
2.90E-06	2,500

NEVER OPERATE TOOL DRY

Running a dry tool will result in permanent seal damage

Appendix D – Supplemental 2D Model Information

Pressure time series along segment AA':

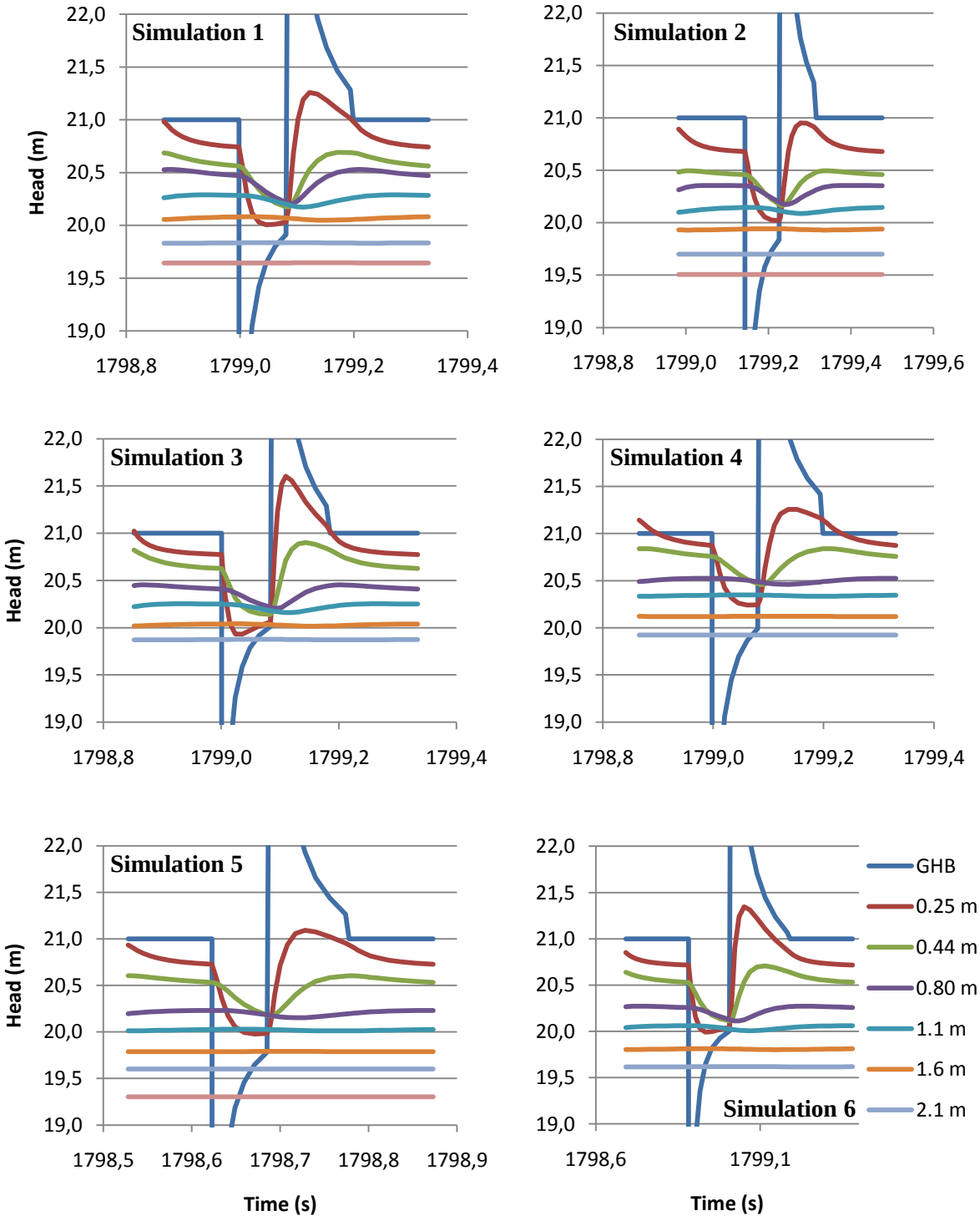

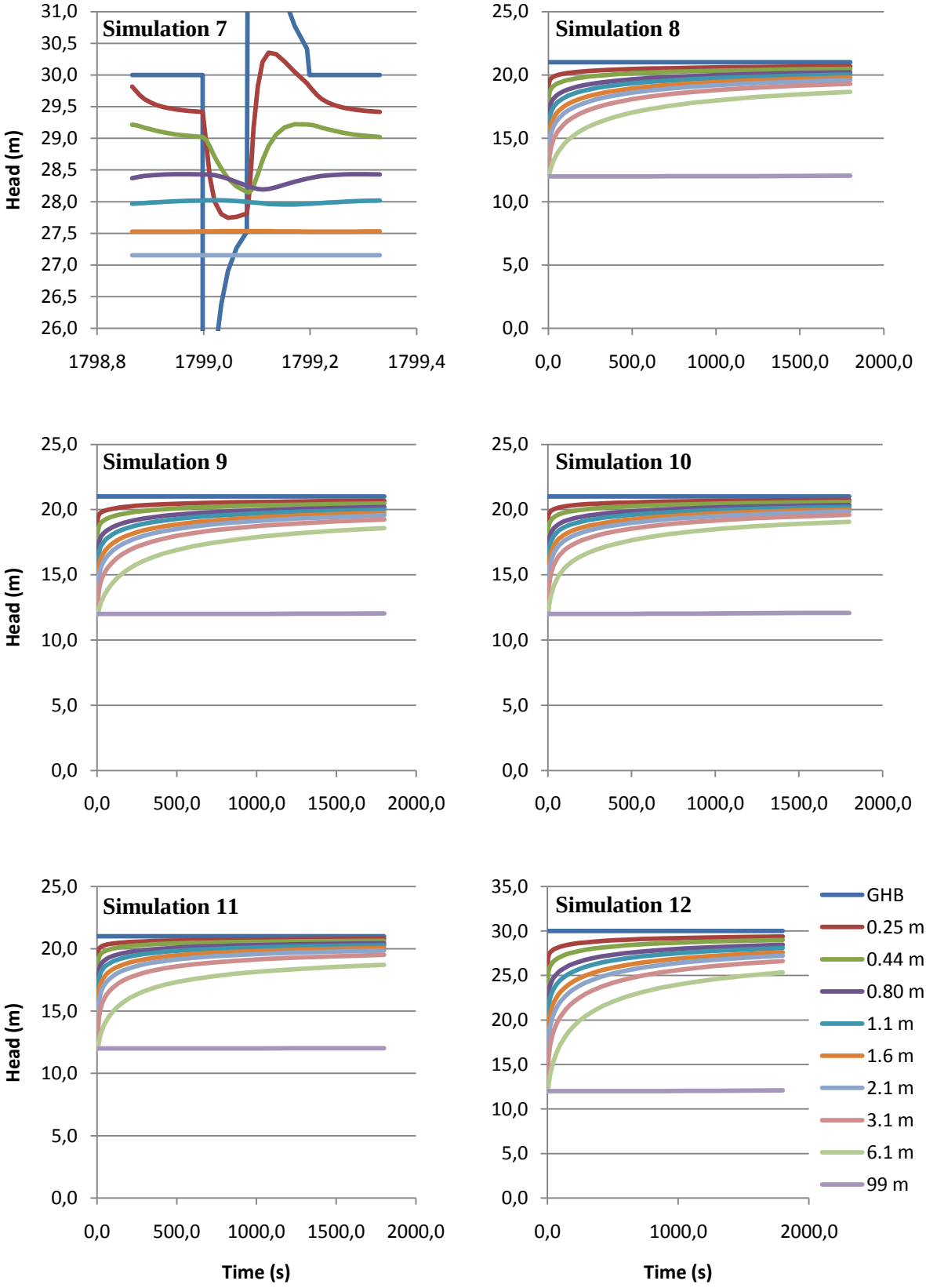
Simulation 7
Simulation 8
Simulation 9
Simulation 10
Simulation 11
Simulation 12
Head (m)
Time (s)
GHB
0.25 m
0.44 m
0.80 m
1.1 m
1.6 m
2.1 m
3.1 m
6.1 m
99 m

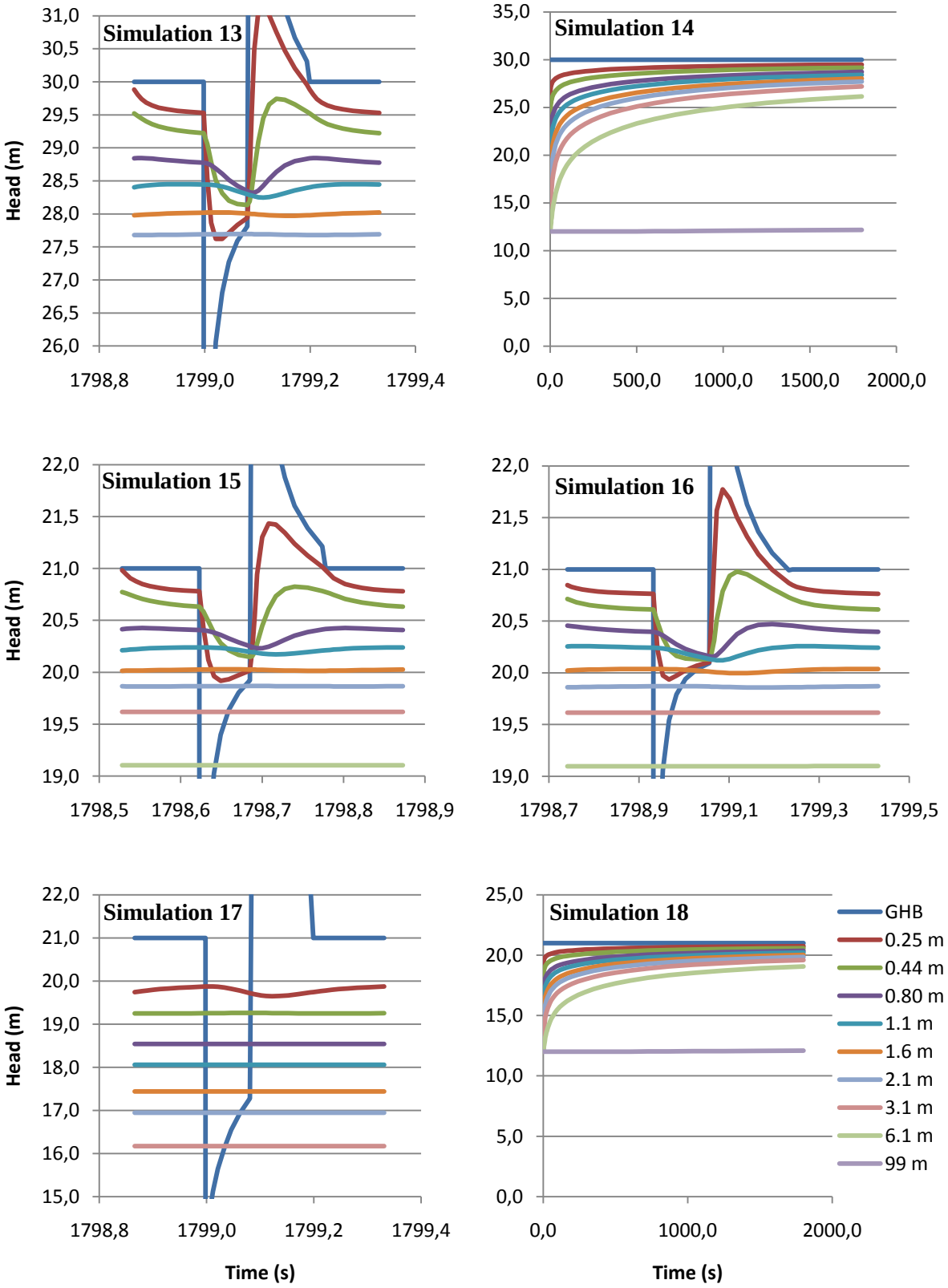
Simulation 13
Head (m)
31,0
30,5
30,0
29,5
29,0
28,5
28,0
27,5
27,0
26,5
26,0
1798,8
1799,0
1799,2
1799,4
Simulation 14
35,0
30,0
25,0
20,0
15,0
10,0
5,0
0,0
0,0
500,0
1000,0
1500,0
2000,0
Simulation 15
Head (m)
22,0
21,5
21,0
20,5
20,0
19,5
19,0
1798,5
1798,6
1798,7
1798,8
1798,9
Simulation 16
22,0
21,5
21,0
20,5
20,0
19,5
19,0
1798,7
1798,9
1799,1
1799,3
1799,5
Simulation 17
Head (m)
22,0
21,0
20,0
19,0
18,0
17,0
16,0
15,0
1798,8
1799,0
1799,2
1799,4
Time (s)
Simulation 18
25,0
20,0
15,0
10,0
5,0
0,0
0,0
1000,0
2000,0
Time (s)
GHB
0.25 m
0.44 m
0.80 m
1.1 m
1.6 m
2.1 m
3.1 m
6.1 m
99 m

Pressure time series along segment BB':

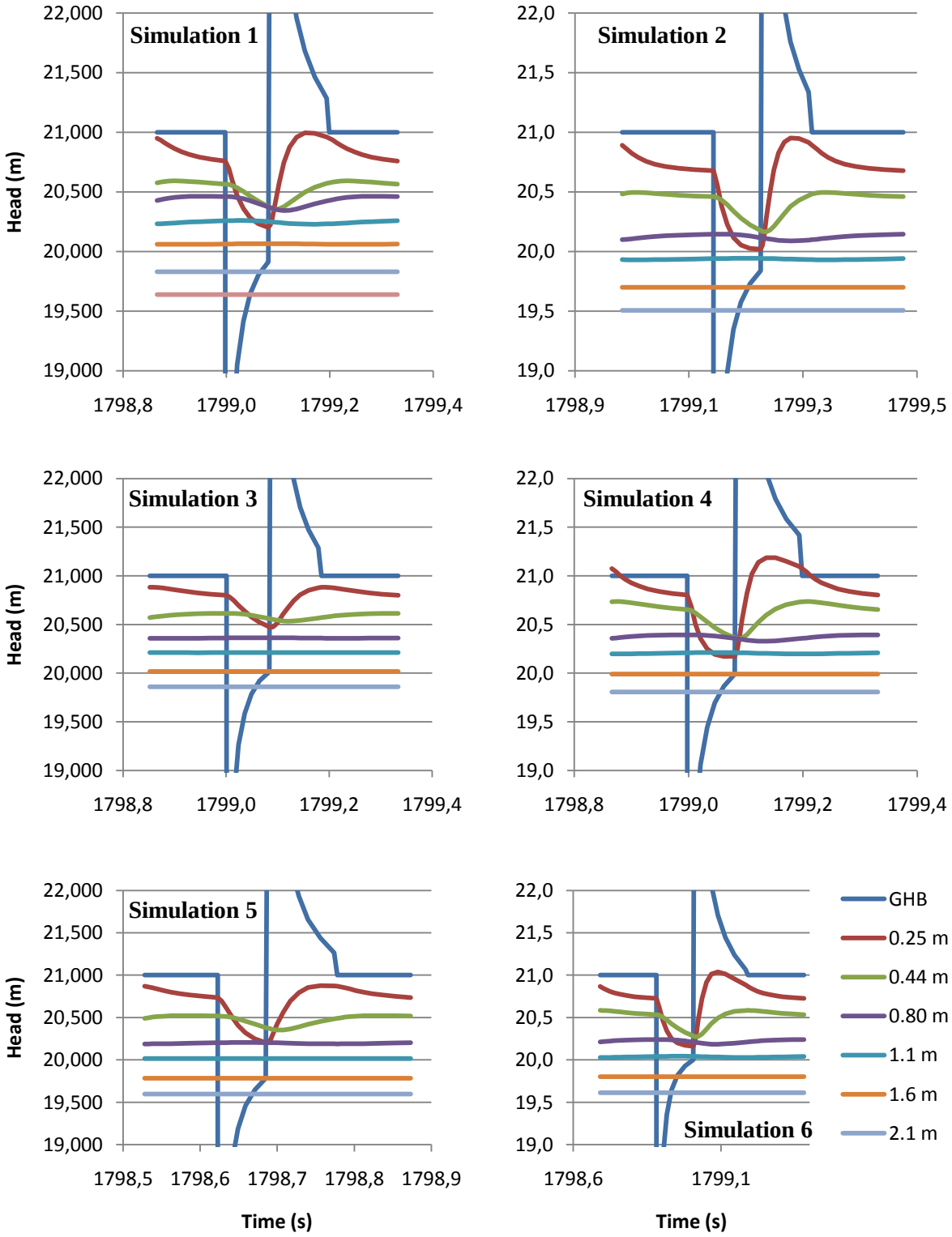

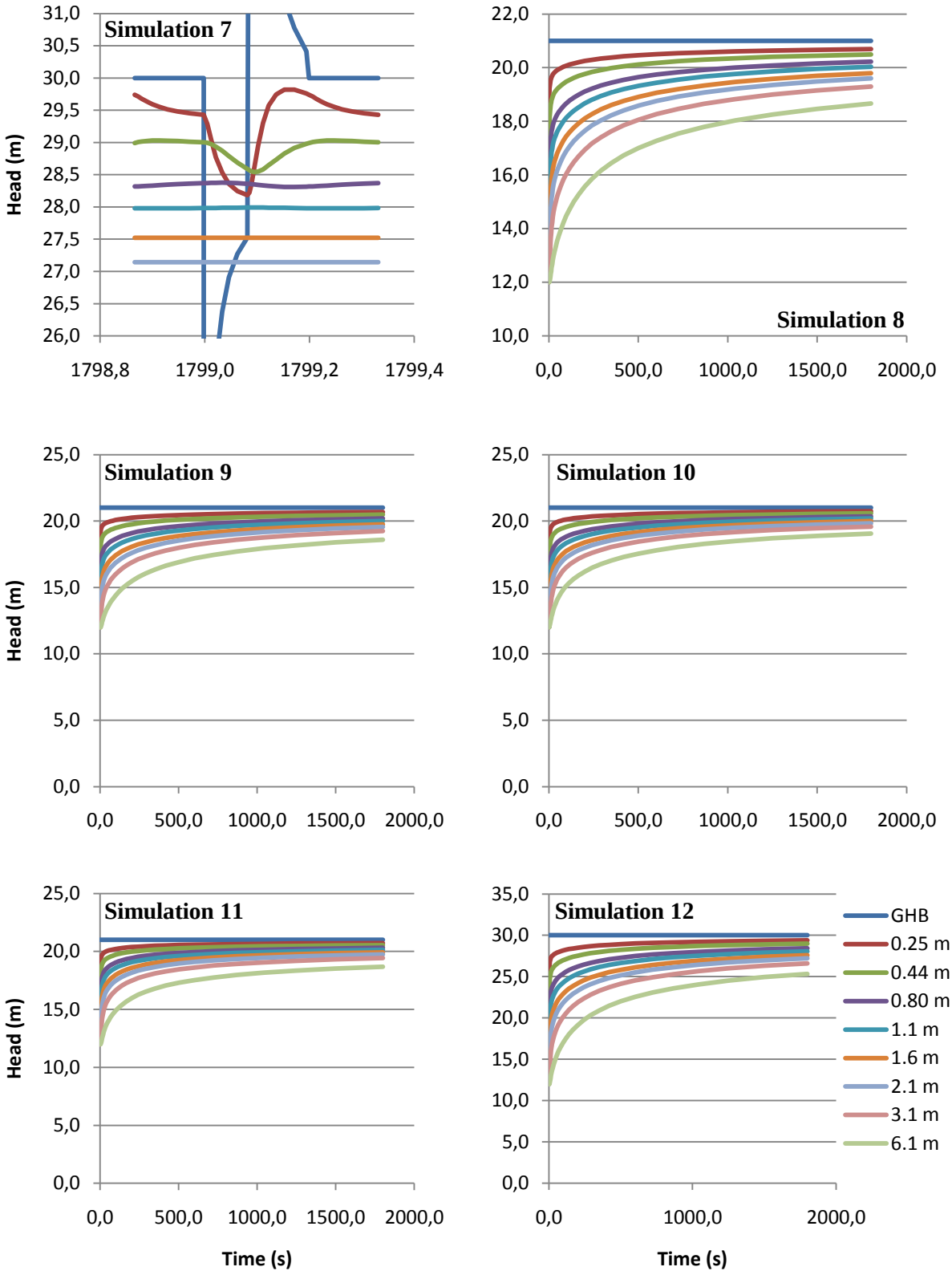
Simulation 7
Simulation 8
Simulation 9
Simulation 10
Simulation 11
Simulation 12
Head (m)
Time (s)
GHB
0.25 m
0.44 m
0.80 m
1.1 m
1.6 m
2.1 m
3.1 m
6.1 m

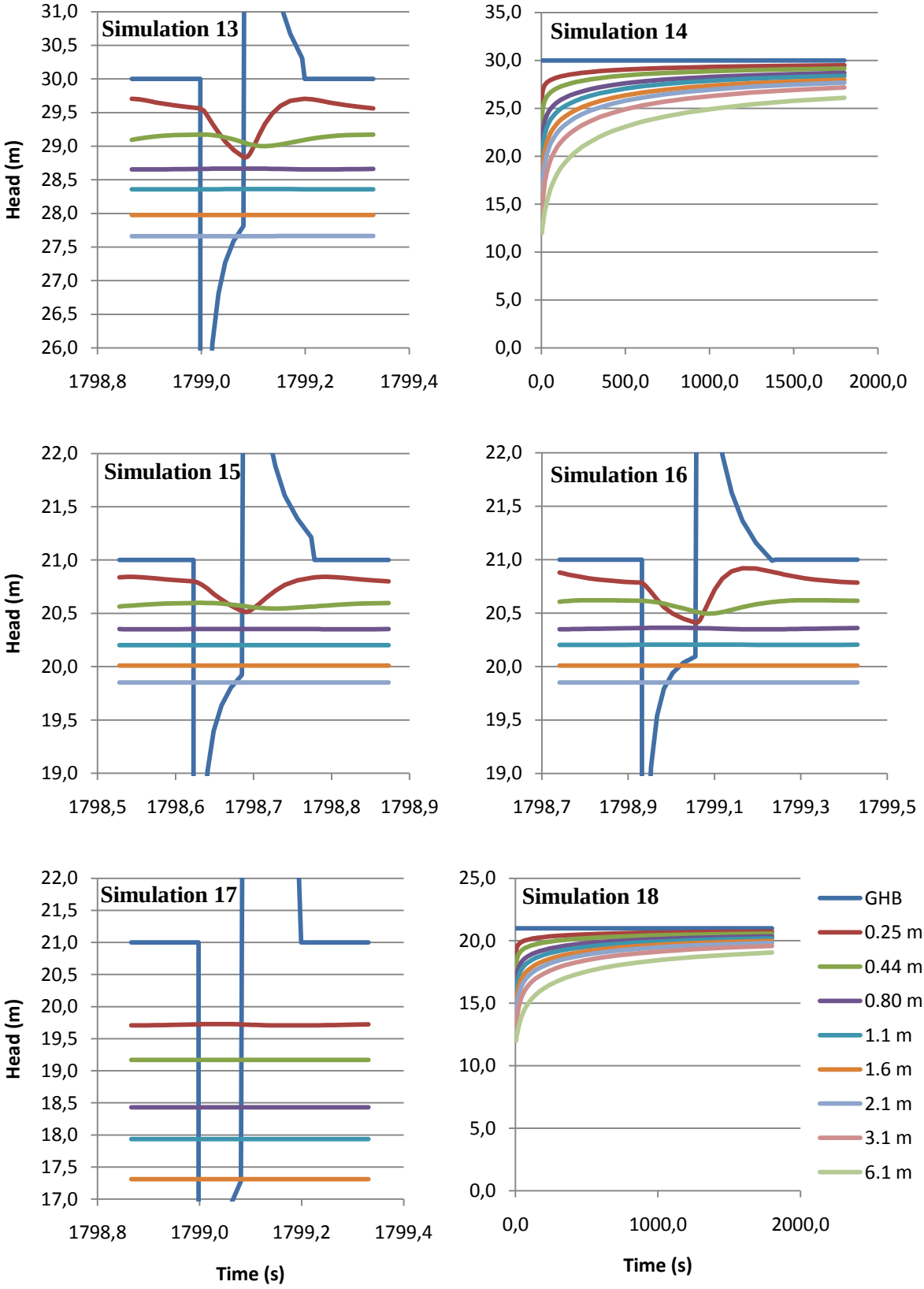
Simulation 13
Head (m)
31,0
30,5
30,0
29,5
29,0
28,5
28,0
27,5
27,0
26,5
26,0
1798,8
1799,0
1799,2
1799,4
Simulation 14
35,0
30,0
25,0
20,0
15,0
10,0
5,0
0,0
0,0
500,0
1000,0
1500,0
2000,0
Simulation 15
Head (m)
22,0
21,5
21,0
20,5
20,0
19,5
19,0
1798,5
1798,6
1798,7
1798,8
1798,9
Simulation 16
22,0
21,5
21,0
20,5
20,0
19,5
19,0
1798,7
1798,9
1799,1
1799,3
1799,5
Simulation 17
Head (m)
22,0
21,5
21,0
20,5
20,0
19,5
19,0
18,5
18,0
17,5
17,0
1798,8
1799,0
1799,2
1799,4
Time (s)
Simulation 18
25,0
20,0
15,0
10,0
5,0
0,0
0,0
1000,0
2000,0
Time (s)
GHB
0.25 m
0.44 m
0.80 m
1.1 m
1.6 m
2.1 m
3.1 m
6.1 m

Simulated Tracer Breakthrough Curves:

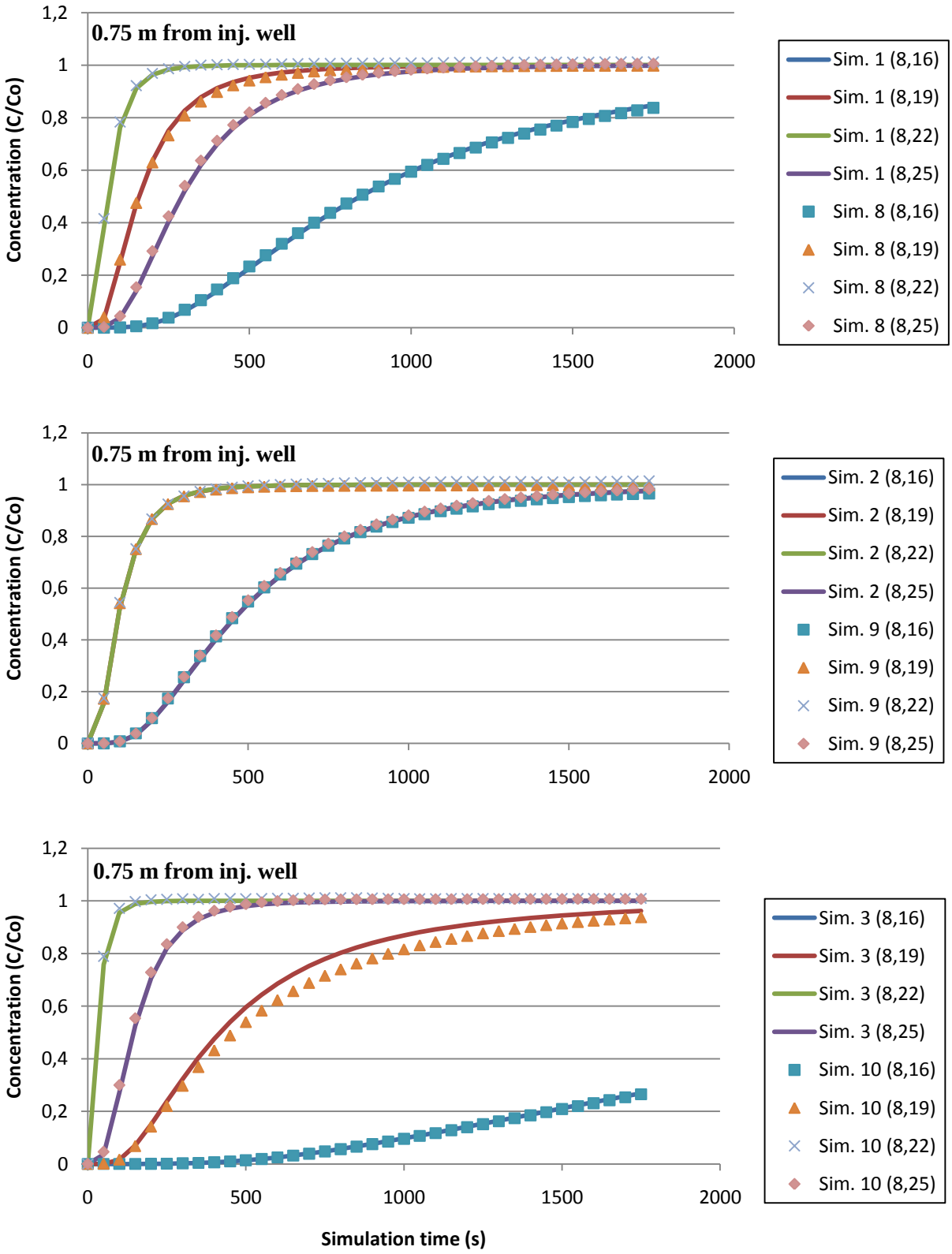

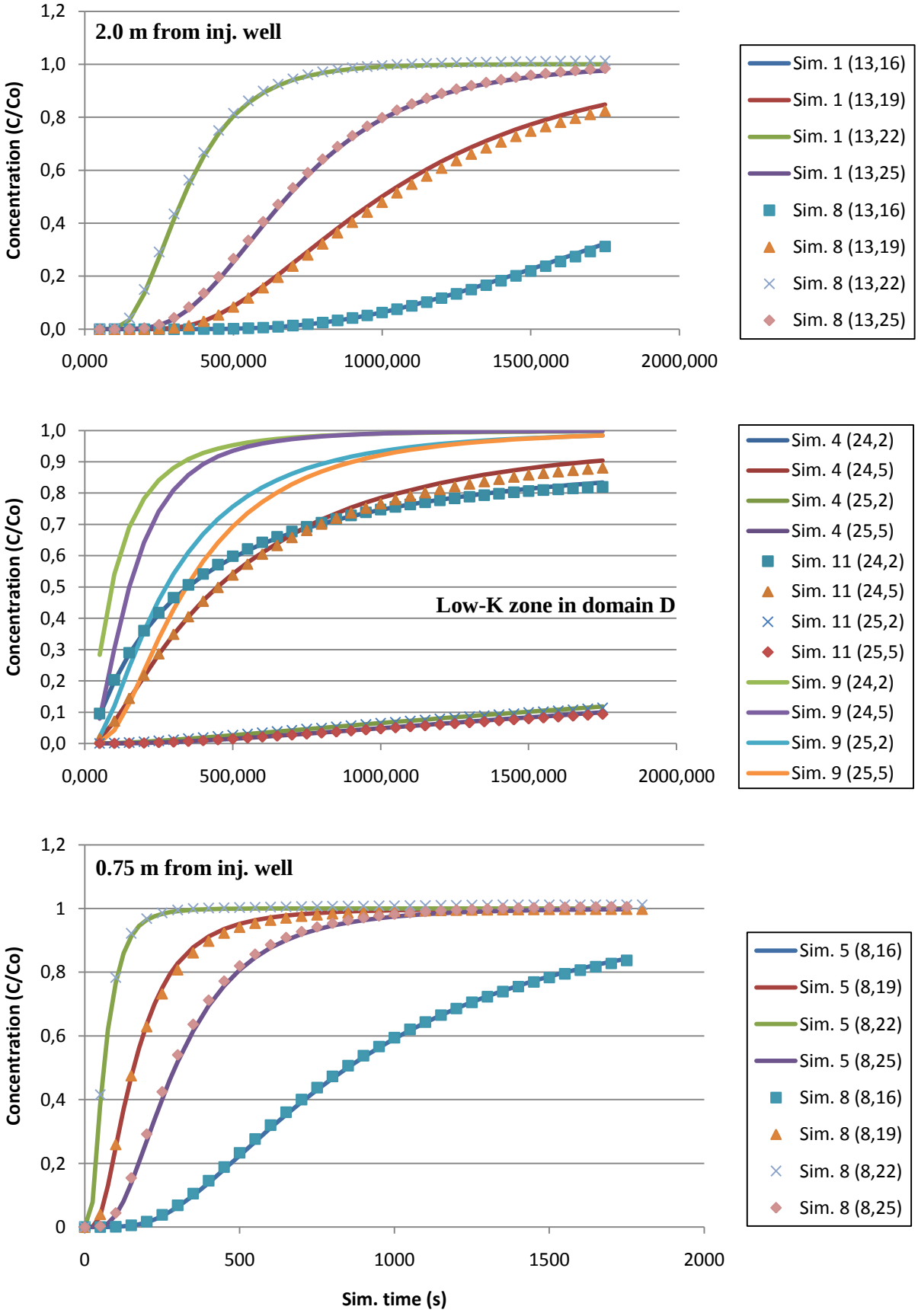
2.0 m from inj. well
Concentration (C/Co)
1,2
1,0
0,8
0,6
0,4
0,2
0,0
0,000
500,000
1000,000
1500,000
2000,000
Sim. 1 (13,16)
Sim. 1 (13,19)
Sim. 1 (13,22)
Sim. 1 (13,25)
Sim. 8 (13,16)
Sim. 8 (13,19)
Sim. 8 (13,22)
Sim. 8 (13,25)
Low-K zone in domain D
Concentration (C/Co)
1,0
0,9
0,8
0,7
0,6
0,5
0,4
0,3
0,2
0,1
0,0
0,000
500,000
1000,000
1500,000
2000,000
Sim. 4 (24,2)
Sim. 4 (24,5)
Sim. 4 (25,2)
Sim. 4 (25,5)
Sim. 11 (24,2)
Sim. 11 (24,5)
Sim. 11 (25,2)
Sim. 11 (25,5)
Sim. 9 (24,2)
Sim. 9 (24,5)
Sim. 9 (25,2)
Sim. 9 (25,5)
0.75 m from inj. well
Concentration (C/Co)
1,2
1
0,8
0,6
0,4
0,2
0
0
500
1000
1500
2000
Sim. time (s)
Sim. 5 (8,16)
Sim. 5 (8,19)
Sim. 5 (8,22)
Sim. 5 (8,25)
Sim. 8 (8,16)
Sim. 8 (8,19)
Sim. 8 (8,22)
Sim. 8 (8,25)

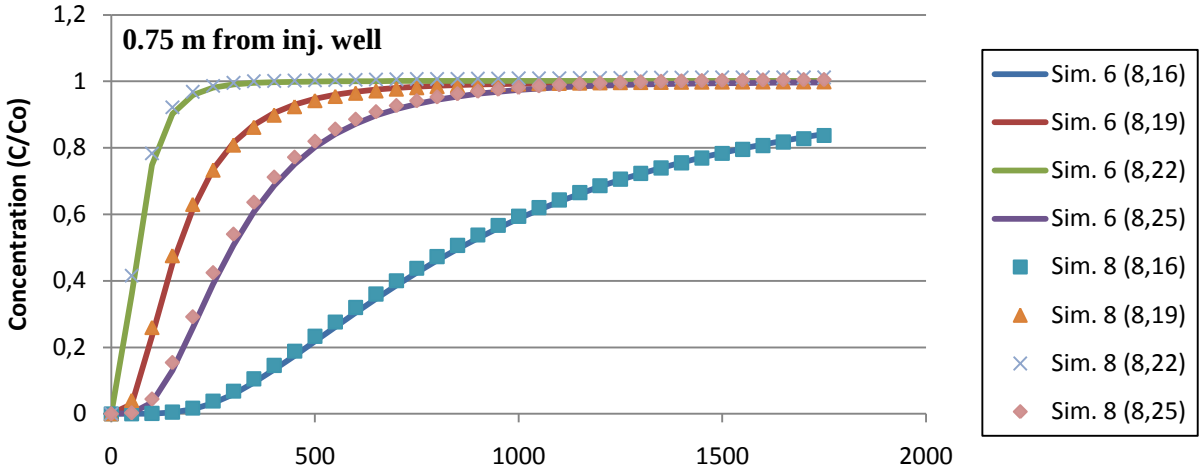
0.75 m from inj. well
Concentration (C/Co)
1,2
1
0,8
0,6
0,4
0,2
0
0
500
1000
1500
2000
Sim. 6 (8,16)
Sim. 6 (8,19)
Sim. 6 (8,22)
Sim. 6 (8,25)
Sim. 8 (8,16)
Sim. 8 (8,19)
Sim. 8 (8,22)
Sim. 8 (8,25)

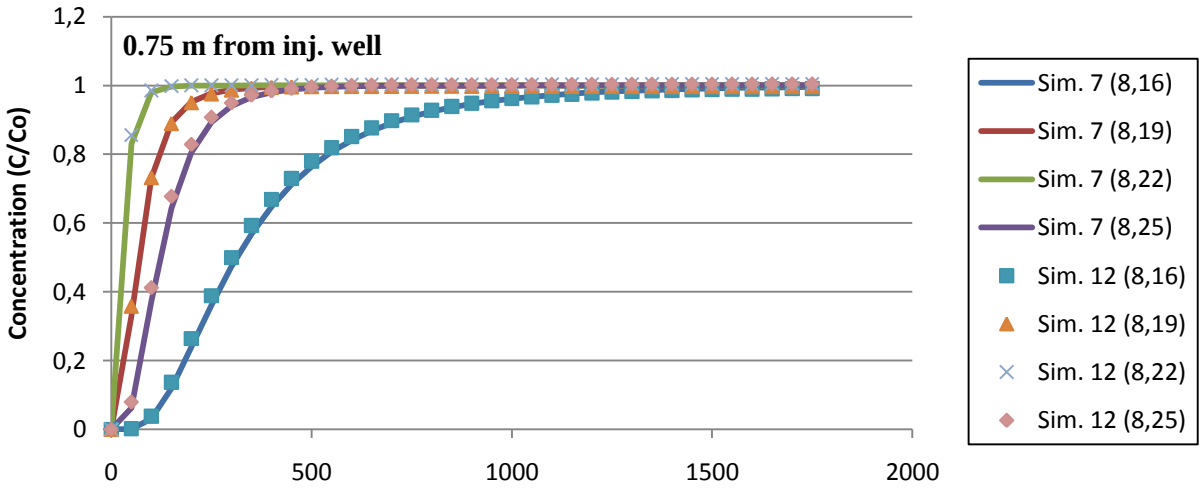
0.75 m from inj. well
Concentration (C/Co)
1,2
1
0,8
0,6
0,4
0,2
0
0
500
1000
1500
2000
Sim. 7 (8,16)
Sim. 7 (8,19)
Sim. 7 (8,22)
Sim. 7 (8,25)
Sim. 12 (8,16)
Sim. 12 (8,19)
Sim. 12 (8,22)
Sim. 12 (8,25)

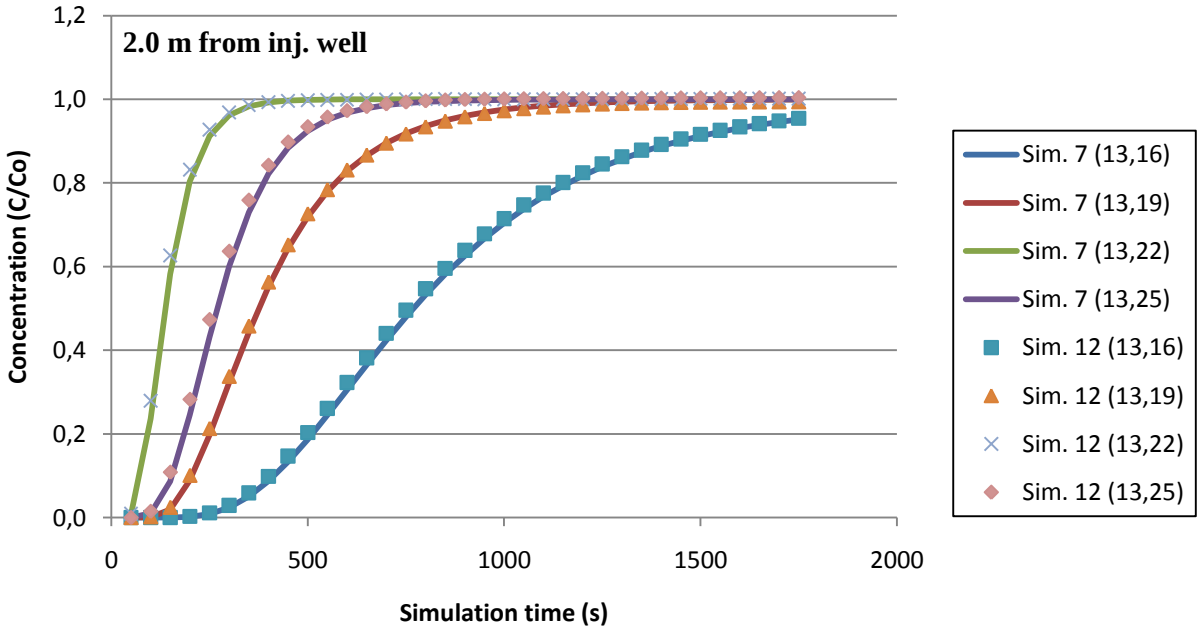
2.0 m from inj. well
Concentration (C/Co)
1,2
1,0
0,8
0,6
0,4
0,2
0,0
0
500
1000
1500
2000
Simulation time (s)
Sim. 7 (13,16)
Sim. 7 (13,19)
Sim. 7 (13,22)
Sim. 7 (13,25)
Sim. 12 (13,16)
Sim. 12 (13,19)
Sim. 12 (13,22)
Sim. 12 (13,25)

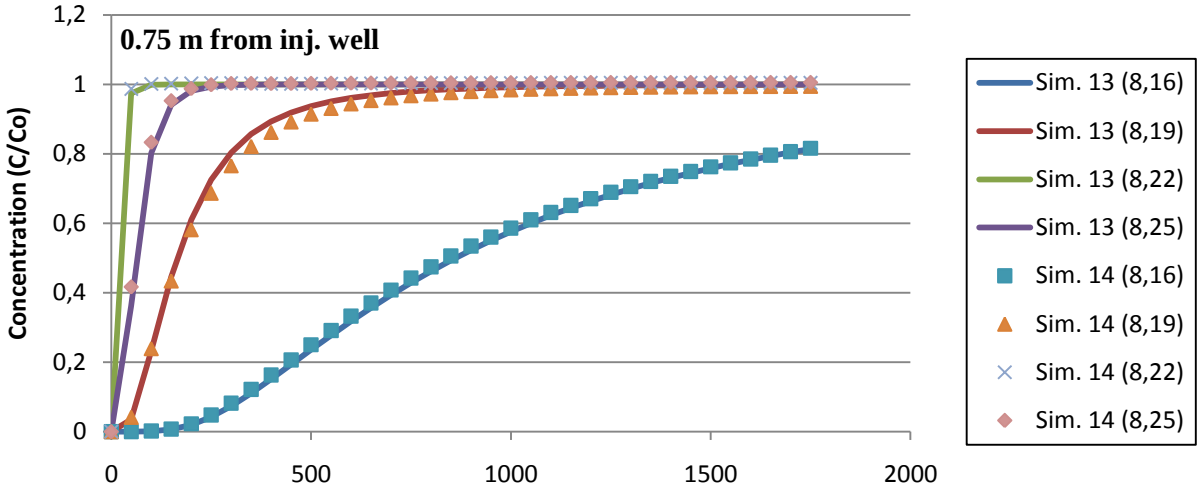
0.75 m from inj. well
Concentration (C/Co)
1,2
1
0,8
0,6
0,4
0,2
0
0
500
1000
1500
2000
Sim. 13 (8,16)
Sim. 13 (8,19)
Sim. 13 (8,22)
Sim. 13 (8,25)
Sim. 14 (8,16)
Sim. 14 (8,19)
Sim. 14 (8,22)
Sim. 14 (8,25)

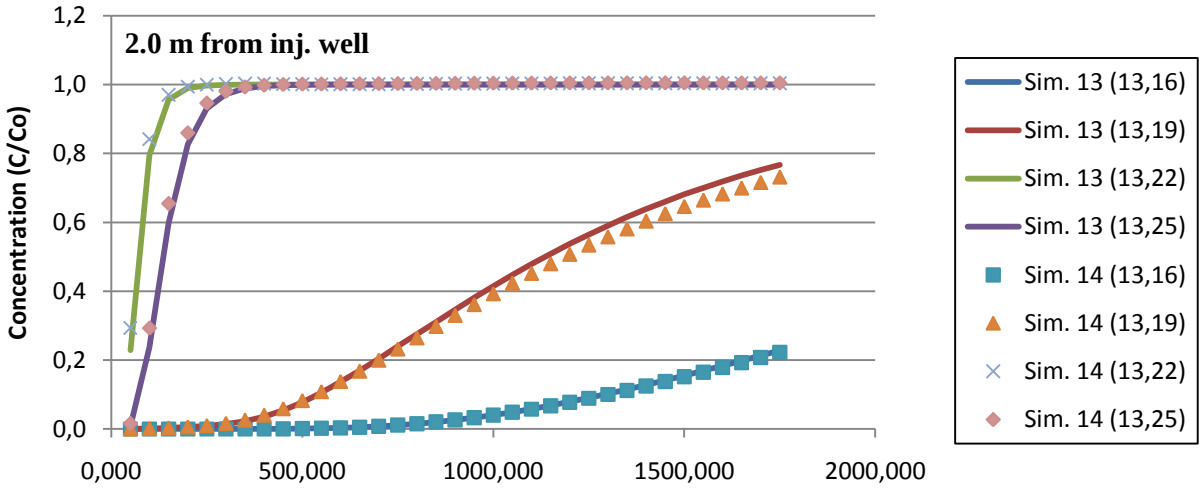
2.0 m from inj. well
Concentration (C/Co)
1,2
1,0
0,8
0,6
0,4
0,2
0,0
0,000
500,000
1000,000
1500,000
2000,000
Sim. 13 (13,16)
Sim. 13 (13,19)
Sim. 13 (13,22)
Sim. 13 (13,25)
Sim. 14 (13,16)
Sim. 14 (13,19)
Sim. 14 (13,22)
Sim. 14 (13,25)

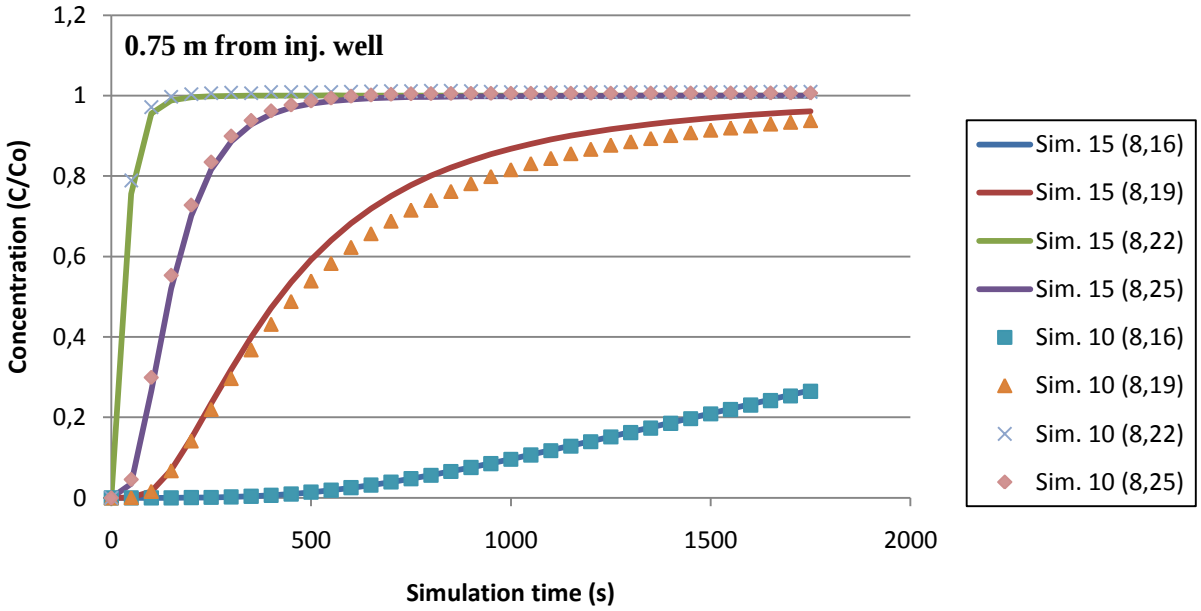
0.75 m from inj. well
Concentration (C/Co)
1,2
1
0,8
0,6
0,4
0,2
0
0
500
1000
1500
2000
Simulation time (s)
Sim. 15 (8,16)
Sim. 15 (8,19)
Sim. 15 (8,22)
Sim. 15 (8,25)
Sim. 10 (8,16)
Sim. 10 (8,19)
Sim. 10 (8,22)
Sim. 10 (8,25)

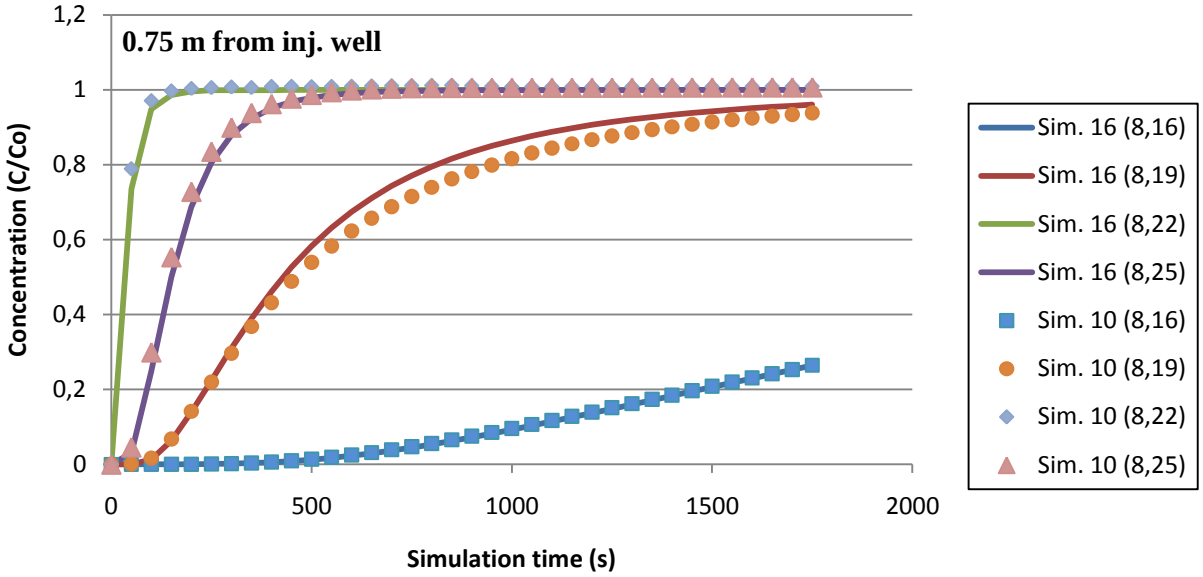

Head contour maps:

Head distribution near the injection well during the final simulation time step are shown for conventional injection simulations. Three different times during a quasi steady-state pulsing cycle are shown for pressure pulsing simulations. These include the following:

(1) During pressure pulsing stress period 1 (Boundary pressure is H_{Steady})
(2) Begging of pressure pulsing stress period 3 (recovery 1)
(3) Beggining of pressure pulsing stress period 5 (recovery 2)

Head contour maps were not generated for simulations 17 and 18.

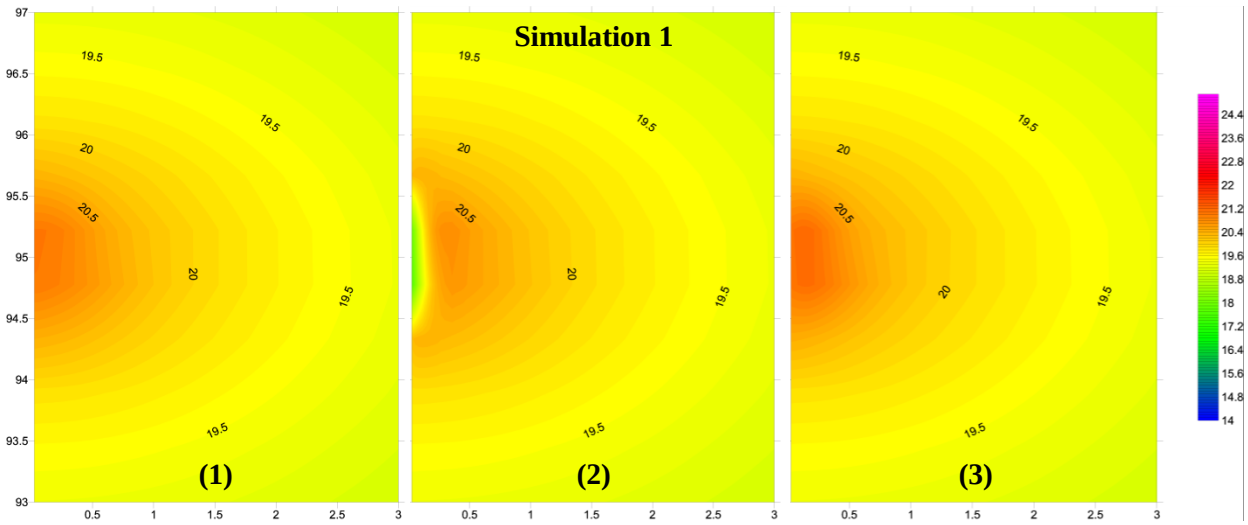

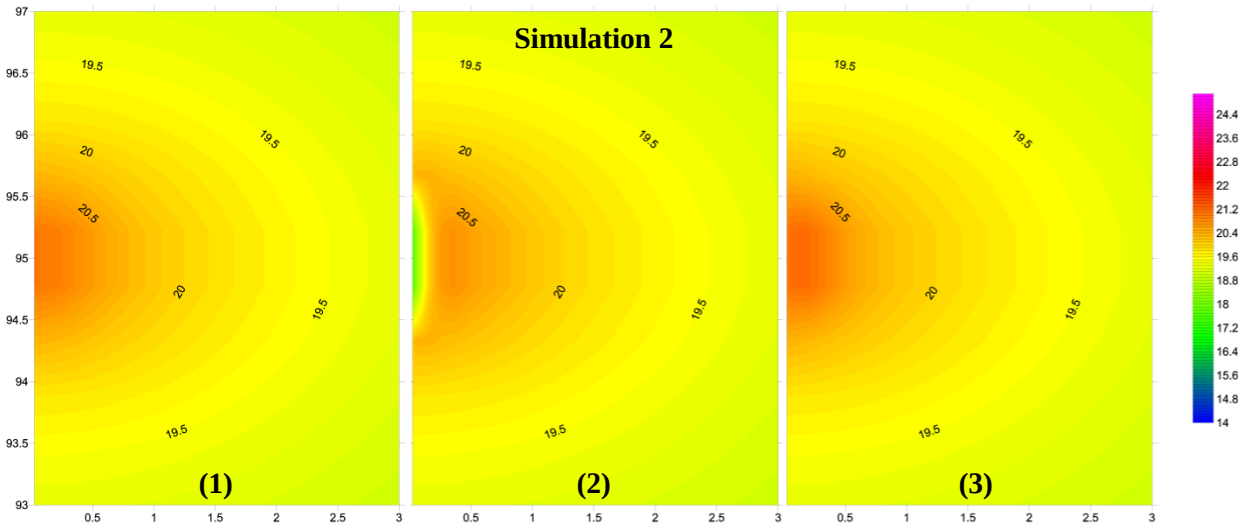
Simulation 2
(1)
(2)
(3)

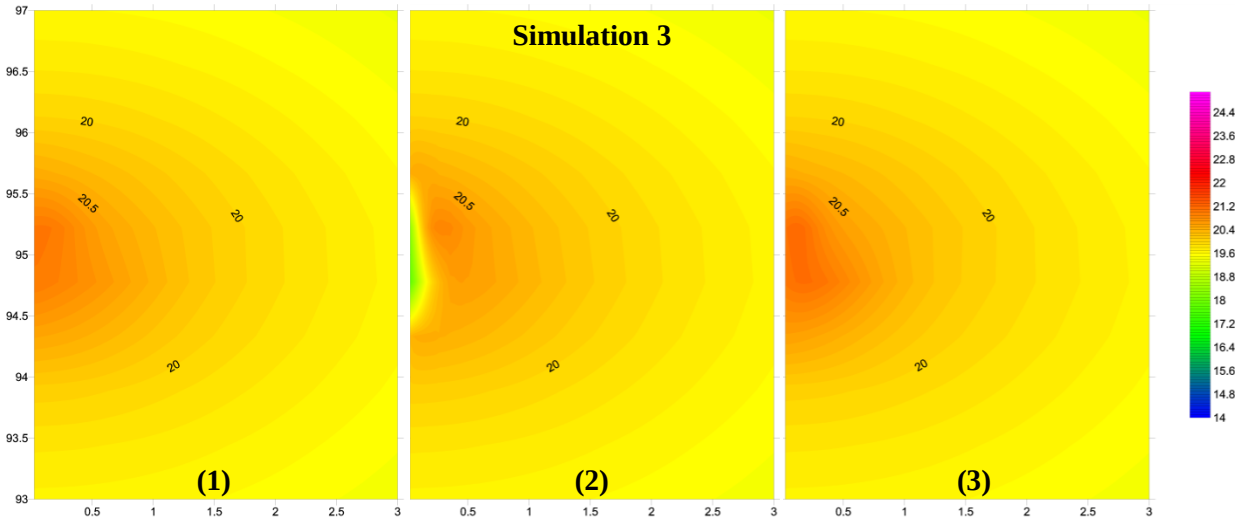
Simulation 3
(1)
(2)
(3)

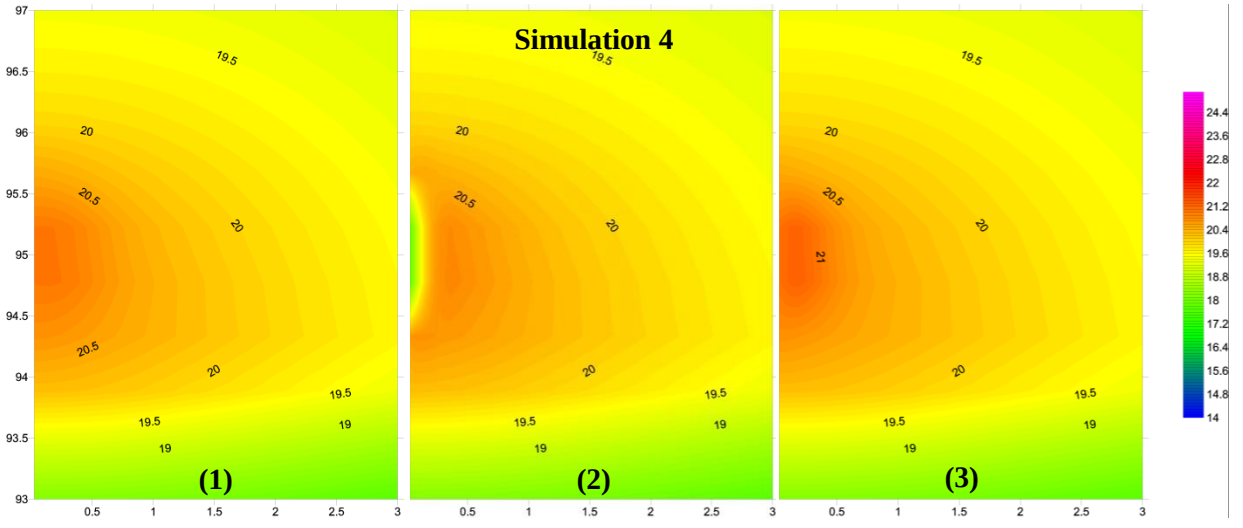
Simulation 4
(1)
(2)
(3)

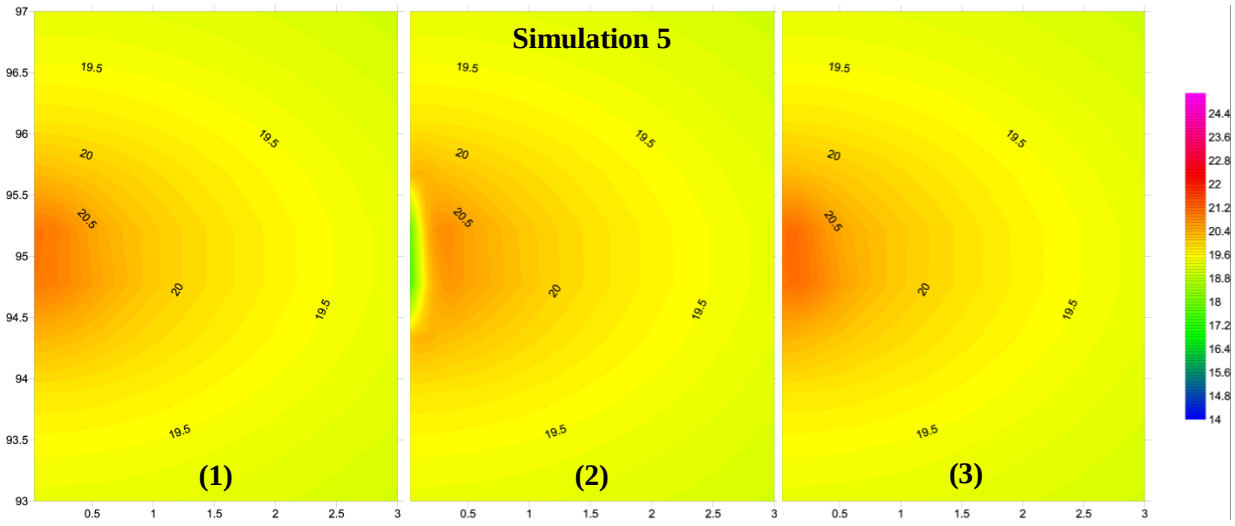
Simulation 5
(1)
(2)
(3)

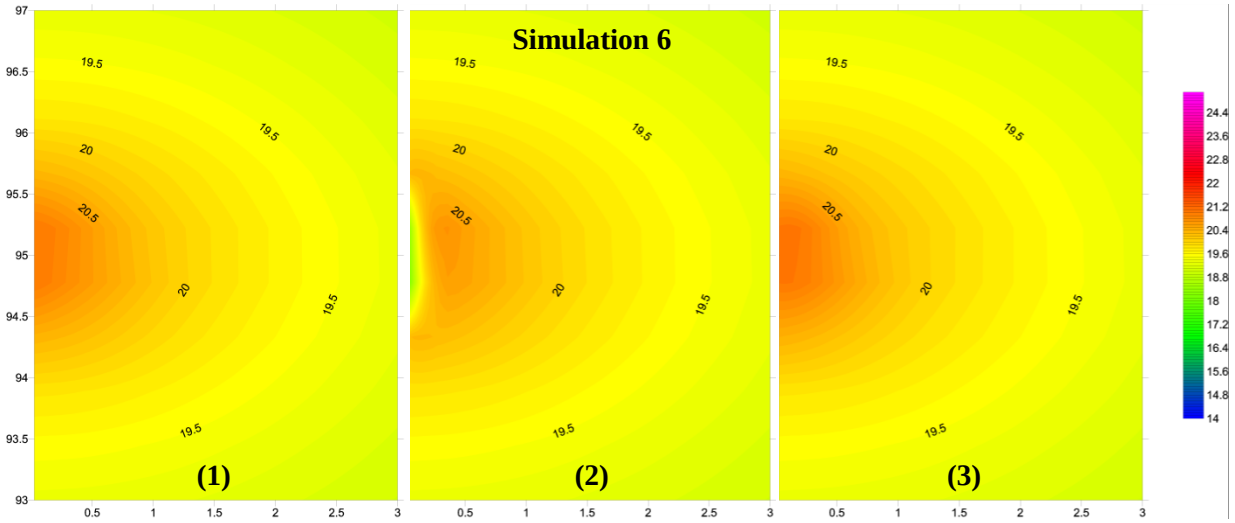
Simulation 6
(1)
(2)
(3)

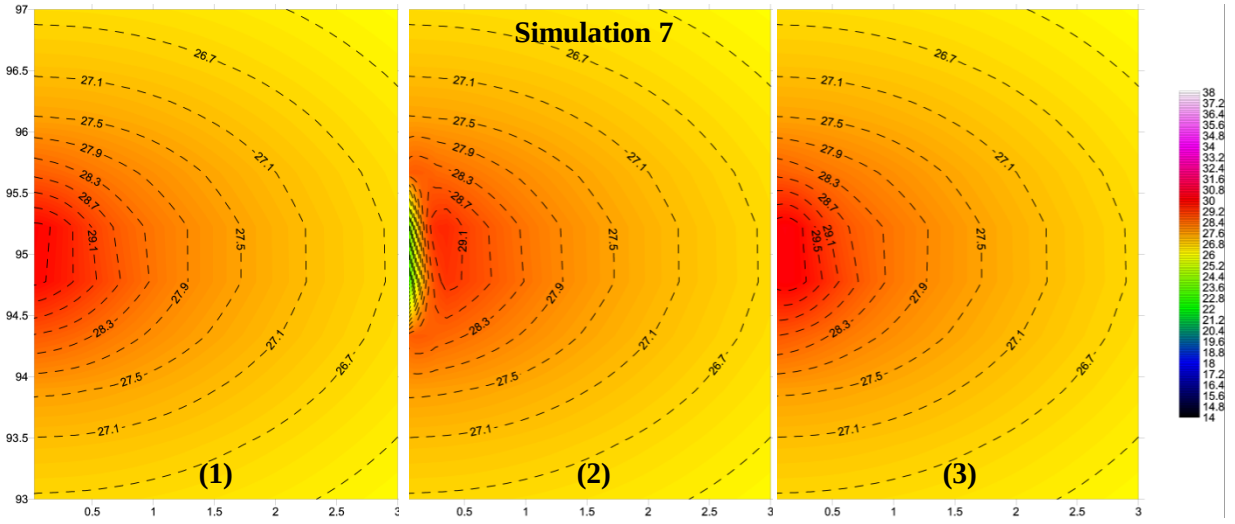
Simulation 7
(1)
(2)
(3)

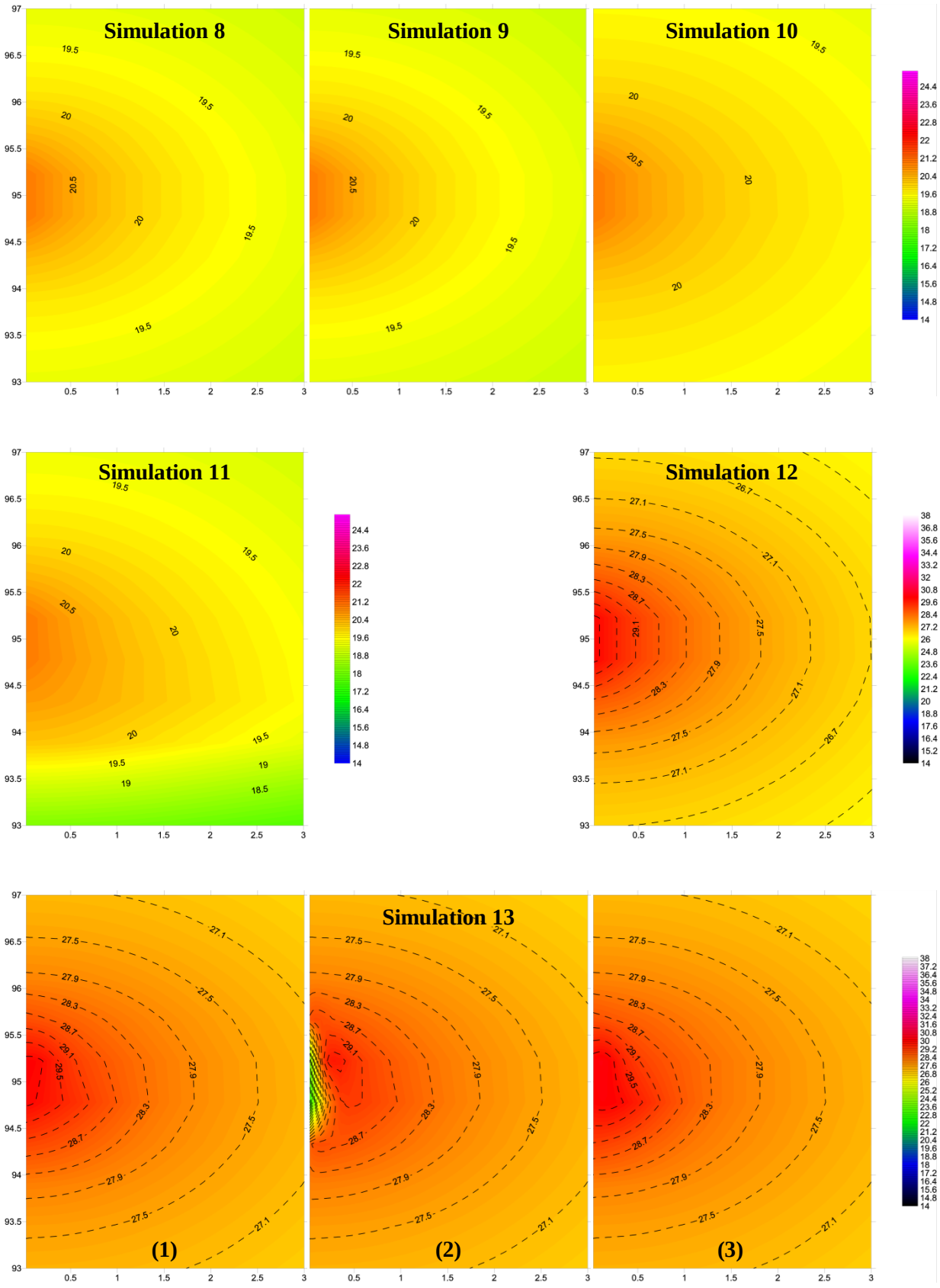
Simulation 8
Simulation 9
Simulation 10
Simulation 11
Simulation 12
Simulation 13
(1)
(2)
(3)

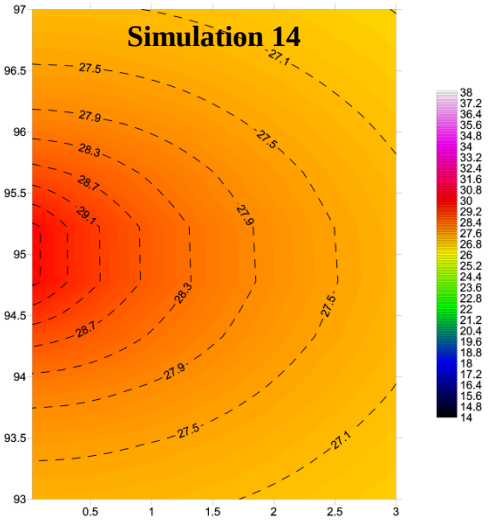
Simulation 14

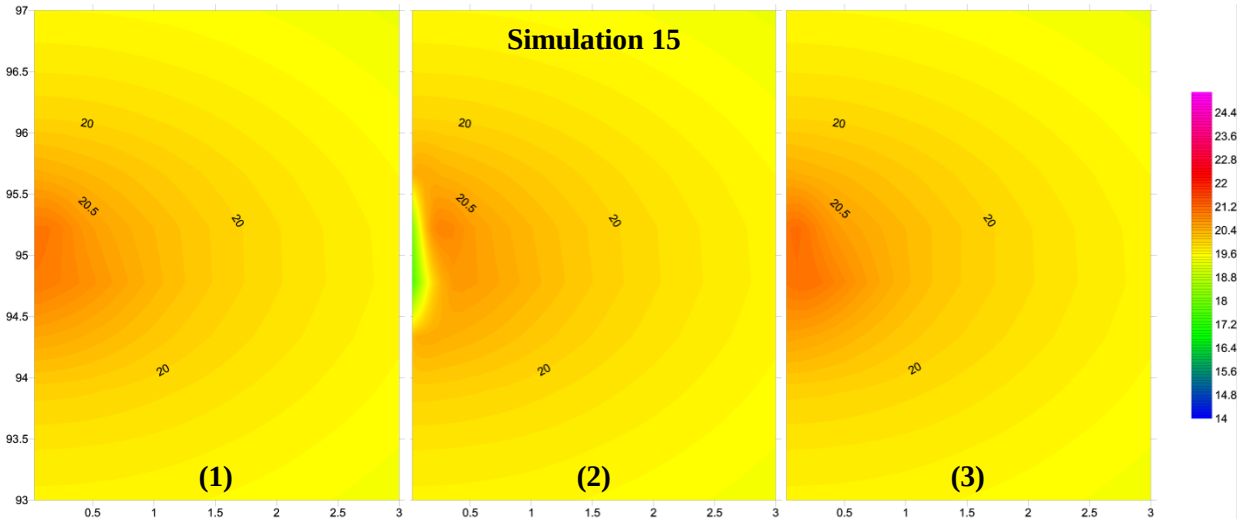
Simulation 15
(1)
(2)
(3)

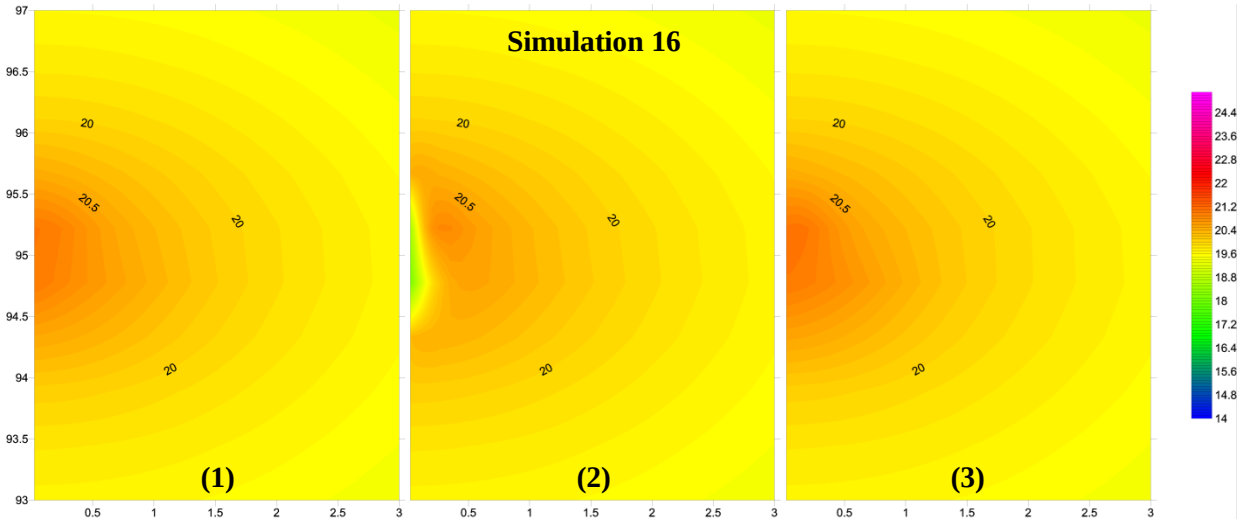
Simulation 16
(1)
(2)
(3)

Concentration contour maps:

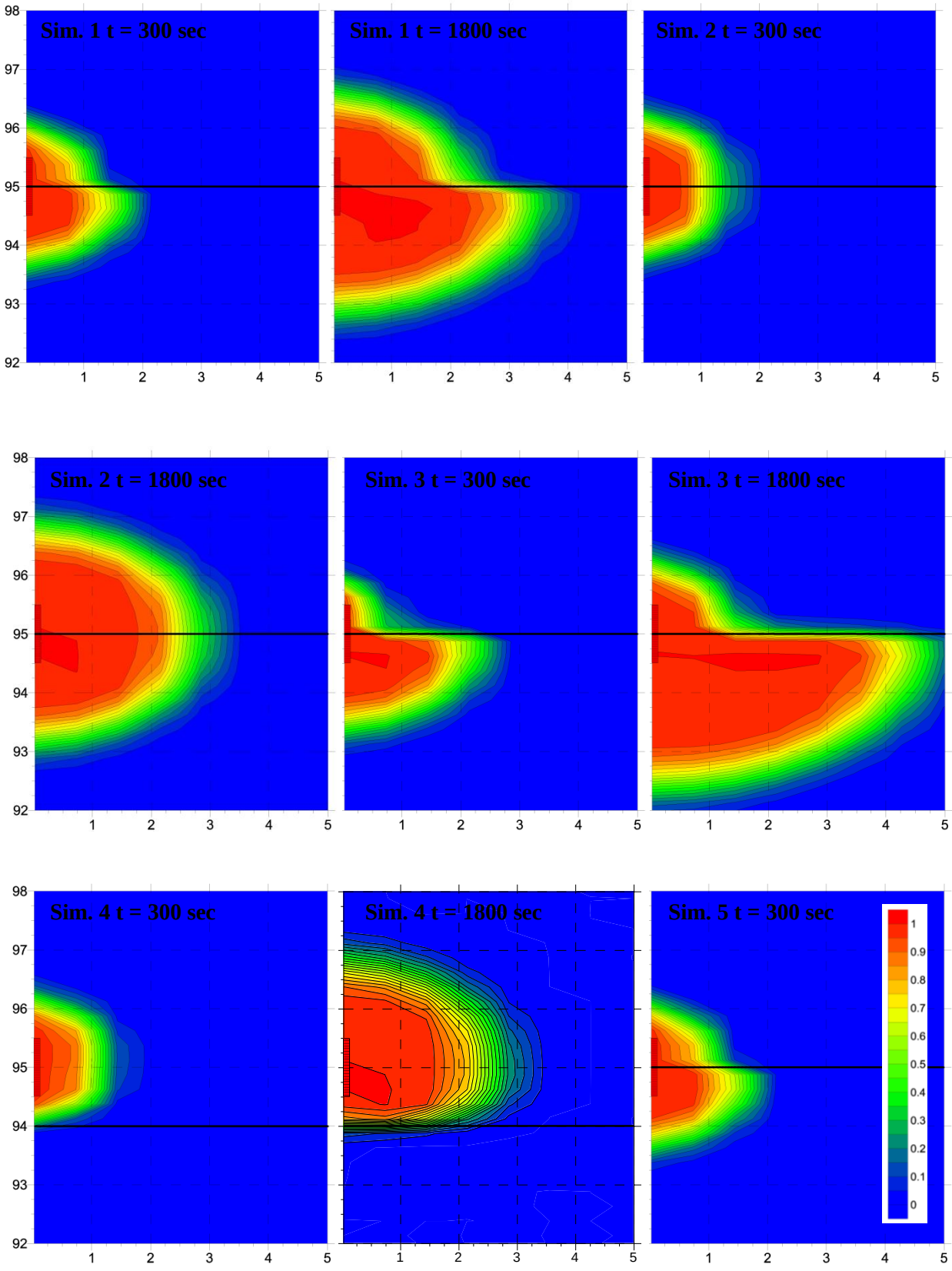

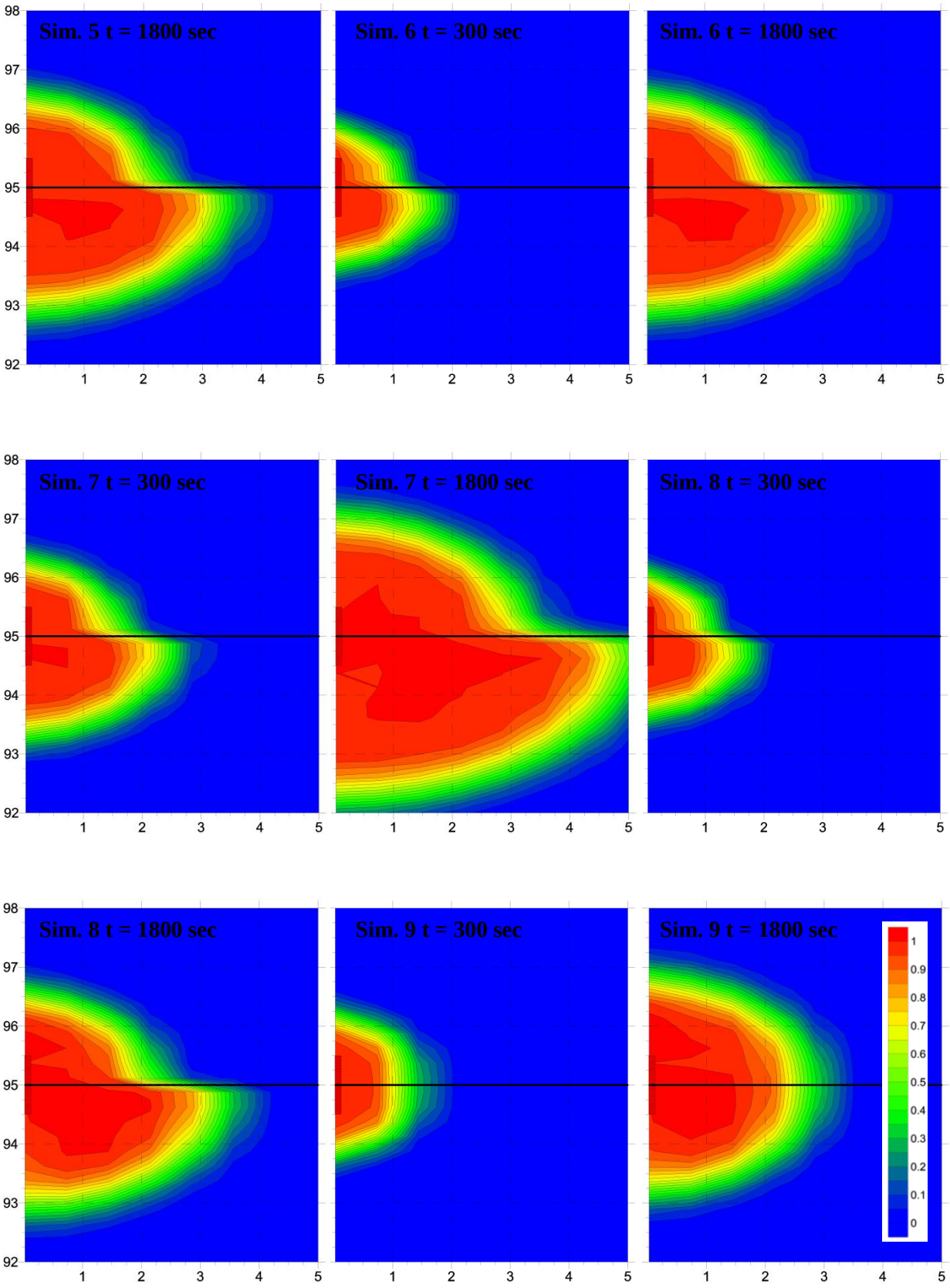
Sim. 5 t = 1800 sec
Sim. 6 t = 300 sec
Sim. 6 t = 1800 sec
Sim. 7 t = 300 sec
Sim. 7 t = 1800 sec
Sim. 8 t = 300 sec
Sim. 8 t = 1800 sec
Sim. 9 t = 300 sec
Sim. 9 t = 1800 sec
98
97
96
95
94
93
92
1
2
3
4
5
1
0.9
0.8
0.7
0.6
0.5
0.4
0.3
0.2
0.1
0

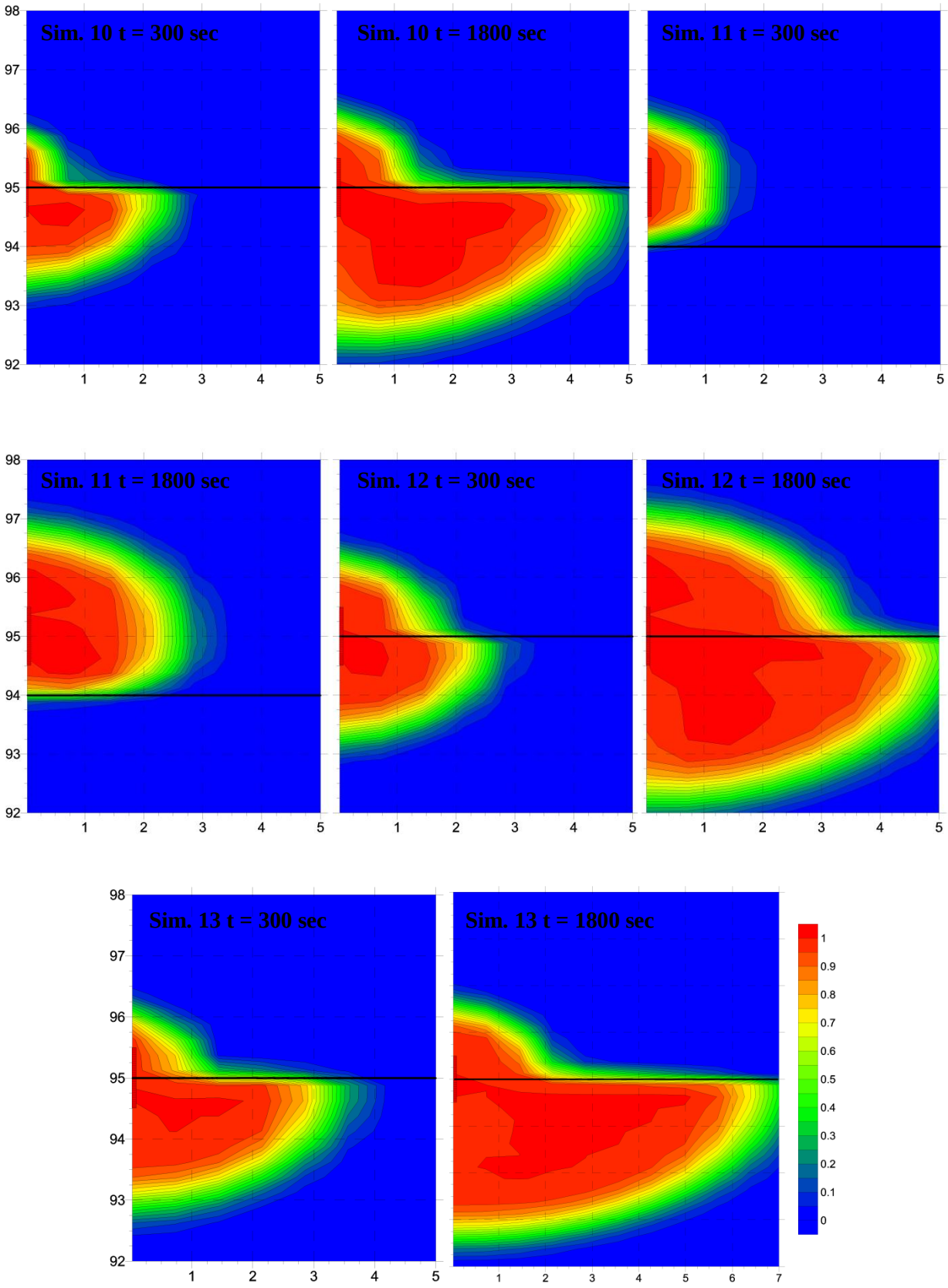
Sim. 10 t = 300 sec
Sim. 10 t = 1800 sec
Sim. 11 t = 300 sec
Sim. 11 t = 1800 sec
Sim. 12 t = 300 sec
Sim. 12 t = 1800 sec
Sim. 13 t = 300 sec
Sim. 13 t = 1800 sec
98
97
96
95
94
93
92
1
2
3
4
5
6
7
0.9
0.8
0.7
0.6
0.5
0.4
0.3
0.2
0.1
0

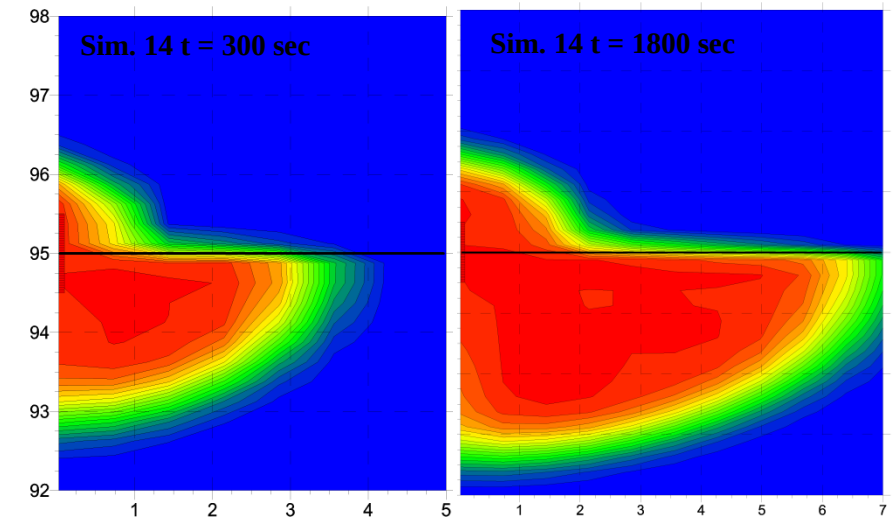
Sim. 14 t = 300 sec
Sim. 14 t = 1800 sec
98
97
96
95
94
93
92
1
2
3
4
5
6
7

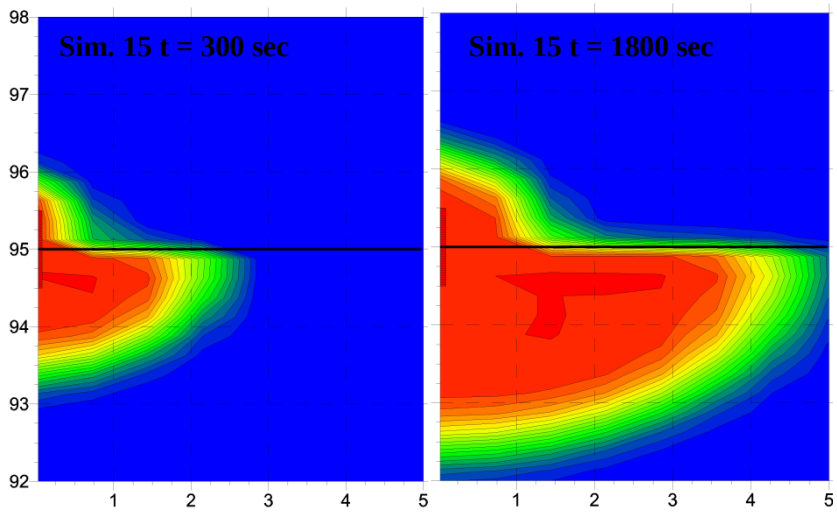
Sim. 15 t = 300 sec
Sim. 15 t = 1800 sec
98
97
96
95
94
93
92
1
2
3
4
5

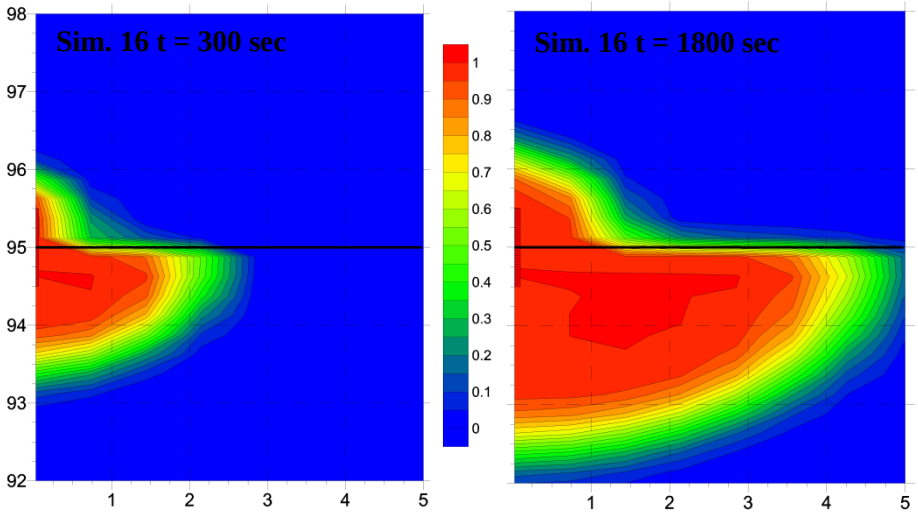
Sim. 16 t = 300 sec
Sim. 16 t = 1800 sec
98
97
96
95
94
93
92
1
2
3
4
5
1
0.9
0.8
0.7
0.6
0.5
0.4
0.3
0.2
0.1
0

Concentration Difference Contour Maps:

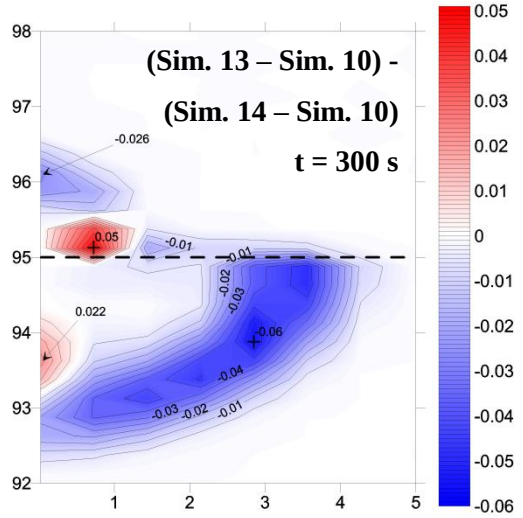

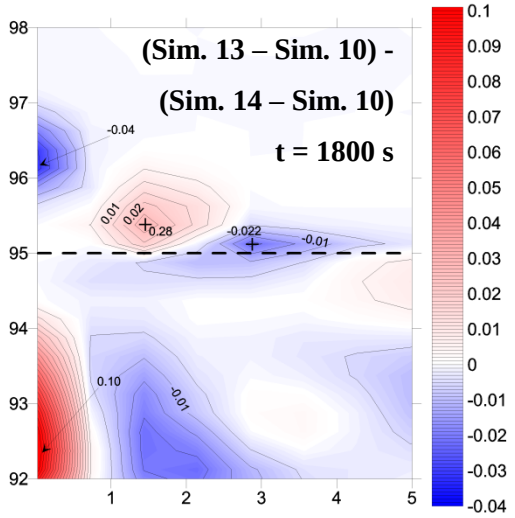

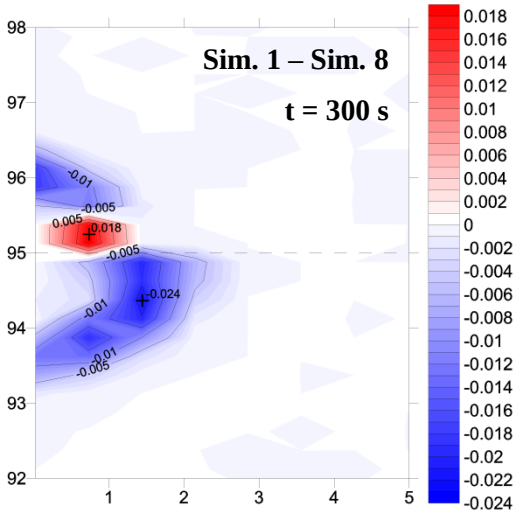

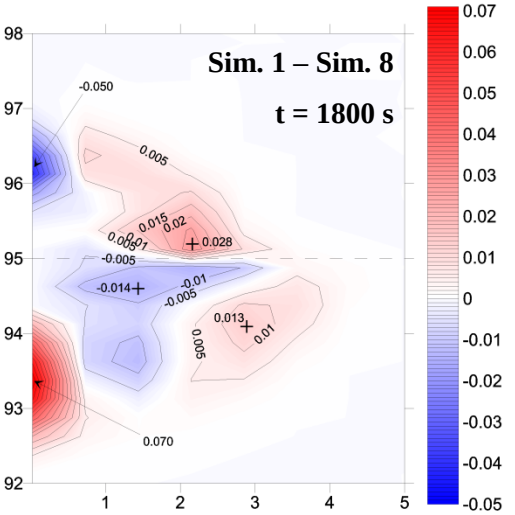

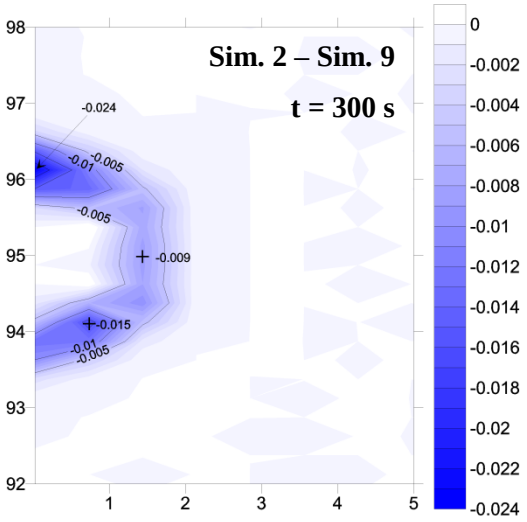

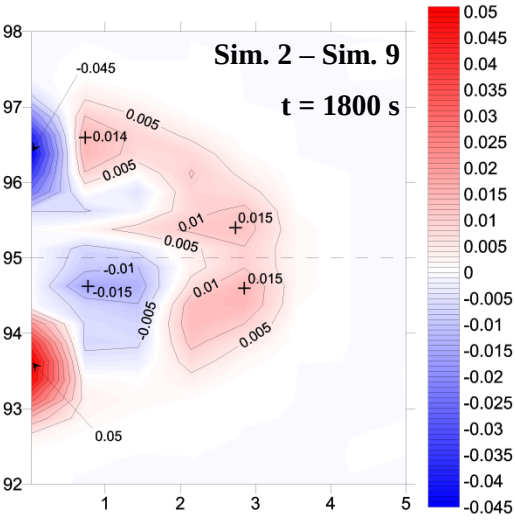

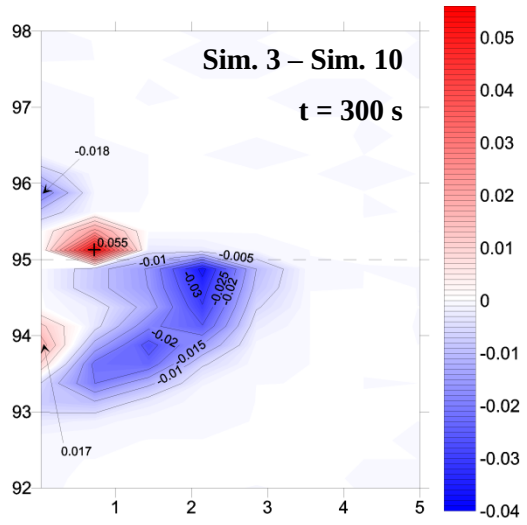
Sim. 3 – Sim. 10
t = 300 s

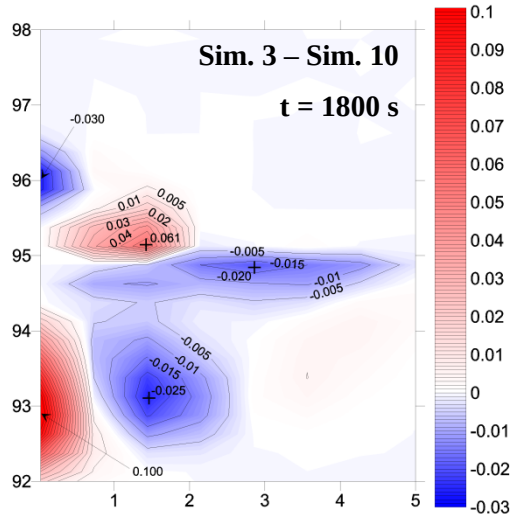
Sim. 3 – Sim. 10
t = 1800 s

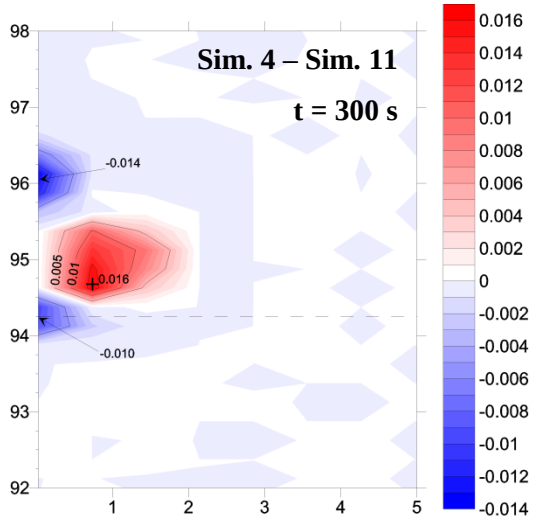
Sim. 4 – Sim. 11
t = 300 s

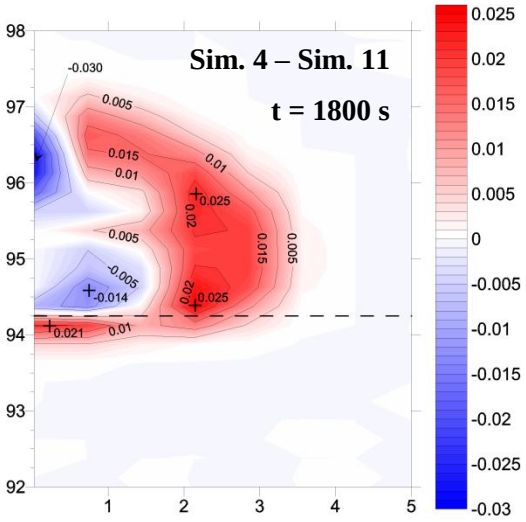
Sim. 4 – Sim. 11
t = 1800 s

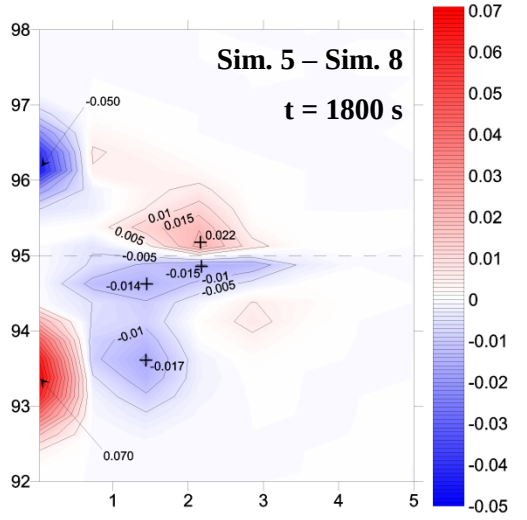
Sim. 5 – Sim. 8
t = 1800 s

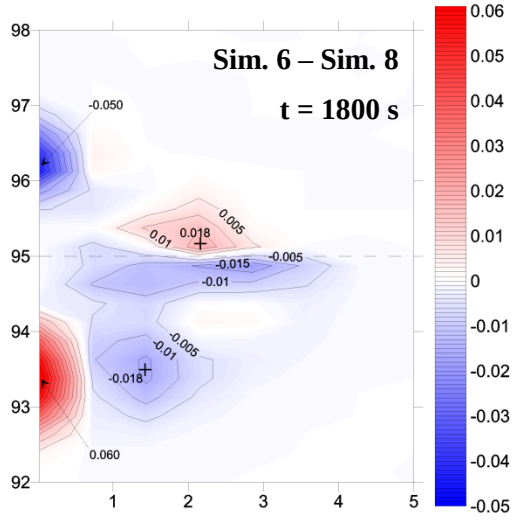
Sim. 6 – Sim. 8
t = 1800 s

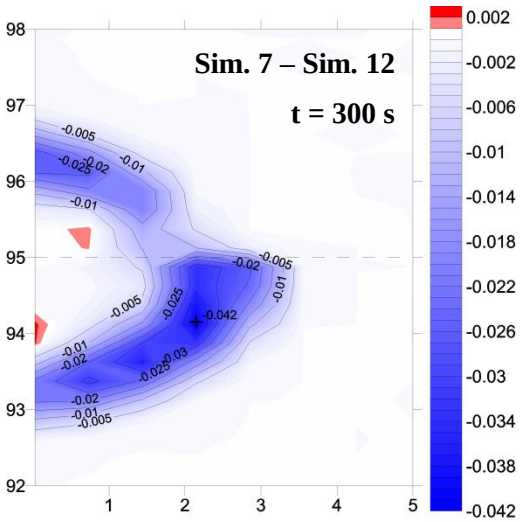
Sim. 7 – Sim. 12
t = 300 s

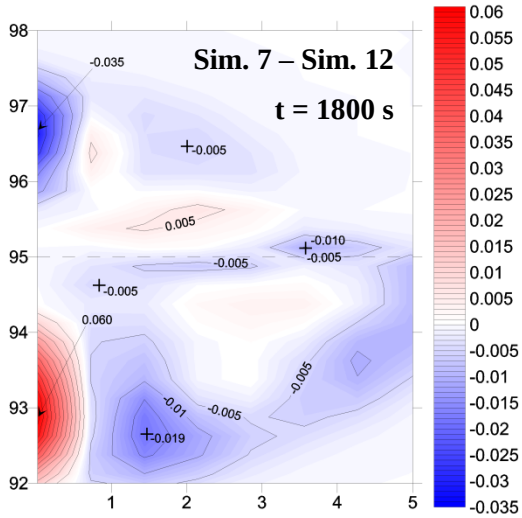
Sim. 7 – Sim. 12
t = 1800 s

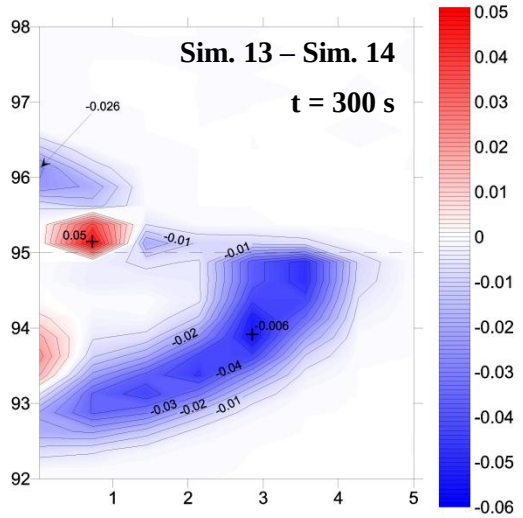
Sim. 13 – Sim. 14
t = 300 s

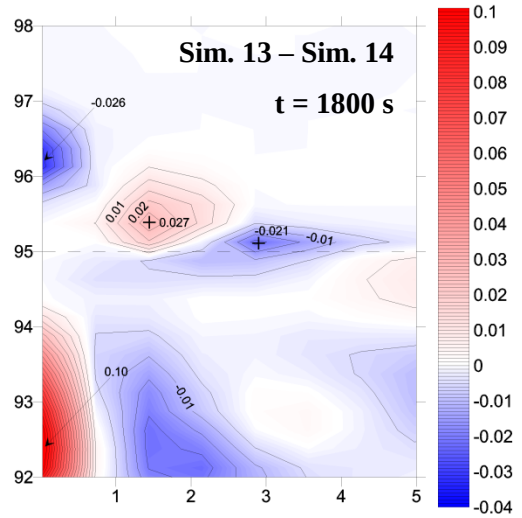
Sim. 13 – Sim. 14
t = 1800 s

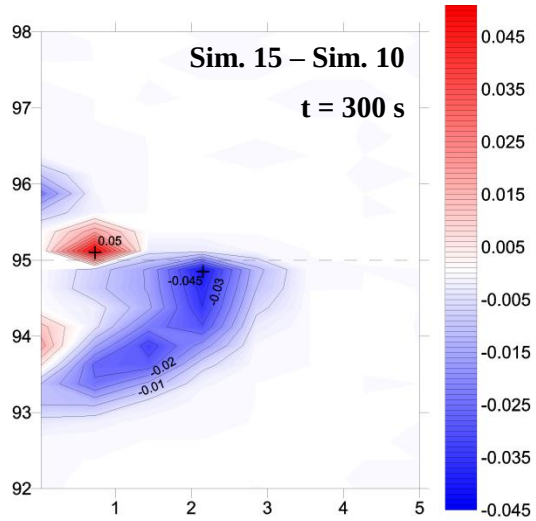
Sim. 15 – Sim. 10
t = 300 s

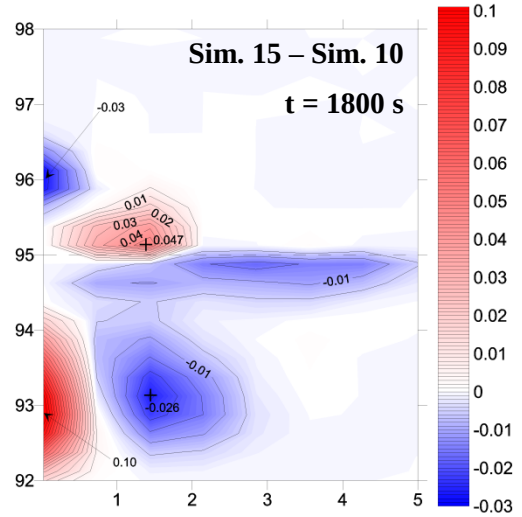
Sim. 15 – Sim. 10
t = 1800 s

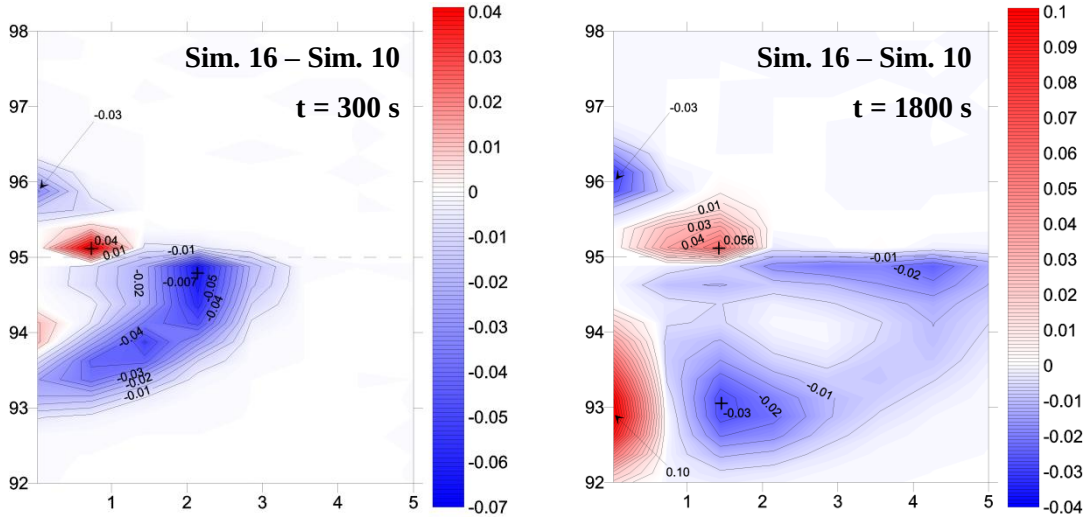

Zone Budget Time Series:

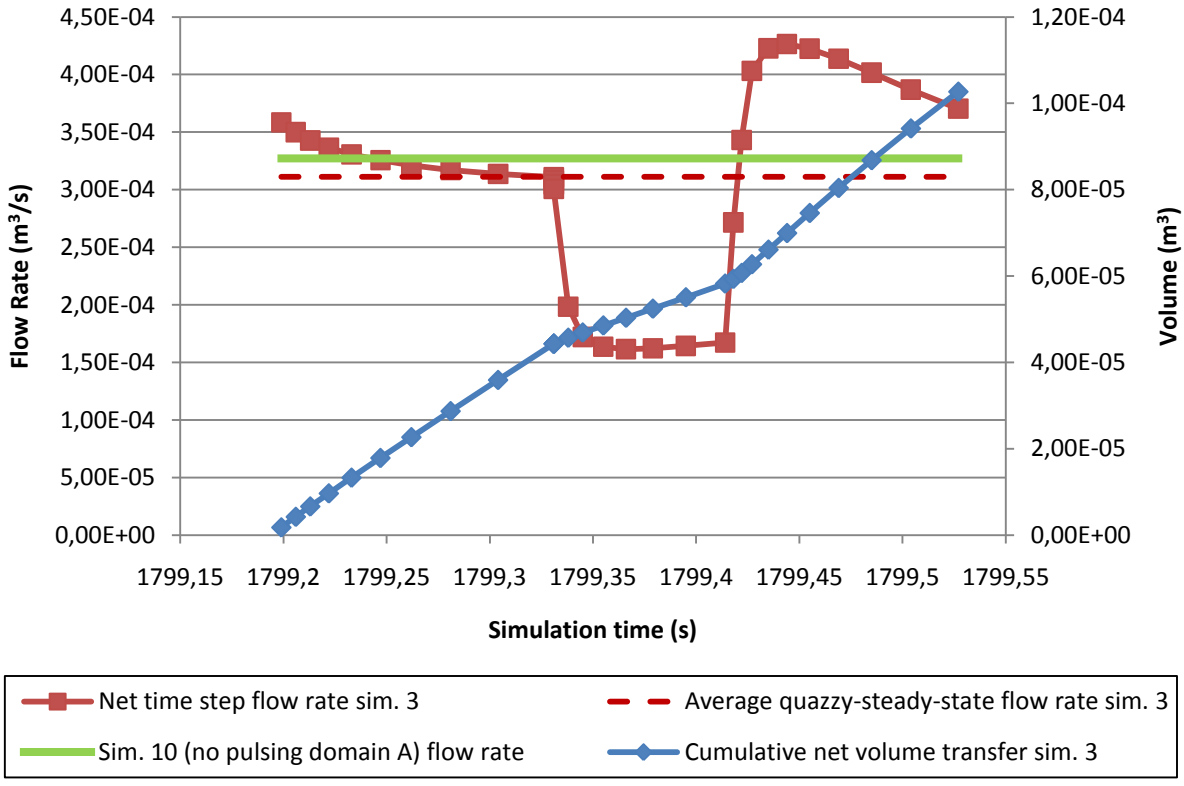

Zone budget time series for simulations 3 (pulsing) and 10 (conventional)

Quality Control Datasets:

Head differences spanning simulated injection well over a pulsing cycle (simulation 1)

Stress Period	Time Step	Time	Head at GHB Cells (C,L) (m)		Difference (m)
			1,19	1,22	
26992	1	1798.998	14.004	14.004	0.000
26992	2	1798.998	14.000	14.000	0.000
26992	3	1798.998	14.000	14.000	0.000
26993	1	1799.005	17.158	17.158	0.000
26993	2	1799.012	18.424	18.424	0.000
26993	3	1799.021	19.052	19.052	0.000
26993	4	1799.033	19.415	19.415	0.000
26993	5	1799.046	19.647	19.647	0.000
26993	6	1799.062	19.803	19.803	0.000
26993	7	1799.081	19.913	19.913	0.000
26994	1	1799.085	25.000	25.000	0.000
26994	2	1799.089	25.000	25.000	0.000
26994	3	1799.094	25.000	25.000	0.000
26995	1	1799.102	23.635	23.635	0.000
26995	2	1799.111	22.843	22.843	0.000
26995	3	1799.122	22.325	22.325	0.000
26995	4	1799.136	21.958	21.958	0.000
26995	5	1799.152	21.681	21.681	0.000
26995	6	1799.171	21.463	21.463	0.000
26995	7	1799.194	21.285	21.285	0.000
26996	1	1799.199	21.000	21.000	0.000
26996	2	1799.206	21.000	21.000	0.000
26996	3	1799.213	21.000	21.000	0.000
26996	4	1799.222	21.000	21.000	0.000
26996	5	1799.233	21.000	21.000	0.000
26996	6	1799.247	21.000	21.000	0.000
26996	7	1799.262	21.000	21.000	0.000
26996	8	1799.281	21.000	21.000	0.000
26996	9	1799.304	21.000	21.000	0.000
26996	10	1799.331	21.000	21.000	0.000

Changes in hydraulic head over successive pulsing cycles indicating approach to quasi steady-state

Distance from GHB	Upper layer		Lower Layer	
	Δh_1 (m)[1]	Δh_2 (m)[2]	Δh_1 (m)[1]	Δh_2 (m)[2]
0 (at GHB)	0.00004	0.00000	0.00005	0.00000
0.25 m	0.00005	0.00004	0.00005	0.00003
0.44 m	0.00006	0.00005	0.00006	0.00006
0.80 m	0.00008	0.00008	0.00008	0.00008
1.1 m	0.00009	0.00010	0.00010	0.00009
1.6 m	0.00011	0.00011	0.00012	0.00011
2.1 m	0.00014	0.00014	0.00013	0.00013
3.1 m	0.00015	0.00015	0.00015	0.00015
6.1 m	0.00021	0.00020	0.00021	0.00021

1. Measured at last time step of pulsing stress period 5 (end of recovery 2)
2. Measured at last time step of pulsing stress period 1

Hydraulic head measured at last time step of simulation adjacent to constant head boundary

Simulation no.	Hydraulic Head (m)
1	12.049
2	12.041
3	12.092
4	12.029
5	12.049
6	12.048
7	12.097
8	12.048
9	12.042
10	12.089
11	12.030
12	12.098

Note: Inital hydraulic head = 12.0 m

Average Pressure Pulsing Injection Pressure

Simulation no.	Avg inj. pressure (m)
1	20.98
2	20.98
3	21.0
4	21.05
5	20.96
6	20.96
7	29.85
13	29.92
15	20.99
16	21.0

Appendix E – Supplemental 3D Model Information

Hydraulic Head Time Series:

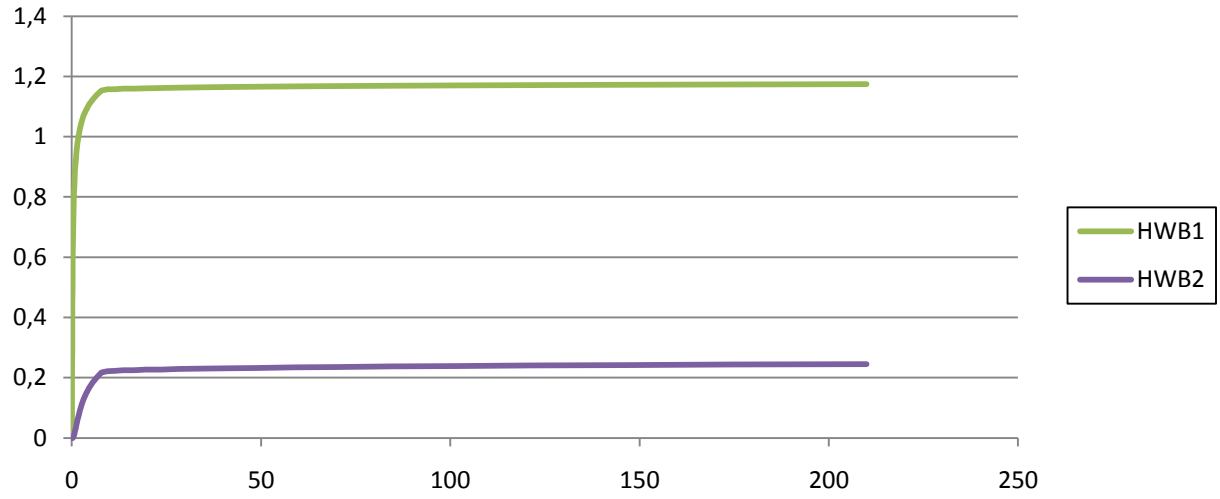

Simulation 3D-1 Hydraulic Head Time Series

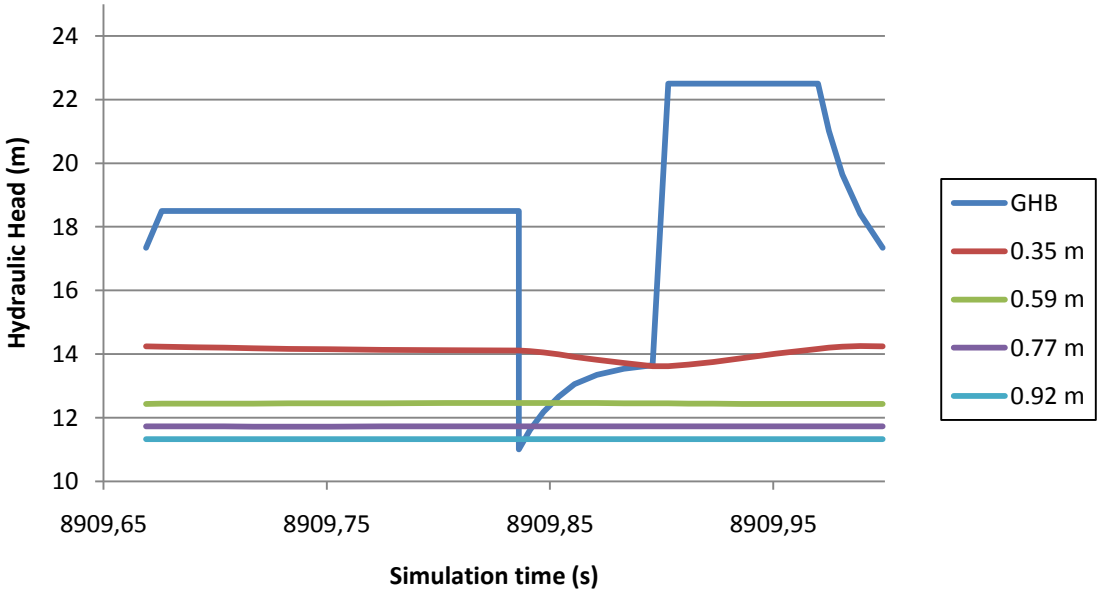

Simulation 3D-2 hydraulic head time series for a quasi steady-state pulsing cycle at layer 25

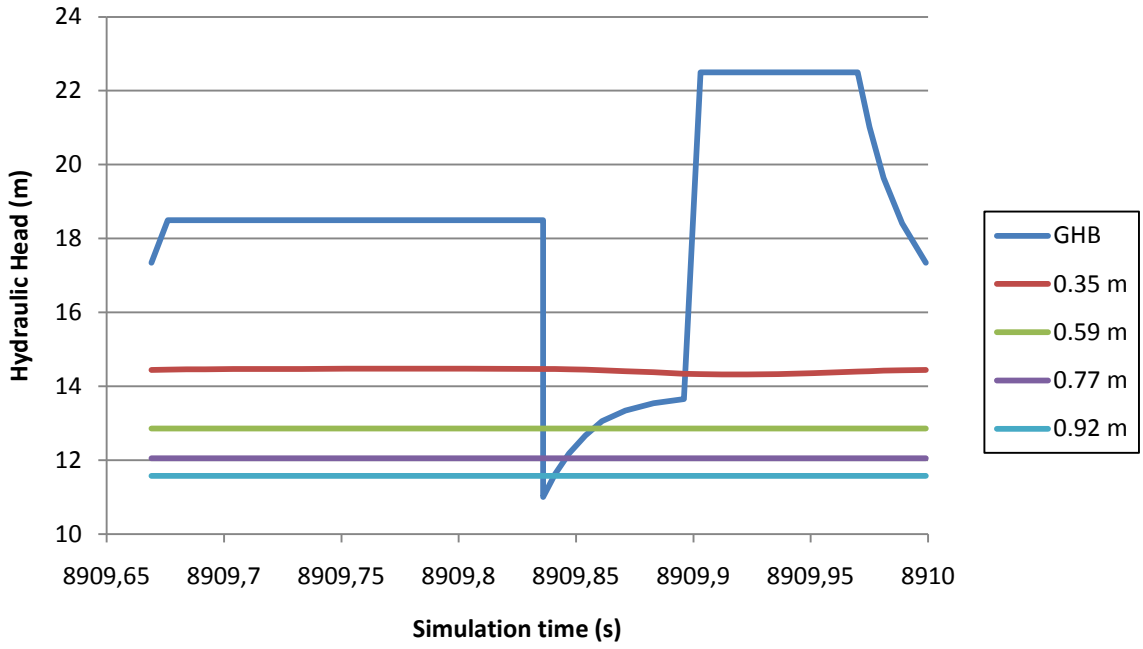

Simulation 3D-2 hydraulic head time series for a quasi steady-state pulsing cycle at layer 28

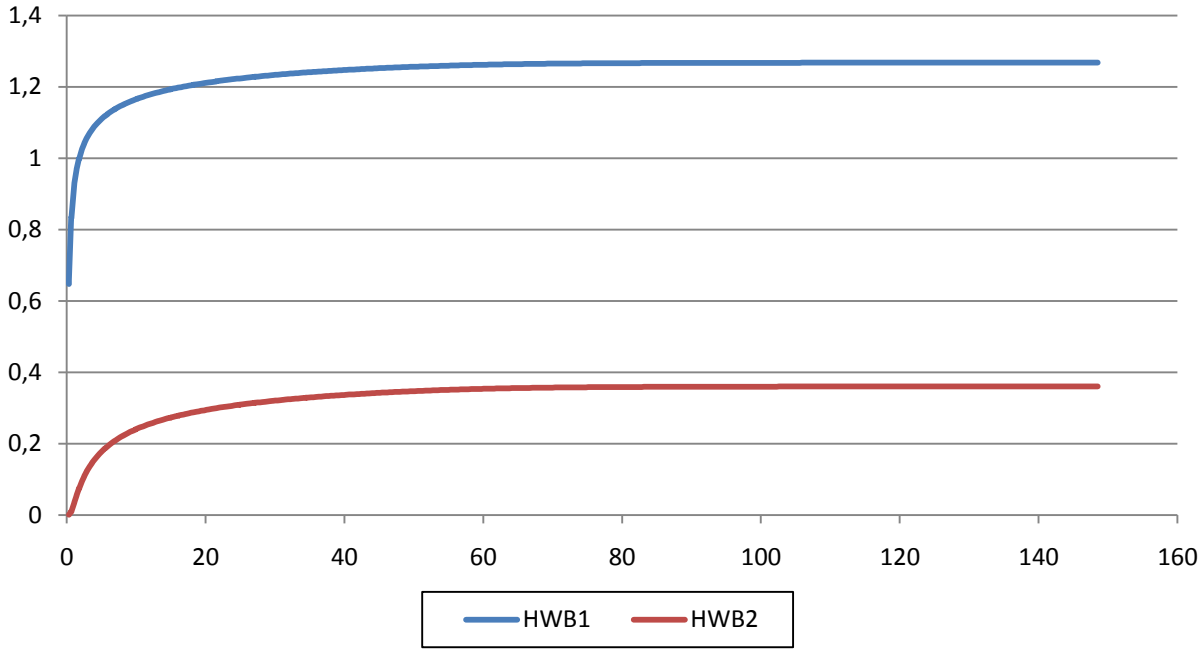

Simulation 3D-2 hydraulic head time series 1.0 and 2.0 m from injection well for complete duration

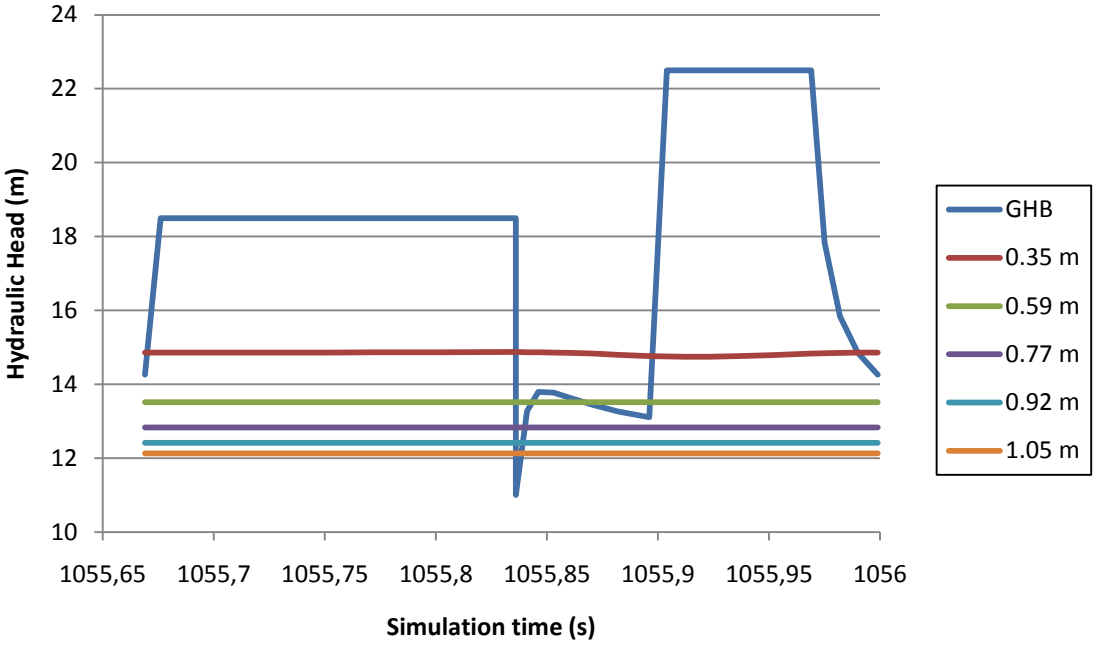

Simulation 3D-3 hydraulic head time series for a quasi steady-state pulsing cycle at layer 25

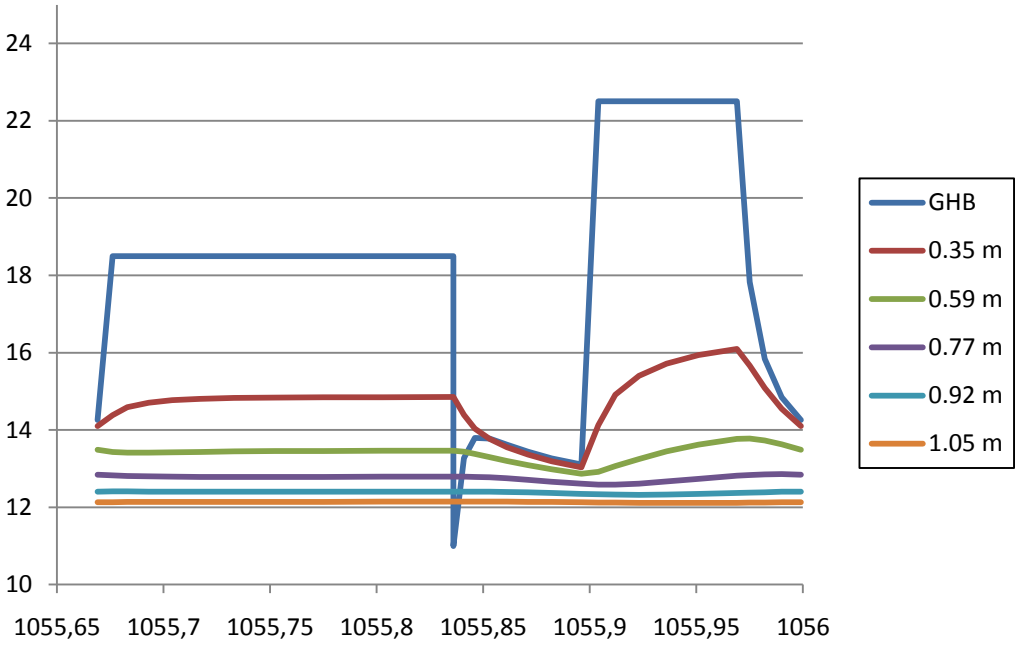

Simulation 3D-3 hydraulic head time series for a quasi steady-state pulsing cycle at layer 28

Hydraulic Head Contour maps:

Three different times during a quasi steady-state pulsing cycle are shown for pressure pulsing simulations. These include the following:

(1) During pressure pulsing stress period 1 (Boundary pressure is H_{Steady})
(2) Begging of pressure pulsing stress period 3 (recovery 1)
(3) Beggining of pressure pulsing stress period 5 (recovery 2)

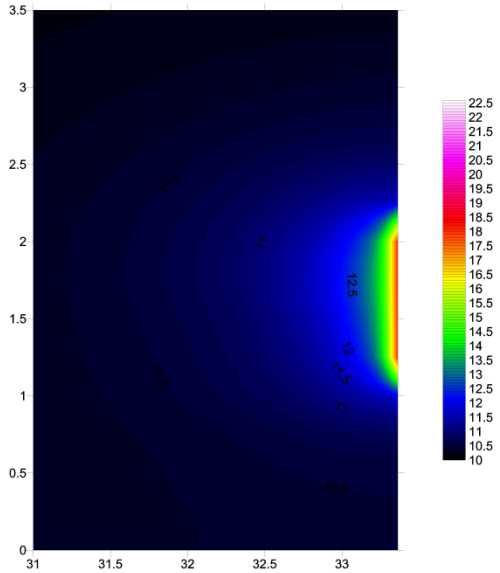

Sim. 3D-1 head distribution during the final simulation time step

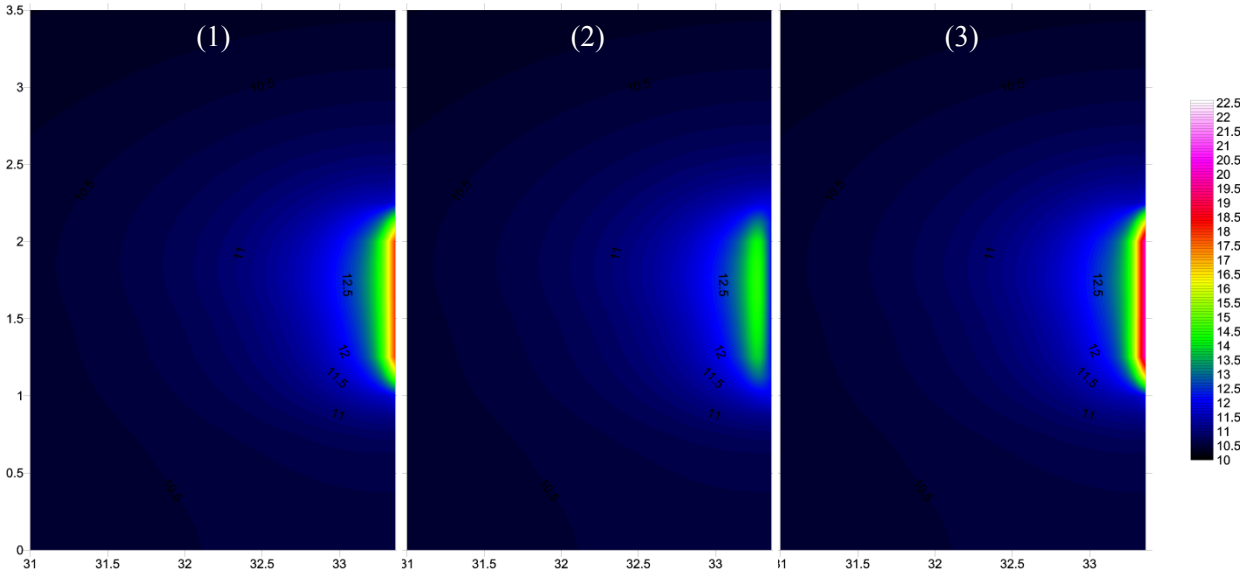

Sim. 3D-2

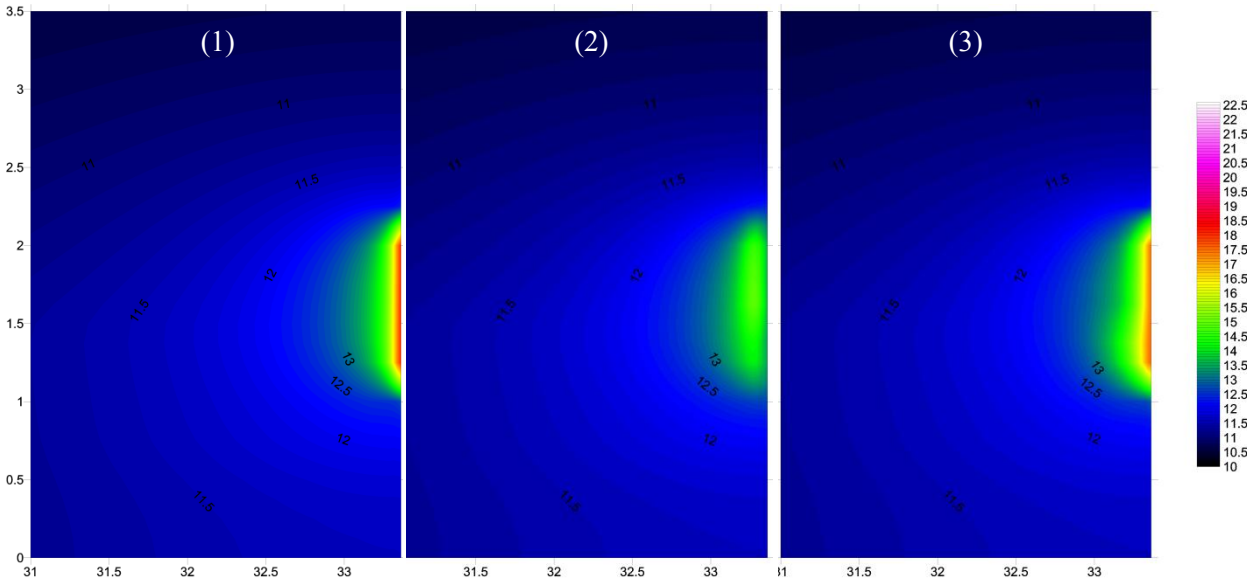

Sim. 3D-3

Zone Budget Time Series:

Zone Budget zone legend

Zone no.	Description
1	Simulated injection well
97	Upper hydrostratigraphic layer
98	Middle hydrostratigraphic layer
99	Lower stratigraphic layer

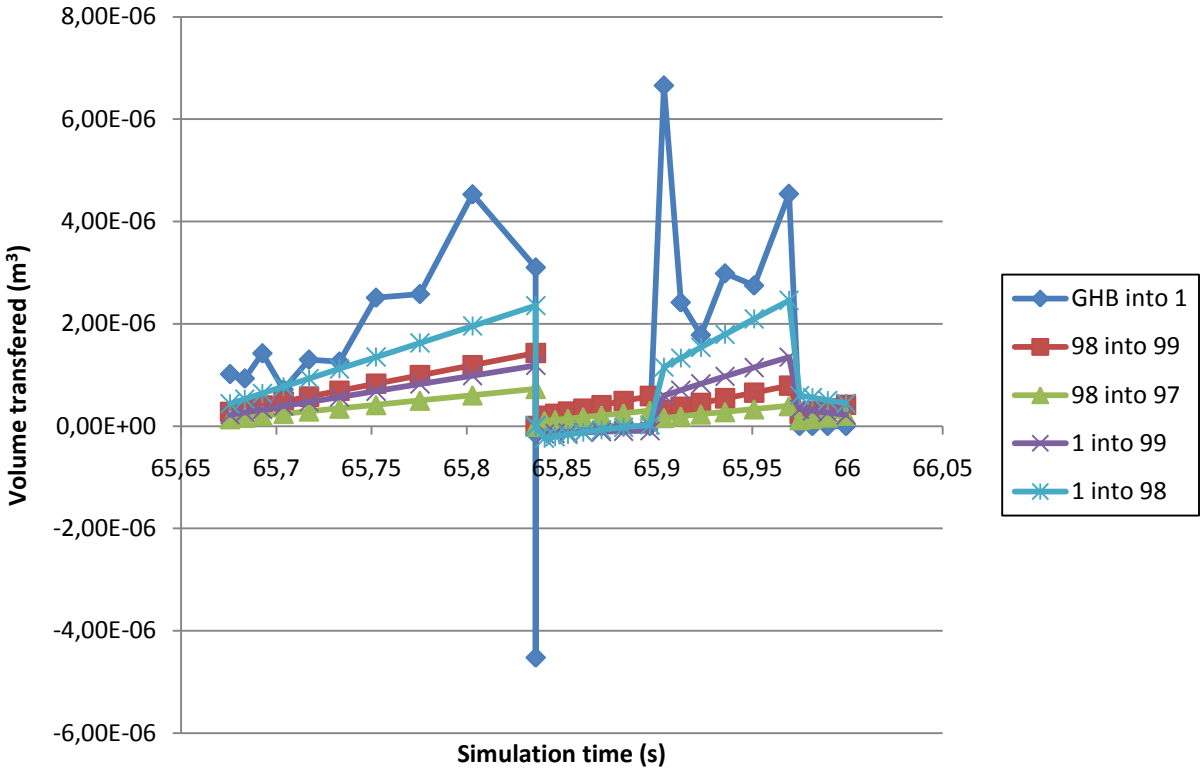

Simulation 3D-2 flow volumes transferred during a quasi steady-state pulsing cycle

Average flow rates at quasi steady-state (pulsing) or steady-state (conventional)

Border	Average flow rate (L/min)			
	Sim. 3D-1	Sim. 3D-2		
		Net	in	out
GHB into 1	6.54	6.51	4.05E-05	4.69E-06
98 into 99	1.53	2.58	1.87E-05	4.47E-06
98 into 97	1.56	1.31	2.28E-05	1.56E-05
1 into 99	2.21	2.14	1.26E-05	8.57E-07
1 into 98	4.38	4.25	2.43E-05	8.68E-07

Quality Control Data:

Head differences spanning simulated injection well over a pulsing cycle (simulation 3D-2)

Time	Head at GHB Cells (R,C,L) (m)			Difference (m)		
	58,58,28 (1)	58,58,23 (2)	58,58,25 (3)	(1)-(2)	(1)-(3)	(2)-(3)
599.0182	14	14	14	0	0	0
599.0374	20.65284	20.65284	20.65286	0	-2E-05	-2E-05
599.0605	19.67415	19.67415	19.67417	0	-2E-05	-2E-05
599.0882	18.61891	18.61891	18.61893	0	-2E-05	-2E-05
599.1214	17.80071	17.80071	17.80072	0	-1E-05	-1E-05
599.1613	17.14688	17.14687	17.14688	1E-05	0	-1E-05
599.2091	16.60471	16.6047	16.60471	1E-05	0	-1E-05
599.2665	16.14351	16.1435	16.14351	1E-05	0	-1E-05
599.3354	15.7445	15.74449	15.7445	1E-05	0	-1E-05
599.418	15.39541	15.3954	15.39541	1E-05	0	-1E-05
599.5172	15.08774	15.08774	15.08774	0	0	0
599.5365	36	36	36	0	0	0
599.5596	36	36	36	0	0	0

Changes in hydraulic head for successive pulsing cycles indicating approach to quasi steady-state

Simulation Time (s)	Δh (m) at cells of interest			
	56,58,25	56,56,25	57,57,25	58,56,25
60	0.00213	0.00236	0.00170	0.00213
180	0.00050	0.00056	0.00040	0.00050
600	0.00012	0.00013	0.00009	0.00012

Δh measured at first time step of pulsing stress period 3 (pulse peak)